CHRONIC INTRACORTICAL ELECTRODES: MODULATION OF THE BLOOD-BRAIN BARRIER AND THE FUNCTIONAL IMPLICATIONS

A Dissertation
Presented to
The Academic Faculty

by

Jessica Dominique Falcone

In Partial Fulfillment
of the Requirements for the Degree
Doctorate in Philosophy in the
School of Electrical and Computer Engineering

Georgia Institute of Technology
May 2018

CHRONIC INTRACORTICAL ELECTRODES: MODULATION OF THE BLOOD-BRAIN BARRIER AND THE FUNCTIONAL IMPLICATIONS

Approved by:

Dr. Ravi V Bellamkonda, Advisor
Pratt School of Engineering
Duke University

Dr. Thomas Barker
School of Biomedical Engineering
University of Virginia

Dr. Robert Butera, Co-advisor
Wallace H. Coulter Department of Biomedical Engineering and the School of Electrical and Computer Engineering
Georgia Institute of Technology and Emory University

Dr. Garrett Stanley
Wallace H. Coulter Department of Biomedical Engineering
Georgia Institute of Technology and Emory University

Dr. Themis Kyriakides
School of Pathology and Biomedical Engineering
Yale University School of Medicine

Dr. Stephen DeWeerth
P.C. Rossin College of Engineering and Applied Science
Lehigh University

Date Approved: December 07, 2017

To my family,

Your strength and support make all things possible.

Thank you.

ACKNOWLEDGEMENTS

I would like to thank my family, my friends, and my colleagues for their constant encouragement and support. The PhD has been long road full of professional and personal growth. As I complete my 12th year at Georgia Tech, I am reminded of the excellent caliber of faculty, researchers, and students. It has been an absolute pleasure.

First, I would like to thank Dr. Ravi Bellamkonda. I appreciate you taking a chance on me (6+) years ago. The experience in your lab has been like no other. I was thrown headlong into the world of *in vivo* work and exposed to research beyond neural interfaces (cancer, TBI, immunology to name a few). Most importantly, through my thesis, I have become comfortable with tackling the unknown. Thank you for cultivating an environment of freedom and flexibility. I am a strong and independent researcher because of it.

I would like to thank Dr. Robert Butera. After the Duke Move of '16, you incorporated me into your lab and found me wet lab and surgery space. An entire aim of my thesis would not have been possible without your help. Following that, I would also like to thank Dr. Michelle LaPlaca for allowing me to "borrow" her lab and surgery space. I am grateful for her patience as I wrap up at Tech.

To my committee members, your stimulating conversation and advisement has been invaluable. I am constantly amazed how a different voice and background allows me to approach an old problem with a new idea. With faculty moving to new universities, I am especially appreciative that time was made for my thesis, allowing me to complete

the final leg of this journey. I would like to thank Dr. Themis Kyriakides for allowing me to explore the CCR2 pathway, providing excellent guidance on the world of foreign body reactions, and being readily available when I had questions and new data to discuss. Thank you to Dr. Thomas Barker with your excellent thoughts on the biological interpretation. Thanks to Dr. Stephen DeWeerth for your input on signal analysis. Also, thank you to Dr. Garrett Stanley for your scientific method and guidance on signals in the barrel cortex.

To the members of the Bellamkonda lab, past and present, thank you for your help and support. I especially want to thank Dr. Akhil Srinivasan for taking time to walk through my research and offer advice. Another big thank you to Dr. Tarun Saxena for offering guidance on experiments and reading drafts of papers. I would like to thank Sheridan Carroll for her mRNA work. Thanks to Ketki Patil for being an awesome lab manager and helping me out after the lab moved. Also thanks goes to our new lab manager, Sean Meehan, for ensuring I get the supplies I need at Georgia Tech. I would also like to thank Dr. Nalini Mehta, Dr. Kristin Loomis, Dr. Nassir Mokarram, Dr. Johnathan Lyon, Dr. Adriana Vest, Dr. Bala Pai, Melissa Alvaredo, Martha Betancur, Faaiz Enam, Ashley Alva, and Kelly Rockwell. (Also, additional thanks to Melissa, Martha, and Ashley for letting me stay on their couch while I imaged at Duke!)

The PRL staff at Georgia Tech is awesome, and none of this animal work would be possible without them. Thank you to Dr. Laura O'Farrell and Dr. Richard Noel for training on techniques and guidance on animal experiments. Thanks to Kim Benjamin for running a tight ship, and thank you to everyone who works in the rat room for your hard work and fun conversation, including Ogeda Blue, Altair Rivas, and Andrea Gibson.

A big thank you to my mother, Felicia Stone Falcone, for being my fan of 30 years! You provide the perfect level of comfort and pragmatism, and I have needed both through this process. My favorite quote from you (when I'm complaining) is "It's a PhD. If it were easy, everyone would have one." I am where I am today, because of the drive and work ethic you have instilled in me. Thank you for all your sacrifice and hard work.

To my friends, old and new, thank you being there to talk and give me laughs. My undergrad GT group has remained a rock, and it is awesome celebrating 10 years of friendship with y'all. To my Atlanta/Rotaract friends, I am so glad I went to a Rotaract meeting. A whole new world of friendships has blossomed for me, and it has been a ton of fun getting to know you and Atlanta at the same time.

Last, but certainly not least, I would like to thank my amazing husband, Yogi Pai. Thank you for the hugs, the food, the constant words of encouragement, and the (occasional) weekend trips into lab. You are my biggest cheerleader, and I am so honored to be your partner in life. I cannot wait to start our next chapter together!

TABLE OF CONTENTS

LIST OF TABLES

LIST OF FIGURES

LIST OF SYMBOLS AND ABBREVIATIONS

Abl	Abelson murine leukemia viral oncogene homolog 1
Arg	Ableson-related gene
BBB	Blood-brain barrier
BMI	Brain machine interface
Casp3	Caspase 3
CCL2	C-C chemokine ligand type 2
CCR2	C-C chemokine receptor type 2
ColIV	Collagen IV
DAPI	4’,6-diamidino-2-phenylindole
DBS	Deep brain stimulation
DMSO	Dimethyl sulfoxide
EBA	Endothelial barrier antigen
EAE	Experimental allergic encephalomyeliti
FIJI	FIJI is just ImageJ
GFAP	Glial fibrillary acidic protein
IACUC	Institutional Animal Care and Use Committee
IC	Intracerebral
IgG	Immunoglobulin G
ISI	Interspike interval
IP	Intraperitoneal
KO	Knockout
LFP	Local field potential

MCP-1	Monocyte chemoattractant protein 1
MMP	Matrix metalloproteinase
MS	Multiple sclerosis
MSA	Mouse serum albumin
NeuN	Neuronal nuclei
PDGFRs	Platelet-derived growth factor receptors
SEM	Scanning electron microscopy
SCI	Spinal cord injury
SNR	Signal-to-noise ratio
TBI	Traumatic brain injury
tPA	Tissue plasminogen activator
ZO	Zona occludens

SUMMARY

Brain machine interfaces have the potential to connect patients living with paralysis to prosthetics and devices, dramatically improving quality of life[1]–[3]. Intracortical electrodes provide the electrode-tissue interface and record action potentials from neurons. Over time, the strength of the recorded action potentials diminishes, making repeat trials and device control difficult[4]–[6]. The biological cause was believed to be the formation of the astroglial scar physically separating the neurons from the recording sites[7], [8]. Local neurodegeneration was then identified at the electrode interface[9], and a new theory emerged suggesting that a leaky blood-brain barrier (BBB) leads to neurodegeneration[10], [11]. A negative correlation was found between recording performance and BBB breach in different implanted electrode types[12]. This work led to the questions of what impact could therapeutic modulation of the BBB have on electrophysiological function, and what mechanisms regulate the BBB in an intracortical electrode implant model?

Here we administered a therapeutic inhibitor to modulate the BBB in an electrode implant model, while evaluating the functional electrophysiology. We also sought to better understand the molecular cues in the electrode implant model and correlated electrophysiology and mRNA at a chronic time point. Specifically, the CCL2/CCR2 pathway was inhibited to prevent pro-inflammatory monocytes recruitment to the electrode interface and to also modulate the BBB[13]. Functional Michigan electrodes were implanted for 2 and 12 weeks and administered a CCR2 antagonist. The number of animals with active recording electrodes was increased at 12 weeks when compared to controls, and histological outcomes were improved at 2 weeks in the treatment group. Then, in a

chronic (>12 weeks) microwire model, mechanisms regulating the BBB, neuroinflammation, leukocyte infiltration, and inflammation were analyzed at 1 and 14 weeks. A significant correlation was found between SNR and PDGFR-β expression, suggesting a potential pathway to regulate for improved recording performance.

The significance of this work is the increased understanding of the biological mechanisms at play in an intracortical electrode implant model. Additionally, these mechanisms have been correlated with electrophysiology, assessing functionality. Future work would include delving into the temporal aspects of the CCL2/CCR2 pathway, as well as exploring the effects of PDGFR-β. MMP-9, and MMP-2 knock models on electrophysiology. Alternatively, from a device design perspective, the presence of an external connector suggests that the meninges (a part of the BBB) may never heal. Removing the connector and creating wireless recording electrodes will be the next generation of neural interfaces. Evaluation of this device design *in vivo* will further elucidate the impact of targeted BBB biological mechanisms and the subsequent electrophysiological performance.

INTRODUCTION

Neural interfacing to regulate and replace lost sensory and motor abilities is now entering clinical trials[2], [3], [6]. Guaranteeing reliable, chronic neural interfacing is critical for the success of BMIs. There are ~5.4 million people estimated to be living with some form of paralysis in the United States, and the primary causes are stroke, spinal cord injury, and multiple sclerosis[14]. BMIs provide the opportunity to improve quality of life for these populations by allowing brain connection to a computer or a robotic prosthetic[15], [16]. Additionally, BMIs can bypass the damaged neural circuits to reanimate paralyzed arms[2], [3] and legs[17]. Deep brain stimulation is a standard therapeutic tool for patients living with Parkinson's disease and the use of BMIs can provide a closed-loop system to adjust stimulation parameters based on neural recordings[18]–[21].

Both pre-clinical and clinical research has shown that action potential strength diminishes over time[2], [3], [6], [22]–[24]. Currently, all clinical trials use some form of spikes (or that frequency range) as the input data for prosthetic control[2], [3], [5], [6], [16]. Therefore, continued strength of action potentials is key for improved device control. It has been previously thought that the main biological cause for signal deterioration was the development of the astroglial scar which physically separated neurons from the recording sites[8], [25], [26]. Neurodegeneration was then identified at the electrode-tissue interface at a chronic timepoint (16 weeks), suggesting that the biological cause for signal failure was neural death[9]. Blood-brain barrier (BBB) breach was identified at the electrode interface[11], [27], and the BBB is a therapeutic target to curb neurodegeneration

in several neurodegenerative diseases[28]–[32]. Subsequent work showed a correlation between electrode failure and BBB leakage[12].

The *objective* of this thesis was to identify and target BBB repair mechanisms in an intracortical electrode model and observe the functional outcomes. Acute BBB breach in the intracortical electrode model is caused by vasculature injury due to implant insertion. As a result, infiltrating leukocytes, plasma proteins, and inflammatory chemokine and cytokines are able to enter the brain[33]. Chronically, it is believed that the foreign body presence of the electrode keeps inflammation levels elevated, resulting in continued BBB leakage[12]. Through this work, a specific pathway (CCL2/CCR2) was targeted to evaluate the impact of BBB modulation. Additional BBB mechanisms were also correlated with electrode functionality to develop a guide for future studies.

Specific Aim 1: Explore BBB modulation strategies in Michigan electrodes through inhibition of the CCR2 pathway

Following BBB rupture, circulating leukocytes enter the brain[34]. Pro-inflammatory monocytes are one of the first responders to an injury. These cells are CCR2+, and by blocking this receptor, the injury site can be turned into a more anti-inflammatory environment[35]–[38]. Additionally, CCR2 is also present on endothelial cells and when activated, tight junction proteins are disrupted[39]–[41]. The *working hypothesis* was that infiltrating pro-inflammatory monocytes play a critical role post-implantation. By antagonizing the CCR2 pathway, pro-inflammatory monocytes would be prevented from infiltrating at the electrode-tissue interface. CCR2 antagonism would also improve the fidelity of the BBB by maintaining tight junction proteins.

The *objective* for this aim was to systemically inject a CCR2-antagonist *in vivo* and evaluate outcome metrics via histology and electrophysiology. Michigan electrodes were implanted for 2 and 12 weeks in the barrel cortex of Sprague Dawley rats. Weekly electrophysiological recordings were conducted, and at the specified endpoints, histology was performed focusing on neuroinflammation, vasculature, and BBB breach. The *outcomes* of this aim are discussed in 0.

Specific Aim 2: Identify chronic BBB mechanisms related to performance variability in microwires

Currently, the biological mechanisms influencing chronic electrode performance are not well understood. The *working hypothesis* was that mRNA expression of BBB components would correlate with recordings and suggest mechanisms behind animal-to-animal variability. The *objectives* for this aim were to evaluate mRNA expression of tissue explanted at the electrode interface and correlate these profiles with electrophysiology by animal. The selected mRNA was divided into four categories of interest: 1) neuroinflammation, 2) blood-brain barrier, 3) leukocyte infiltration, and 4) inflammation. Each of these foci are related to either the physical BBB breach or the subsequent results of BBB breach. mRNA expression was evaluated at 1 and 14 weeks after microwire implantation and compared to chronic electrophysiology collected at 14 weeks. The *outcomes* of this aim are discussed in **Error! Reference source not found.**.

LITERATURE REVIEW

Intracortical electrodes are the biological-to-electronic connection in brain machine interfaces (BMIs). Research shows that signal amplitude diminishes over time[2], [4], [5], and identifying biological mechanisms for this failure can improve clinical outcomes. Chronic neurodegeneration occurs at the tissue electrode interface, and one potential biologic cause is disruption of the BBB[12]. By targeting the BBB and modulating this system, neural health can potentially be improved, resulting in improved signal strength and longevity. This review will delve into details about electrode failure, neurodegeneration and the BBB, and identify potential BBB therapeutic targets for the intracortical electrode model.

1.1 Clinical significance of intracortical electrodes

Three different clinical trials are currently being conducted for neural prosthesis, which include BrainGate2, Battelle Memorial Institute, and the University of Pittsburgh. All clinical subjects have been implanted with the 10 x 10 Blackrock Microsystems “Utah” array, which is the only recording electrodes approved by the FDA for clinical use. It is well-understood in the field that the quality of action potentials will degrade over time. For BrainGate2, over the course of 500 days, a significant decrease in spike amplitude and number of units was observed for two subjects[42]. For Battelle, wavelet power decreased for the first 150 days, but stabilized afterwards in one subject[2]. For the University of Pittsburgh, reduction in number of single was noted after 21 days in one subject[5]. The decrease in signal strength heavily impacts the pre-processing methodology. Therefore, many have suggested that the algorithms cannot rely on spikes alone and must also use

local field potentials (LFPs). The three clinical groups each have their own strategy for managing the neural signals, which will be reviewed here.

Currently, BrainGate2 has the longest running clinical trial for intracortical electrodes, with one of their patients having been implanted with Blackrock arrays for over 1000 days with successful recordings[43]. Between two patients, only 23% of electrodes recorded spike activity post 500 days implantation. However, for one patient, ~70% of electrodes were recording local field potentials (LFPs) while for the other patient, only 30% of electrodes were recording LFPs[42]. Power spectrum analysis of LFPs focuses on four brain wave frequency categories: 1) delta (0.5 – 3 Hz), 2) theta (3.5 – 7 Hz), 3) alpha (8 – 13 Hz), and 4) gamma (30 – 70 Hz)[44]. The BrainGate2 group was interested in high frequency LFPs, and added two more frequency categories of interest: 5) high gamma (70 – 200 Hz) and epsilon (200 to 400 Hz)[42]. In future algorithms, spikes and high-frequency LFPs (250 to 2500 Hz) were used for motor decoding[3]. BrainGate2 has conducted studies to control a computer mouse in a 2 dimensional space[4], [15], [42], [43], [45], a robotic arm with 7 degrees of freedom[16], and most recently controlling functional electrode stimulation (FES) electrodes implanted into the patient's paralyzed arm[46], [47].

Battelle tested a patient implanted with a Blackrock Microsystems array for 15 months (~450 days), and the signals from the array were used to stimulate external FES electrodes on the paralyzed patient's arm to control movement and grasp with 6 degrees of freedom[2]. A previous non-human primate study acknowledged the steady decline of SNR and number of units over the course of 200 days. A 11-level wavelet analysis was used over spikes for the decoding, and the wavelets fell into three categories: 1) LFP (0 to 200 Hz), 2) multi-units (300 Hz to 1 kHz), and 3) single units (>1 kHz)[24]. The 4 wavelets in

the multi-unit frequency were selected for use in the decoder during the clinical trials[2], [46]. Wavelets in the multi-unit frequency were selected as they did not significantly correlate with the decline in single unit amplitude[24].

The University of Pittsburgh demonstrated a subject's control of a robotic arm with 7-degrees of freedom over a 13 week time period following implantation of two Blackrock arrays[5]. Firing rates from single and multi-units were inputted into the neural decoders[5], [6]. The most recent study compared 2 subjects (both with two implanted Blackrock arrays) controlling a robotic arm with 7-degrees of freedom with shared control by vision-guided robotic assistance. Both subjects were more successful at completing reaching, grasp, and object selection tasks[6]. This group has also shown efficacy of microstimulation in the somatosensory cortex to elicit tactile sensation[1]. Closed-loop tactile sensations are critical for improving reach and grasp tasks[48]–[50].

In these trials, the neural signals that are inputted into the decoders for prosthesis control provide guidelines for pre-clinical electrophysiological research. No clear consensus has been made as to whether spikes or LFPs are the preferred input signal. It is also important to remember that these studies are extremely underpowered (n = 1 or 2), so more subjects are needed before a path forward can be determined. Interestingly, it appears that the traditional LFP range (0 to 200 Hz) does not appear sufficient. Both the BrainGate2 and the Battelle group have selected frequencies (<250 Hz) that correspond with spiking activity[2], [3], [46]. To supplement poor signal recording, improvements in decoders[4] and implementation of decoder and neural adaptation algorithms[51] have been proposed, and additional assistance from vision-guided robotics have been successfully used[6].

Regardless, improvement in the strength and fidelity of action potentials over the course of months (and years) would greatly benefit clinical trials.

1.2 Chronic intracortical electrode recording failure

As mentioned in the previous section, a reduction in signal amplitude over time has been observed clinically[2], [4], [5]. Additionally, chronic electrode failure has been well documented in pre-clinical models[12], [22]–[24], [52]–[54]. A study using Utah electrodes in a monkey reported a steady decrease in SNR starting at day 31 until day 227[24]. Utah electrodes were implanted into the cerebral cortex of 4 cats, and a decrease in signal amplitude was observed at 60 days and then again at 200 days[53]. A separate study focused on the electrophysiological and histological effects of Utah electrodes at 12 weeks in rats. Out of 10 implanted rats, only 2 had action potentials and discernable units at 12 weeks[52]. In rats, functional electrophysiology was compared across implanted Michigan, Utah, and microwire electrodes for 12 weeks. Microwires outperformed both Michigan and Utah electrodes in terms of SNR, but all SNRs had reduced by 12 weeks[22].

Table 1 – Overview of specs for recording electrodes used in research

Electrode Type	Insulation	Site Material	Dimensions	Shape	Size of Array
Microwire	Polyimide/ Teflon	Stainless steel/ Tungsten	Ø = 50 µm	Cylinder	16 to 96
Michigan	Silicon Dioxide/ Silicon Nitride	Iridium	thk: 15 or 50 µm wd: 50 to 100 µm	Tapered Prism	1 to 8
Utah	Parylene-C	Platinum/ Iridium oxide	Ø = 50 µm	Cone	16 to 96
Tethered Microwire	Parylene-C	Platinum/ Iridium	Ø = 75 µm	Cylinder	16 to 32

Chronic recordings conducted in mice using Michigan electrodes also saw a decrease in SNR after 1 month[23].

1.2.1 Material – electrode failure

It is important to acknowledge that different intracortical electrodes are used throughout the literature. As seen in **Table 1**, the most commonly used electrodes are microwires, Michigan electrodes (NeuroNexus, MI), Utah electrodes (Blackrock Microsystems, UT), and tethered microwires (Microprobes, MD). Utah electrodes are the intracortical electrode that has received FDA approval and are therefore the only electrode used in clinical trials[43]. Electrophysiology is the standard *in vivo* measurement for function, however, in addition to material and mechanical damage, the cellular environment impacts this measurement as well.

Compromised insulation and damaged recording sites have been observed on TDT microwires[55], Microprobes floating microwires[56], NeuroNexus "Michigan" probes[57], and BlackRock Microsystems "Utah" needle electrodes[54], [58] following chronic *in vivo* implantation, as well as through accelerated failure lab bench testing[59]. This damage leads to increased impedance and non-functioning electrodes. SNR will be the highest within the first 2 weeks of implantation (particularly on the day of surgery) followed by a steady decline and eventual plateau[12], [22]–[24], [60]. Therefore, the impact of compromised insulation and recording site degradation should be taken into consideration.

The type of damage the electrodes encounter is design related. The electrodes fall into two categories, NeuroNexus probes and protruding electrodes. For the protruding

electrodes, which are Microprobes, Blackrock Microsystems, and TDT, the electrodes consist of an inductive material (platinum iridium, platinum-coated silicon, and gold-coated tungsten) coated with insulation (parylene-C, parylene-C, and polyimide) and a single recording site exposed at the distal end of the electrode. The failure points are at the electrode sites and in the insulation. For the electrode sites, insulation can delaminate, extending the recording site surface area, and damage can occur to the recording site in the form of cracks, corrosion, and deformation. Insulation can be compromised be delamination and fissures[54]–[56], [58], [59].

NeuroNexus probes have a different design with multiple insulated traces feeding into multiple recording sites on a single shank. The electrodes are fabricated from silicon and the recording sites are coated in iridium and the insulation on the traces is silicon nitride. Kozai et al. demonstrated how mechanical strain can lead to device deterioration. The NeuroNexus probes have the traces running under the sputtered iridium (which is larger than the recording site). Kozai used an FEM to show the increase in strain at the traces at the iridium interface and replicated this result with SEM images from chronically implanted electrodes that had increased insulation degradation at the trace-iridium interface. Additionally, electrodes that ceased to record had insulation degradation either in the vicinity of the recording site or further up the electrode at one of these interfaces. For the recording sites, the main issue with the NeuroNexus probes is cracking and corrosion of the iridium. For the traces, it is severe cracking in the insulation[57].

1.2.2 Biomechanical – micromotion

A study revealed that micromotion at the electrode interface the day of implantation is caused by respiration (6–11 μm) and heart beat (2–4 μm)[61]. While this effect is reduced by 8 weeks, micromotion is still present[62]. Most notably, this micromotion is observed in an anesthetized, stereotaxed animal and does not include micromotion from active movement or from plugging in the electrophysiology connectors. Modeling work has also shown the impact of strain on the surrounding tissue and the electrode itself[57], [63], [64].

To reduce the biological effects of micromotion, significantly "softer" electrodes have been developed and have been shown to reduce the chronic biological response at the electrode interface[65]–[73]. A caveat to flexible electrodes is that they are difficult to insert into the brain. This has also resulted in a field designing coatings and material strategies for easy insertion[68], [74], [75]. An alternate approach is to miniaturize the electrodes. Karumbaiah et al demonstrated a reduced immune response using smaller NeuroNexus probes (thickness = 15 μm) compared to thicker NeuroNexus probes (thickness = 50 μm) of the same length and width[22]. Kozai et al. fabricated carbon nanofibers for functional recordings and demonstrated *in vivo* proof-of-concept for electrophysiology and reduced immune response when compared to NeuroNexus probes[69].

Tethered electrodes are another strategy to reduce the effects of micromotion. By tethering, the electrodes can move with the brain and therefore reduce inflammation. However, these tethered electrodes are not truly "free floating" as forces are still exerted from the ribbon cable which is dental cemented to the skull at an alternate location. Previous work has shown that tethered electrodes induce an increased neuroinflammation

response when compared to untethered, fixed electrodes of the same material and dimensions[22].

1.2.3 Biological – cellular milieu

Following electrode insertion, within 100 microns of the electrode-tissue interface, astrocytes and microglia are highly activated. During the acute timeframe (between implantation and two weeks post-implantation), reactive astrocytes and reactive microglia are heavily recruited to the implant sight, and significant neuronal loss occurs as well [11]. Reactive microglia levels peak at two weeks. In the post-acute window (between two and eight weeks post-implantation), reactive astrocyte recruitment peaks and then plateaus, while reactive microglia decrease. It is important to note that while there is a reduction in activated microglia, astrocytes still remain in a more elevated reactive state. During the post-acute phase, the neural population remains stable[25], [26]. At chronic time points (from eight to sixteen weeks post-implantation), while reactive astrocyte and microglia levels remain stable, significant neurodegeneration is observed[11], [76]. The main biotic theory for failure is electrode encapsulation by the astroglial scar, which physically distances the electrodes from the neurons. However, as the astroglial scar stabilizes within the first 4 weeks[11], the data suggests that an alternative cascade is set in motion at 8 weeks to incite neurodegeneration.

Experiments revealed the presence of IgG at the electrode interface at acute and chronic timepoints[11], [27]. More recently, BBB disruption has been identified as a potential cause for neurodegeneration and reduction in recording quality. Research in the Bellamkonda lab showed significantly different SNRs between animals implanted with

microwires versus animals implanted with Michigan electrodes. Further histology revealed that there was less IgG expression at the interface of the microwire animals (better SNR performance) while the Michigan electrodes (worse SNR performance) had significantly increased IgG expression[12]. Tresco's lab furthered this result by comparing IgG expression of inner electrodes (worse SNR performance) to outer electrodes (better SNR performance) within each Utah electrode array. The results showed that electrodes with better SNR had reduced IgG expression and visa versa[52].

1.3 The blood-brain barrier and neurodegeneration

1.3.1 Physiology of the blood-brain barrier

Surrounding the brain is the meninges which contains cerebrospinal fluid and is divided into three layers: the dura, the arachnoid, and the pia. As seen in **Figure 1A**, vasculature runs through these layers in a series of venules and arterioles that penetrate into the brain and divide into microvessels[77], [78]. The BBB is a critical organ in the regulation of homeostasis in the brain and is responsible for immune surveillance,

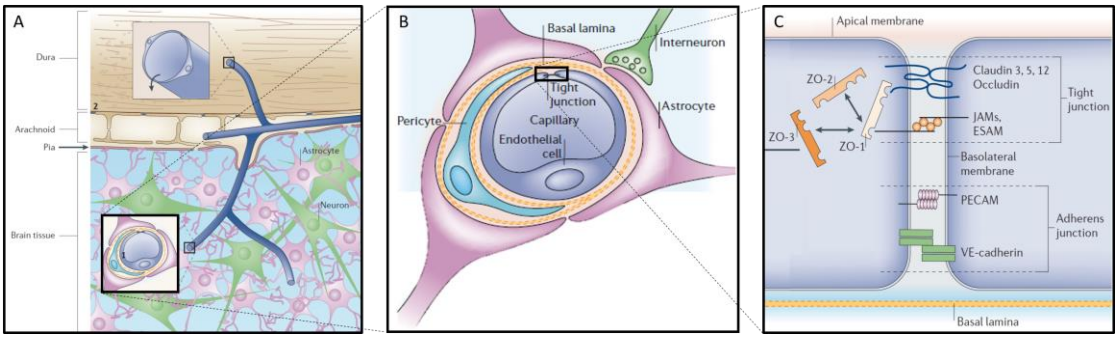

Figure 1 – (A) View of vasculature within the brain, including the meninges, which is compromised of the dura, arachnoid, and pia layers. (B) Cross section of brain vasculature including endothelial cells connected by tight junction proteins, basal lamina, pericytes, and astrocyte end feet. (C) Illustration of cell-to-cell junctions including tight and adherens junctions. Adapted from [29]**.**

molecular trafficking, and ionic regulation. The BBB is composed of several cellular layers (see **Figure 1B**), which include endothelial cells, pericytes, basal lamina, and astrocyte endfeet[29], [79].

Connecting the endothelial cells are a unique set of tight junction proteins, which can be divided into transmembrane (claudins, occludins, junctional adhesion molecules) and intramembrane (zonola occludens) proteins. As seen in **Figure 1C**, zonola occludens (ZOs) anchor the transmembrane proteins to the cytoskeleton in the endothelial cell. Adheren junctions are responsible for direct endothelial-endothelial linking and include PECAM and VE-cadherin proteins[29], [79], [80]. Pericytes, which are imbedded within the basal lamina, control blood flow and directly connect with endothelial cells to maintain

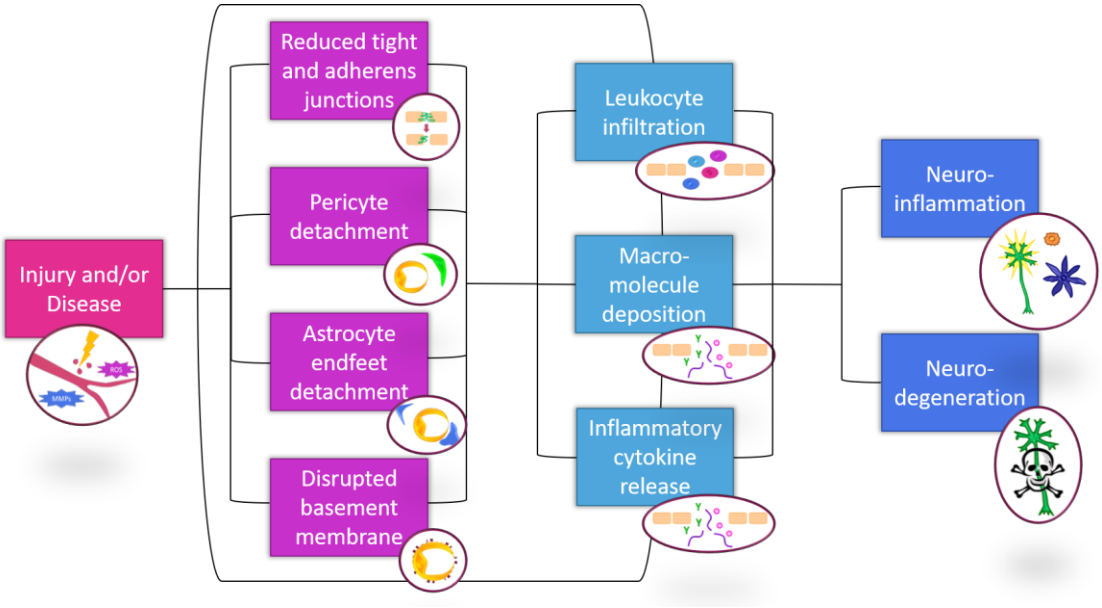

Figure 2 – Illustration of BBB disruption caused by injury and/or disease (pink) which leads to breakdown of the cellular and protein components of the BBB (magenta). This leads to leukocyte, protein, and cytokine infiltration (light blue). These causes of BBB breach can create a positive feedback loop, creating additional disruption. The result of continued BBB breach is neuroinflammation and neurodegeneration (blue).

vasculature health and promote angiogenesis[81], [82]. The basal lamina is composed of several basement membrane proteins, including collagen IV and laminin[79]. The astrocyte endfeet also regulate blood flow and directly connect neurons with vasculature[83]. When there is disruption at any of these layers, the neural health of the brain is severely compromised[29].

1.3.2 Blood-brain barrier disruption and neurodegeneration

Each of the cellular and protein components of the BBB are a potential source for failure. First and foremost, injury can perturb and rupture blood vessels which directly leads to a compromised BBB. More subtly, loss of each layer leads to BBB leakage, including tight and adherens junctions[84], pericytes, basal lamina[85], and astrocytes. The effects of a disrupted BBB include leukocyte infiltration[81], macromolecule deposition, neuroinflammation, and neurodegeneration (See **Figure 2**).

Specific examples can be found throughout different neurodegenerative pathophysiology (**Figure 3**). Recent work from the Akassaglou lab delved into the mechanism behind demyelination in multiple sclerosis using an EAE model. They demonstrated that fibrinogen leakage into the brain activated microglia, which in turn phagocytosed the myelin of nearby axons[31], [32], [86]. In an Alzheimer's disease model, pericyte loss led to increased BBB leakage and early neuronal loss[87]. A compromised BBB can lead to epilepsy by the uptake of albumin via astrocytes, causing excitotoxicity in surrounding neurons[88]–[91]. Work in stroke models have shown how an increase in matrix metalloproteinases degrades tight junctions and worsens infarct size[92].

1.4 Blood-brain barrier modulation in an intracortical electrode model

With mounting evidence suggesting that the BBB is a therapeutic target for intracortical implants, the next question is how do we target the BBB? Thus far, reactive oxygen species, general inflammation, and pro-inflammatory monocytes have been targeted. The Capadona lab has explored anti-oxidants to reduce reactive oxygen species at the tissue-electrode interface thought two different compounds, curcumin and resveratrol. Both curcumin and resveratrol have shown success in repairing the BBB and reducing neurodegeneration in stroke, Alzhemier's, multiple sclerosis, Parkinson's, and spinal cord injury[93]–[100]. Curcumin and resveratrol controlled release hydrogel coatings were developed for Michigan electrodes. These coatings both reduced the immune response at 2 weeks, but not at 16 weeks around single shank Michigan electrodes implanted in rats[101], [102]. Next, a systemic daily injection of resveratrol was analyzed for implanted single shank Michigan electrodes in rats, but again while there was a reduced immune response at 2 weeks, this effect was not sustained at 16 weeks[103].

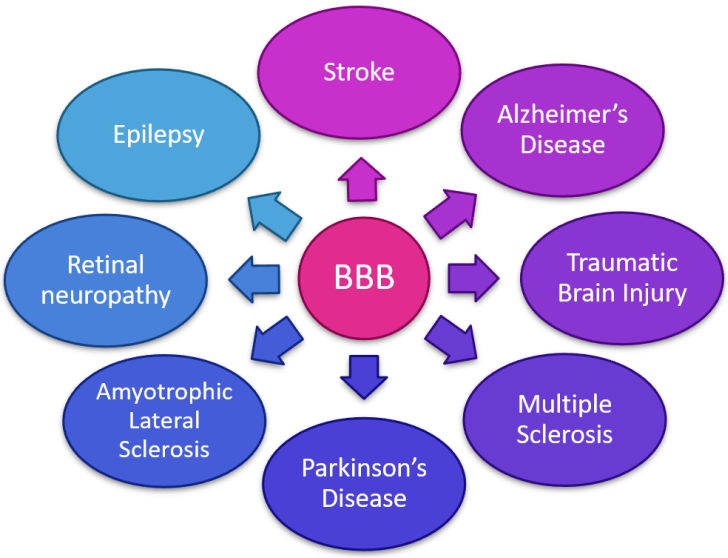

Figure 3 – Illustrative figure demonstrating neurodegenerative diseases that have BBB breach that causes neurodegeneration.

Kozai et al explored inhibiting a general inflammation marker, caspase-1, which has shown promise in stroke, traumatic brain injury, Huntington's, and Amyotrophic Lateral Sclerosis[104]–[108]. Functional single-shank Michigan electrodes were implanted into a caspase-1 knockout mouse model. Improved single unit and SNRs were seen in the caspase-1 knockout mice compared to wildtype controls[60]. For a more specific look at inflammation, Kyriakides' lab used a CCL2 knockout mouse model to analyze the impact of preventing recruitment of pro-inflammatory monocytes in a single shank Michigan electrode implant model. At 8 weeks, knockout mice had reduced GFAP and albumin expression with increased NeuN expression. qRT-PCR showed a shift towards an anti-inflammatory profile at 2 weeks[13]. A final study examined the impact the neuroprotective and anti-inflammatory effects of minocycline on a microwire electrode implant model in rats. At 4 weeks, improved SNRs were observed in minocycline treated rats compared to control. GFAP activation was reduced at 1 week in minocycline treated rats, but not at 4 weeks[109].

For this work, two mechanisms have been proposed. The first, imatinib, is novel for application to the electrode implant model. Imatinib targets various aspects of the vasculature and wound healing and has shown promise in various neurodegenerative disease models. The second, RS 102895, is a CCR2-antagonist used in the Kyriakides' lab work. As no functional analysis was conducted in that work, the implementation of the CCR2-antagonist with a functional electrode implant model is the logical next step.

1.4.1 Imatinib: Restoring the BBB through vasculature modulation

Imatinib mesylate, an FDA-approved tyrosine kinase inhibitor (aka Gleevec), was originally developed to inhibit the mutated BCR-ABL in chronic myelogenous leukemia. Further research has revealed that imatinib also inhibits c-KIT, which is upregulated in gastrointestinal stromal tumors, and platelet-derived growth factor receptors (PDGFRs). Imatinib has proven usual at attenuating symptoms in several disease categories, including fibrosis, hypertension, and most recently neurodegeneration.

More importantly, imatinib administration in several neurodegenerative models has resulted in a reduction in BBB breach. Originally, Su and colleagues were investigating the molecular pathway in stroke after the administration of tissue plasminogen activator (tPA) and how to prevent the deleterious side effects of tPA. Su et al. validated that tPA increased the production of PDGF-CC, and when the receptor (PDGFR-α) was inhibited with imatinib, tPA treatment greatly reduced the infarct size and BBB breach in the stroke model[110]. Another group used imatinib in a pericyte-deficient mouse model to reduce BBB leakage caused by missing pericytes[111]. Imatinib has also proven successful at reducing BBB breach in multiple sclerosis[112] and spinal cord injury[113].

1.4.1.1 Astrocytes and PDGFR-α inhibition with imatinib to reduce MMP-9 production

PDGFR-α are common on astrocyte endfeet (which interact with the BBB) and may play a role in the efficacy of imatinib [110]. MMP-9 is associated with BBB disruption and astrocytes are the main resident brain cells to produce MMP-9 [114]. Interestingly, Yang et al. have recently identified the impact of IL-1ß on the release of MMP-9 from astrocytes through the c-Src/PDGFR/PI3K/Akt-dependent Nox/ROS pathways with the transcription factors NF-κB and AP-1 [115], [116]. Following this pathway, by administering imatinib,

PDGFR would be inhibited, preventing the downstream transcription of MMP-9. Ma et al., 2011 has investigated the importance of PDGFR-α in an *in vivo* intracerebral hemorrhage model, and administration of imatinib showed a decrease in MMP-9.

1.4.1.2 Pericytes and PDGFR-ß inhibition with imatinib to prevent angiogenesis

During angiogenesis, endothelial cells secrete PDGF-BB to recruit pericytes, which have PDGFR-ß. Two theories have emerged within the tumor literature for the effects of targeting pericytes with imatinib or other PDGFR-ß inhibitors: 1) by inhibiting PDGFR-ß, angiogenesis is halted [118], [119], which results in less blood vessel leakage [84] or 2) by inhibiting PDGFR-ß, pericytes start to apoptose, which leads to reduced vasculature stability [120]. Hosaka et al., 2013 conducted an elegant study to investigate the effects PDGFR-ß inhibition in tumor models and explain conflicting results from past studies. Their hypothesis was that the resident PDGF-BB levels of the tumors would predict the efficacy of imatinib on the tumor. By comparing the vasculature of high PDGF-BB tumors to low PDGF-BB tumors for both control and imatinib treatment, it was seen that high PDGF-BB responded positively to imatinib with less dextran leakage into the subcellular space and, interestingly enough, larger pericyte and smaller endothelial cell coverage in the imatinib treated tumors. With low PDGF-BB tumors, imatinib increased dextran extravasation and minimized both pericyte and endothelial cell coverage. However, despite the differences in tumor vessel leakage, imatinib still significantly reduced the tumor size of both high and low PDGF-BB tumors [120].

Other studies have shown that imatinib does decrease pericyte population, which in turn reduces vasculature [121]–[123]. However, comparisons are difficult across the

literature as endothelial cell and pericyte markers are predominantly used to evaluate functional outcomes, but a marker for BBB or blood vessel leakiness is not cross-correlated with these results. Also, when evaluating these studies it is important to keep in mind that more blood vessels or more angiogenesis is not necessarily a good thing. The impact of angiogenesis after injury or tissue disruption in the brain is not well understood. However, the results from Vlahovic et al., 2007 demonstrated that while imatinib reduced vasculature coverage in the tumor model, imatinib concurrently reduced newly forming blood vessels at a similar rate, suggesting that imatinib was preventing the formation of new blood vessels, as opposed to destroying mature blood vessels.

1.4.1.3 Endothelial cells and Abl inhibition with imatinib to improve cell-to-cell contact

The mechanisms behind imatinib-induced sealing of the BBB are not fully understood; however, research from several different disease models have illuminated potential pathways. Within endothelial cells, the relationship between Abl inhibition and decreased endothelial permeability has been studied. Imatinib inhibition of Abl has been shown to strengthen endothelial cell-to-cell VE-cadherin junctions by increasing production of Rac1 and Rap1 GTPases [124]. Within endothelial cells, imatinib also inhibits Abl-related gene (Arg) which also improves cell-to-cell and cell-to-matrix contacts by preventing the disassembly of focal adhesions, as well as increasing production of Rac1 [125]. Inhibition of Abl with imatinib has also been shown to prevent apoptosis in endothelial cells [126], [127].

1.4.2 Targeting monocytes and BBB leakage through the CCR2 pathway

Monocyte chemoattractant protein 1 (MCP-1, also known as CCL2) is the chemokine that attracts monocyte, and its receptor is CCR2. Monocytes are circulating white blood cells that differentiate into macrophages and dendritic cells. CCL2 works with MCP-3 (also known as CCL7) to attract monocytes and regulate macrophage function (See **Figure 4**). When a deficiency for CCL2 exists, alternate chemokines, namely MCP-2 and MCP-3, are activated and attract monocytes to areas of inflammation[128]. Targeted disruption of SCYA2, the gene encoding CCL2, alone interferes with monocyte recruitment to inflammatory sites[129]. However, genetic deletion of both CCL2 and MCP-3 altogether results in a near inhibition of monocyte mobilization from the bone marrow into the blood stream and an inability to recruit monocytes to sites of inflammation[129], [130].

1.4.2.1 CCL2/CCR2 in the CNS and brain

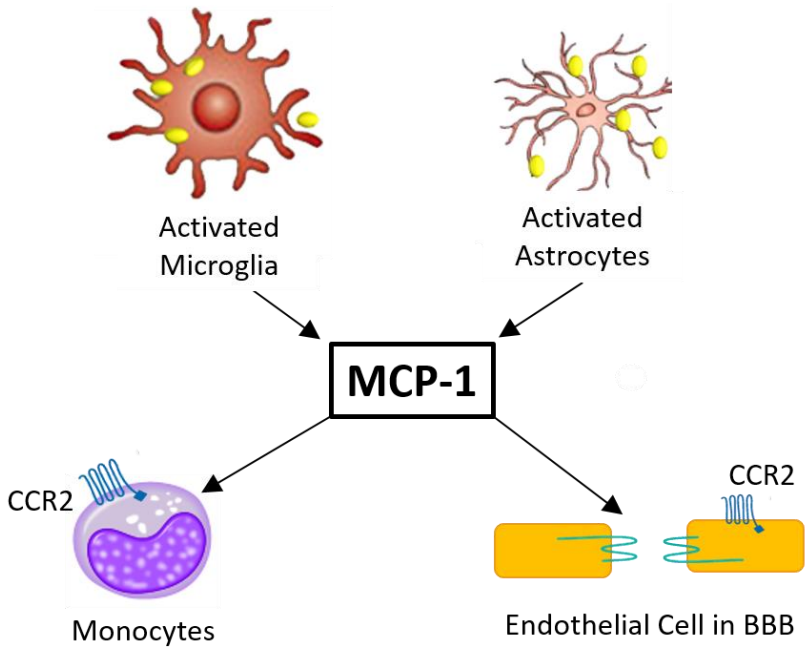

Figure 4 – Pictorial representation of CCL2 recruitment of monocytes and CCL2 activation of tight junction degradation.

CCR2 receptors are present on neurons, astrocyte, microglia, and endothelial cells. During non-injured conditions, expression of CCR2 remains low. However, following injury, astrocyte and microglia CCR2 expression increases. CCL2 is expressed by several CNS cells following injury, including astrocytes, microglia, and neurons. To add literal insult to injury, infiltrating macrophages produce CCL2 as well, creating a positive feedback loop of monocyte recruitment[37].

Finally, several neurodegenerative diseases express CCR2 and CCL2 upregulation at the onset of disease. Autopsied brain tissues of multiple sclerosis (MS) patients have increased CCL2 expression[131], [132]. CCR2 and CCL2 KO MS models exhibited reduced symptoms and less macrophage recruitment when compared to WT[133], [134]. Additional animal work also suggests that instead of initiating onset, CCL2 further amplifies disease progression in MS models[135]. Stroke patients have elevated levels of CCL2 in their serum and cerebral spinal fluid[136], [137]. CCL2 and CCR2 KO stroke models also exhibit reduced infarct volumes and attenuated macrophage recruitment[138], [139]. CCL2 and CCR2 have not been studied as thoroughly in the clinical setting for traumatic brain injury (TBI), but animal work suggests an acute (order of 12 hours) upregulation of CCL2 post injury[37]. CCL2 and CCR2 KO models with induced TBI have reduced cavity sizes and macrophage recruitment [140], [141]

1.4.2.2 CCL2/CCR2 and the blood-brain barrier

CCL2 also affects BBB permeability by altering tight junction proteins[39], [41], [142] (See **Figure 4**). In vitro administration of CCL2 to cultured microvessels depleted ZO-1, occludin, and claudin-5[39], [142]. Intracerebral (IC) injection of CCL2 resulted in

significant FITC-albumin leakage in the brain in vivo. When IC CCL2 was injected into a CCR2 KO mouse, minimal BBB leakage was observed[41]. As a continuation of this work, a middle cerebral artery occlusion to model stroke was applied to a CCR2 KO model. The CCR2 KO had a significant reduction in infarct volume, as well as a reduction of infiltrating cells, including neutrophils and monocytes[138].

1.4.2.3 Monocyte and macrophage inflammatory classifications

Monocytes are a part of the innate immune response and have been divided into two subsets: 1) M1-like (pro-inflammatory) and 2) M2-like (anti-inflammatory). For humans, CD14 and CD16 surface markers identify monocytes (M1-like are CD14+ CD16- and M2-like are CD14+ CD16+). Within mice, Ly6C+ monocytes are M1-like and Ly6C- are M2-like. With rats, CD43- monocytes are M1-like and CD43+ monocytes are M2-like. In all species, M1-like monocytes predominantly have CCR2 surface markers and M2-like monocytes only have CX_3CR1 surface markers[143]–[145].

Table 2 – Murine markers for M1-like and M2-like macrophages

Cell Type	Phenotype Markers	References
Classical (M1-like)	CD86, CD80, iNOS, CCR7	[13], [86], [146], [203], [204], [285]
Wound Healing (M2a,c-like)	Arginase 1, CD163, CD206, CD23	[13], [86], [146], [203], [204], [285]
Regulatory (M2b-like)	CD86, CD163	[13], [86], [146], [203], [204], [285]

Monocytes differentiate into macrophages, which are divided into three subsets as shown in **Table 2**: 1) M1-like (pro-inflammatory), 2) M2a,c-like – wound healing (anti-inflammatory), and 3) M2b-like – regulatory (pro and anti-inflammatory). M1-like macrophages are responsible for phagocytosis and tissue defense following infection and injury. They are the first responders and also regulate reactive oxygen species and nitric oxide production[144], [146]. Wound healing macrophages, as the name suggests, are responsible for tissue repair. M2a cells produce extracellular matrix components and orchestrate fibrosis[144], [146]. M2c cells are responsible for debris clearance and pro-healing[146]. Regulatory macrophages possess both pro and anti-inflammatory phenotypes. These cells suppress innate immunity (classically activated macrophages) for clearance of apoptotic cells[144], [146].

1.4.2.4 Chronic monocyte/macrophage infiltration at electrode interface

In this study, a chimera mouse model was created by harvesting bone marrow cells from a cyan fluorescent protein (CFP)+ mouse and injecting the cells into an irradiated wild type mouse. After 2 weeks, the chimera mice were implanted with single shank Michigan electrodes. Interestingly, CFP+ cells were found up to 16 weeks. Further analysis revealed a 60% co-localization of IBA-1 and CFP+ cells, concluding that 60% of the infiltrating cells were monocytes/macrophages. Within the macrophage/microglia population, co-localization of CD68 and CFP+ cells revealed that only 30% of CD68+ cells were resident microglia across all for time points, confirming that infiltrating monocytes/macrophages dominant the macrophage/microglia response[147].

1.4.2.5 Foreign body response of intracortical electrodes in CCL2 KO model

Sawyer et al. proceeded to investigate the effect of CCL2 elimination on the foreign body response. Single shank Michigan electrodes were implanted into wild-type and CCL2 KO mice over the period of 1, 2, and 8 weeks. Histology revealed that neural density (NeuN) was increased in the CCL2 KO at 2 and 8 weeks. Astrocyte activation (GFAP) was significantly reduced at the 8 week time point as was albumin (MSA). Interestingly, the macrophage population (Mac-3) increased at 2 weeks, but not 1 or 8 weeks, but this reaction has been reported in other work using CCL2 KO models. Wild-type mice were then injected with a CCR2-antagonist, and a significnat increase in NeuN+ cells and a significant decrease in Mac-3+ cells was observed[13].

Next, mRNA gene data was collected at 2 weeks. A significant upregulation was observed in the CCL2 KO mouse for anti-inflammatory markers (CD163, CD206, Arg-1). No significant change was seen in the microglia population (CD68). For the two pro-inflammatory markers, no change was observed for CCR7, while CD80 was significantly upregulated in the CCL2 KO mouse[13].

1.5 Conclusion

Chronically implanted intracortical electrodes have been shown to lose signal amplitude over time in both clinical[2], [4], [5] and pre-clinical models[22], [24], [53], [60]. Many factors, both device and biological, contribute to signal failure. The BBB has been identified as a potential biological target to reduce neurodegeneration at the electrode interface and improve recordings[9], [11], [12], [27]. Breakdown of the BBB following injury is a complicated process. Through this review, two therapeutic strategies have been

identified to modulate the BBB: 1) CCR2-antagonism and 2) Imatinib. The following thesis will evaluate BBB modulation and the impact on functional recordings.

THE IMPACT OF CCR2 ANTAGONISM ON A FUNCTIONAL INTRACORTICAL ELECTRODE MODEL

1.6 Introduction

Intracortical recording electrodes are a key part of brain computer interface, and this technology can allow patients to directly interface with robotics, computers, or their own limbs[2], [3], [17], as well as provide closed-loop systems for deep brain stimulation[19], [148]. These technological advancements require a chronic functional interface, but several studies have demonstrated consistent chronic electrode failure[12], [22]–[24], [52], [53]. Previously, the development of the astroglial scar was credited as the cause of electrode failure. Neurons need to within 100 μm of the recording sites, and the astroglial scar, which develops between the electrode and neural tissue, was thought to separate the neurons this distance[8], [25]. However, McConnell et al. demonstrated that neurodegeneration is initiated at a chronic timepoint (>8 weeks)[9]. Other work has replicated this result[11] and shown that the astroglial scar stabilizes after 8 weeks[9]–[11], [149], which suggests an alternate biological mechanism. Winslow et al identified the presence of IgG, a macromolecule found in the blood, at the electrode-tissue interface, which suggests a breached blood-brain barrier (BBB)[10], [27].

BBB disruption has been implicated as the cause of neurodegeneration in several neurodegenerative diseases[29], [150]. Saxena et al explored the variations in signal-to-noise ratios (SNRs) between different electrode types. The results showed that microwires had higher SNRs for a longer duration of time when compared to Michigan electrodes.

Histological analysis revealed that microwires had significantly less IgG accumulation than Michigan electrodes, suggesting a correlation between BBB breach and SNR[12].

The objective of this research was to modulate the BBB and observe the impact on histology and electrophysiology in an intracortical electrode model. The BBB is composed of endothelial cells, tight and adherens junction proteins, pericytes, basal lamina, and astrocyte endfeet[29]. Removal or disruption of any of these components leads to BBB breach, which is caused by injury or pathology[150]. The results of BBB disruption include leukocyte extravasation, macromolecule deposition, and inflammatory cytokine release, which can lead to neuroinflammation and eventually neurodegeneration[33], [81], [84]. With such a complex system, several modulation strategies exist.

CCL2 removal has been shown to reduce the immune response at 8 weeks in an intracortical electrode model[13]. The CCL2/CCR2 pathway has been heavily explored in terms of pro-inflammatory monocytes and macrophages and has expanded to the CNS[35]–[38]. The CCR2 receptor is common on pro-inflammatory monocytes that are recruited following injury, which then differentiate into pro-inflammatory macrophages. By inhibiting the monocyte recruitment (by blocking CCL2 or CCR2), the influx of anti-inflammatory monocytes to the injury site will create a more anti-inflammatory environment[35]–[38]. Leukocyte extravasation is both a cause and effect of BBB disruption. CCR2 is also present on endothelial cells and its activation disrupts tight junction proteins[39]–[41].

The objective of this study was to apply CCR2 inhibition to a functional electrode implant model. Daily injections of a CCR2-antagonist were administered to rats implanted

with functional Michigan electrodes. Electrodes were implanted in the barrel cortex and weekly electrophysiological recordings were conducted. At 2 and 12 weeks, rats were euthanized, and histology focused on neuroinflammation and BBB leakage was analyzed.

1.7 Methods

1.7.1 Surgical preparation and electrode implantation

All animal procedures were approved by the Institutional Animal Care and Use Committee (IACUC) at the Georgia Institute of Technology. Adult male Sprague Dawley rats (250 – 300 g) were implanted for 2 weeks (non-functional) or 12 weeks (functional). Four shank "Michigan" electrodes (NeuroNexus, MI) with a tetrode recording site design were purchased for implantation. The electrodes were 3 mm long, 83 µm width and 50 µm thick and were spaced 150 µm apart (center-to-center). All electrodes were sterilized by ethylene oxide and degassed for 12 hours. Each rat was anesthetized with 2% isoflurane, and the head was shaved and sterilized with chlorohexidine and isopropanol. After induction, each rat received an intramuscular injection of slow release buprenorphine. Each rat's head was stereotaxtically positioned and a subcutaneous injection of lidocaine was administered to top of the head prior to incision. Following a midline incision, the periosteum was scraped away, and etch gel (Henry Schein, NY) was applied to the skull. Holes for the anchoring screws were then drilled and 5 screws were inserted (1 on the opposite side of the craniotomy, 2 anterior to bregma on either side of the midline, and 2 posterior to lambda on either side of the midline as seen in **Figure 5A**). A 3 x 5 mm craniotomy was drilled at 1.5 mm posterior from bregma and 4 mm lateral to the midline (**Figure 5A**). The dura was retracted using a bent 25-gauge needle and bleeding was

controlled using gel foam (Pfizer, NY) soaked with sterile saline. For the functional electrodes, grounding wires were wrapped around the anchoring screws prior to insertion. Each array was implanted at a 15-degree angle and a depth of 1200 µm, targeting the IV cortical layer of the barrel cortex at a rate of 1 mm/min (**Figure 5B**). Sterile 1.5% SeaKem agarose (Lonza, NJ) was applied above the craniotomy and UV curing dental cement (Henry Schein, NY) was used to secure the electrodes to the skull and the anchor screws. The skin was wound clipped around the connector. After removal from anesthesia, each rat received a subcutaneous injection of enrofloxacin (antibiotic) and ketoprofen (anti-inflammatory), as well as an intraperitoneal injection of either the treatment or vehicle control. Animals received daily subcutaneous injections of enrofloxacin for 2 weeks.

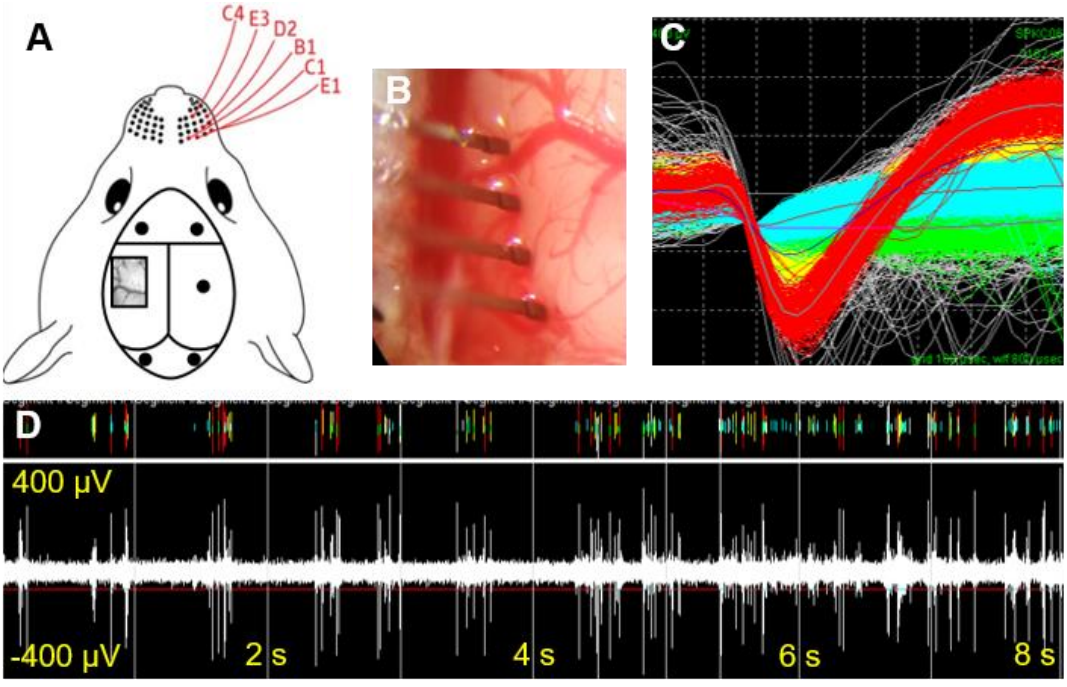

Figure 5 – (A) Location of craniotomy to target the barrel cortex, along with the location of screws. (B) Michigan electrodes implanted in the brain. (C) Sorted units and corresponding (D) filtered recording that has been thresholded.

1.7.2 RS 102895 preparation and administration

Research grade RS 102895 (Santa Cruz, TX) was administered intraperitoneally (IP) at a dose of 3 mg/kg/day. RS 102895 was dissolved in dimethyl sulfoxide (DMSO) at a 10x concentration and stored at -20°C. The day of injection, RS 102895 was diluted to 1x using sterile saline. The total injection volume was 1 mL, so that only 10% DMSO was injected into the animal. RS 102895 was injected every 20 – 28 hours starting immediately after electrode implantation and concluding the day of euthanasia. Control animals received daily 1 mL IP injections of the vehicle (10% DMSO in saline, sterile) for the same duration.

1.7.3 Electrophysiology and analysis

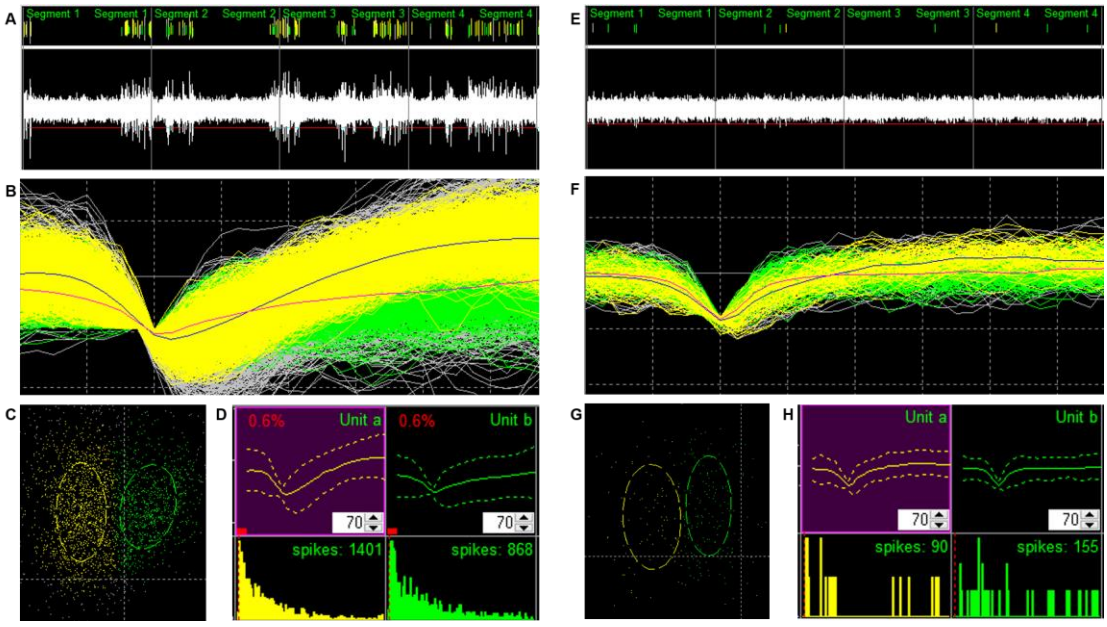

Figure 6 – Example of unit sorting for recording with (A-D) and without (E-H) spikes. (A,E) Filtered signal that has been thresholded (red line) at -4σ and thresholded waveforms are superimposed above. (B,F) Overlaid waveforms for sorted units. (C,G) PCA for sorted units. (D,H) Average waveforms and ISI histograms for sorted units.

Weekly recordings were collected with a 32-channel data-acquisition system (Plexon, TX). Signals were amplified at 1000x gain, band-pass filtered at 500-5000 Hz and sampled at 40 kHz. Animals were anesthetized with ketamine/xylazine/acepromazine cocktail as isoflurane suppresses cortical firing in the barrel cortex. For each recording session, two files were recorded. The first was an evoked file in which the rat's whiskers were rapidly deflected for ~1 minute, generating action potentials. Peak-to-peak voltages ($V_{p\text{-}p}$) were then calculated from the first file following sorting. The second file was a noise file in which no signals were evoked for 10 seconds. Following removal of spontaneous action potentials, the standard deviation of noise was calculated from the second file. The purpose of these recordings is to generate action potentials for proof-of-concept testing of the CCR2-antagonist model.

In Offline Sorter (Plexon, TX), the channels in the evoked files were thresholded at -4σ (standard orders of deviation) as seen in **Figure 6A,E**. Waveforms that crossed the threshold were selected (**Figure 6B,F**), and a PCA plot was generated with a single point for each waveform (**Figure 6C,G**). Units were sorted using K means automatic sorting, and these sorted units usually represented multi-units. The interspike interval (ISI) histograms were calculated for each unit (**Figure 6D,H**). Sorted units for every channel were manually evaluated. If the unit had fewer than 200 waveforms the unit was excluded from analysis. Additionally, if the ISI histogram or waveforms were abnormal, the unit was excluded as well. **Figure 6A-D** shows an example recording with two viable units from an electrode at week 1. **Figure 6E-H** shows the same electrode at week 6. No clear spiking activity is observed in **Figure 6E**. However, waveforms are still detected as crossing the

threshold. With the manual exclusion criteria, both units are excluded from analysis for having less than 200 waveforms and irregular ISI histograms (**Figure 6H**).

To calculate percentage of active electrodes, active electrodes are determined by having at least one viable unit. To calculate percentage of animals with active electrodes, an animal is viable as long as there is one active electrode on the recording array. To calculate SNR, the sorted files were exported from Plexon into Matlab. Custom code was used to calculate the SNR by dividing the peak-to-peak voltage ($V_{p\text{-}p}$) by 2 times the standard deviation of noise, which was recorded from the same electrode in the same animal at the same timepoint (**Equation 1**)[151]–[153]. Prior to calculating the standard deviation of noise, any spontaneous action potentials were removed from the noise file. Animals that never had evoked or spontaneous signal were excluded from the study.

Equation 1 $$\boldsymbol{SNR = \frac{V_{p-p}}{2 * Std_{noise}}}$$

A nested ANOVA model was created to determine significance. As described in **Equation 2**, μ is the grand mean, τ is the effect of time with *I* as the time index, γ is the effect of treatment with j as the treatment index, α is the inter-animal variability with *k* as the index of animals nested with *j* (treatment), β is inter-electrode variability with *l* as the electrode index nested within *k* (animals), and ε is error for time, treatment, animals and electrodes.

Equation 2 $$\boldsymbol{y_{i,j,k} = \mu + \tau_i + \gamma_j + \alpha_{k(j)} + \beta_{l(k)} + \varepsilon_{i,j,k,l}}$$

$$\boldsymbol{i = 1, \dots, 12; j = 1, \dots, 2;\ k = 1, \dots, 4; l = 1, \dots, 4;}$$

1.7.4 Tissue preparation, immunohistochemistry, and microscopy

Three hours prior to euthanasia, 1 mL of 3% Evans Blue (w/v) in sterile saline was intravenously injected into each animal. At 2 and 12 weeks, animals were anesthetized with ketamine (50 mg/kg)/xylazine (10 mg/kg) /acepromazine (1.67 mg/kg) and transcardially perfused with PBS, 4% paraformaldehyde, and 20% sucrose (200 mL, sequentially). The skulls with electrodes still implanted were removed and post-fixed in 4% paraformaldehyde overnight at 4°C and then transferred to 30% sucrose, overnight at 4°C. Electrodes were then carefully extracted from the brains, and the brains was stored at 4°C in 30% sucrose until they sunk to the bottom of the container. Brains were cryosectioned at 14 µm thickness in serial on charged glass slides (VWR, PA).

Please refer to **Table 3** for primary and secondary antibodies used. Sectioned slides were washed with PBS and blocked with blocking solution (4% goat serum and 0.5% Triton X-100 in PBS) for 1 hour. The primary antibodies were incubated at 4°C overnight. The slides were then washed with PBS and washing solution (0.5% Triton X-100 in PBS), and the secondary antibodies were incubated at room temperature for 1 hour. Next, the slides were incubated with 4',6-diamidino-2-phenylindole (DAPI) nuclear stain (Life Technologies,

Table 3 – Antibody chart for immunohistochemistry

Primary antibodies	Company	Catalog #
Rabbit anti-GFAP	DAKO	M0761
Mouse IgG1 anti-NeuN	Millipore	MAB377
Mouse IgM anti-EBA	Biolegend	836802
Rabbit anti-Collagen IV	Abcam	ab19808

Secondary antibodies	Company	Catalog #
Goat anti-mouse IgG1 488	Thermo Fischer Scientific	A-21121
Goat anti-rabbit 647	Thermo Fischer Scientific	A-21244
Goat anti-mouse IgM 488	Thermo Fischer Scientific	A-21042
Goat anti-rat IgG 647	Thermo Fischer Scientific	A21247

NY) for 15 minutes, followed by several washes of PBS and washing solution. The slides were coverslipped with Fluormount-G (Southern Biotech, AL) and left at room temperature overnight in the dark. The coverslip was nailpolished to the slides and stored at -20°C. For Evans Blue, slides were immediately coverslipped and nailpolished.

1.7.5 Quantification and analysis of histology

Slides were imaged at 10X using the inverted DMI8 microscope (Leica Microsystems, IL). Slides from the distal end of the electrode (at the location of the recording sites) were used for analysis in FIJI[154]. For IgG and GFAP, a 400 μm x 100 μm rectangle was centered around each electrode and the intensity profile was calculated. The area under the curve was calculated using custom Matlab code and distances were binned from 0 to 50 μm, 50 μm to 100 μm, 100 μm to 150 μm, and 150 μm to 200 μm. For NeuN, images were thresholded, a 400 μm x 100 μm rectangle was centered around each electrode, and cells were counted using particle analysis. For Col IV and EBA, images were thresholded, a 400 μm x 100 μm rectangle was centered around each electrode, and the percent area was calculated. In addition, at 12 weeks, all thresholded images (NeuN, Col IV, and EBA) were binned from 0 to 50 μm, 50 μm to 100 μm, 100 μm to 150 μm, and 150 μm to 200 μm on the side of the electrode with the recording sites. The intensity analysis for IgG and GFAP were also recalculated using only one side of the electrode.

To determine significance, a nested ANOVA model was calculated in Matlab. As described in **Equation 3**, μ is the grand mean, τ is the effect of time with *i* as the time index, γ is the effect of treatment with j as the treatment index, α is the inter-animal

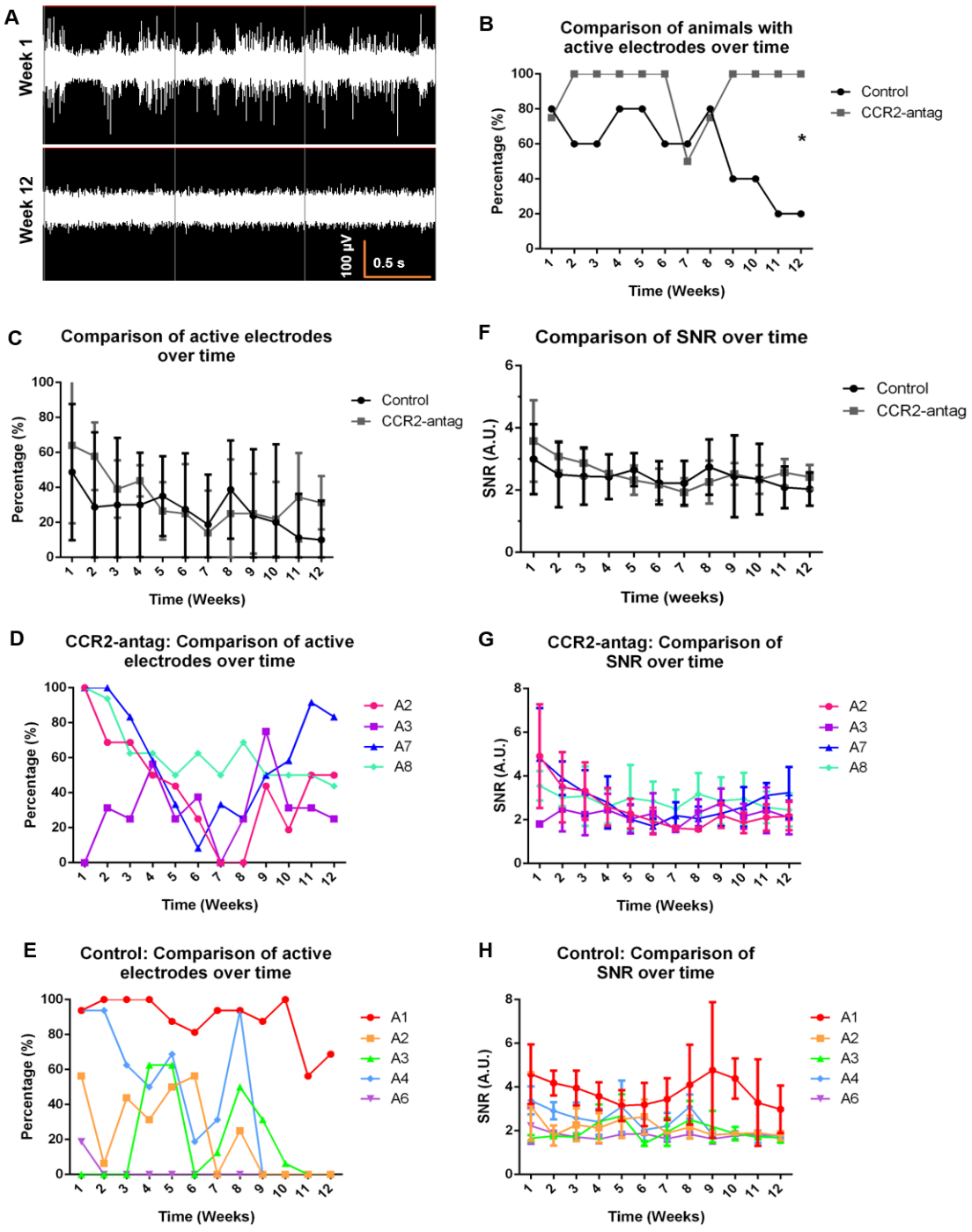

Figure 7 – (A) Example of signal loss between 1 and 12 weeks. Comparison of control and CCR2-antag treated animals over time for (B) percentage of animals with active electrodes ($p < 0.05$), (C) percentage of active electrodes, and (F) SNR. Control has n = 5 and CCR2-antag has n = 4. Individual animal plots for (D,E) percentage of active electrodes and (G,H) SNR for CCR2-antag and control.

variability with *k* as the index of animals nested with *j* (treatment), β is inter-electrode variability with *l* as the electrode index nested within *k* (animals), and ε is error for time, treatment, animals and electrodes.

Equation 3

$$y_{i,j,k} = \mu + \tau_i + \gamma_j + \alpha_{j(k)} + \beta_{k(l)} + \varepsilon_{i,j,k}$$

$$i = 1, \dots, 2; j = 1, \dots, 2;\ k = 1, \dots, 4; l = 1, \dots, 4;$$

1.8 Results

1.8.1 Electrophysiology

Following electrode implantation and daily treatment or vehicle administration, weekly electrophysiological recordings were conducted from the barrel cortex. Briefly, after ketamine anesthetization, a recording of ~10 seconds was taken, which was classified as the noise file. Next, an evoked recording was made by deflecting the rat's whiskers to evoke action potentials in the barrel cortex for ~60 seconds. Recorded signals were thresholded at -4σ and sorted offline using automatic K means sorting. Units were manually validated by excluding units with less than 200 waveforms. Additionally, units with abnormal waveforms or abnormal ISI histograms were excluded as well. Percentage of active electrodes and percentage of animals with active electrodes were calculated from these validated units. SNRs were calculated in custom Matlab software.

Figure 7A demonstrates an example of action potential loss over time, and this is the definition for signal loss. Percentage of animals with active electrodes was calculated in **Figure 7B**. At 12 weeks, each CCR2-antagonist treated rat (n = 4) had active electrodes, while only 1 of the control rats had signal (n = 5). Within the control group, rats lost viable

signal at 2 weeks (1), 9 weeks (2) and 11 weeks (1). There was a significant difference between groups ($p < 0.05$, two-way ANOVA).

Percentage of active electrodes was evaluated next (**Figure 7C**). No significant difference was observed between the two groups. However, for both groups, the percentage of active electrodes significantly decreased over time ($p < 0.05$, two-way ANOVA). **Figure 7E,G** show the individual animal plots of percentage of active electrodes for the CCR2-antagonist and the control group, subsequently.

SNR were then calculated across each electrode for each rat at each time point from the V_{p-p} and standard deviation of noise. No significant difference was observed between CCR2-antag and control (**Figure 7D**). Again, there was a significant decrease in SNR over time between the two groups (4-way nested ANOVA, $p < 0.05$). **Figure 7F,H** show the individual animal plots of SNR for the CCR2-antagonist and the control group, subsequently. There was significant difference in V_{p-p} or noise. V_{p-p} did significantly decrease over time. Noise remained constant until 11 weeks, when there was a significant increase (data not shown).

1.8.2 Histology

Rats were sacrificed at 2 and 12 weeks via transcardially perfusion with paraformaldehyde (n = 4 – 7.) Brains were removed, cryosectioned, and stained with antibodies of interest. The focus of the histology was to analyse the neural population, the vasculature, and BBB leakage. Slides were imaged at 10x and analysed in FIJI via intensity analysis, cell counting, and thresholded percentage area. Four-way nested ANOVAs were used to determine significance.

1.8.2.1 Neural inflammation

NeuN (neuronal nuclei) is a common antibody to detect the neural population. After thresholding the images, a 400 µm x 100 µm rectangle was placed around each electrode and cells were counted. At 2 weeks, NeuN expression was significantly greater in CCR2-antagonist treated animals compared to control (**Figure 8A, C**, $p < 0.05$). By 12 weeks, the effect had disappeared; there was no difference between treatment and control at 12 weeks, and the 12 week control was significantly higher than the 2 week control (**Figure 8A, C**, $p < 0.05$). Further analysis was conducted on the 12 week samples by restring the region of

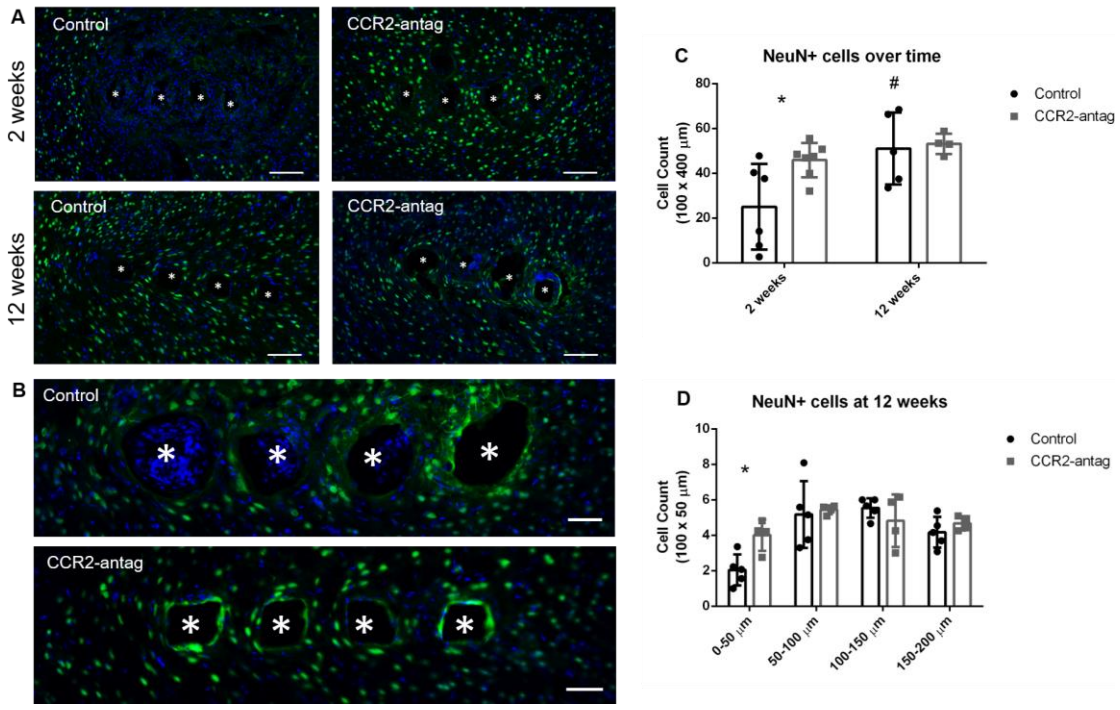

Figure 8 – (A) Representative images of NeuN+ neurons for control and CCR2-antagonist treated tissue at 2 and 12 weeks (Scale bar = 100 µm). (B) Magnified view at 12 weeks for control and treated (Scale bar = 50 µm). (C) Cell count for 2 and 12 week data for CCR2-antagonist and control (* $p < 0.05$ between treatments, # $p < 0.05$ between time). (D) Binned cell count over 200 µm (* $p < 0.05$ between treatments).

interest (ROI) to the side of the electrode with the recording sites, and the 100 x 200 µm ROI was binned into 100 x 50 µm sections. The CCR2-antagonist group had significantly higher NeuN+ cells in the 0 – 50 µm bin compared to control (**Figure 8B, D**, $p < 0.05$). However, this effect disappeared in the subsequent bins.

GFAP is upregulated in reactive astrocytes and is used to evaluate neuroinflammation. A 400 µm x 100 µm rectangle was placed around each electrode and the intensity profile was calculated. There was no significant difference at 2 or 12 weeks between the control and CCR2-antagonist treated animals. GFAP expression did significantly increase between 2 and 12 weeks, which resulted in a localized scar (**Figure 9A, B**, $p < 0.05$). No difference was observed between treatment and control in the binned integral of intensity (**Figure 9C**).

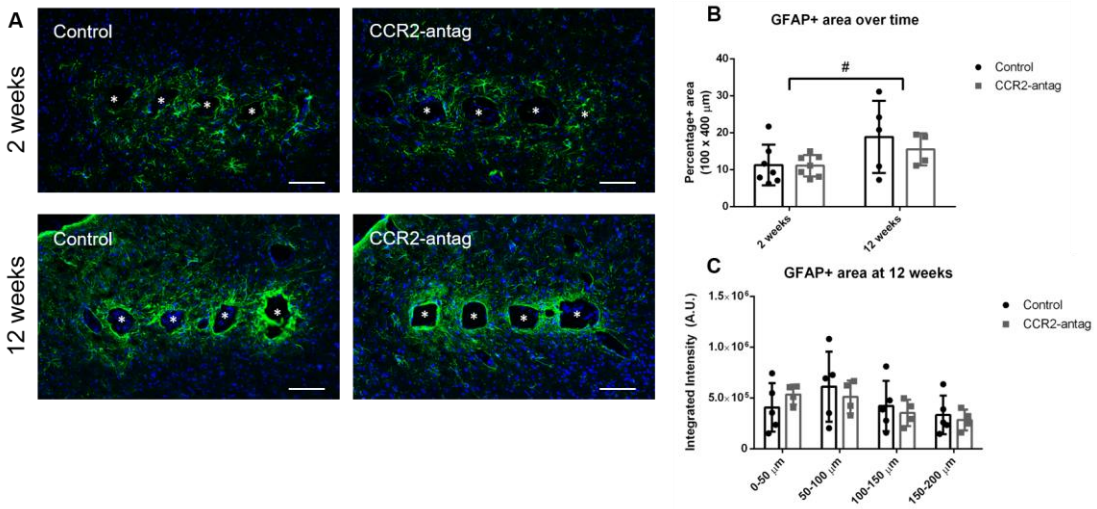

Figure 9 – A) Representative images of GFAP+ astrocytes for control and CCR2-antagonist treated tissue at 2 and 12 weeks (Scale bar = 100 µm). (B) Percentage+ area for 2 and 12 week data for CCR2-antagonist and control (# $p < 0.05$ between time). (C) Binned analysis of GFAP for 12 week data.

1.8.2.2 Vasculature integrity

To build upon the antibody markers of the previous section, the health of the surrounding vasculature was evaluated. Collagen IV (ColIV) stained for vasculature and endothelial barrier antigen (EBA) showed BBB+ vasculature. For both ColIV and EBA, images were thresholded and the percent positive area was calculated for a 400 µm x 100 µm rectangle centered on each electrode. At 2 weeks, there was a significant increase in EBA expression in the CCR2-antagonist treated animals compared to control (**Figure 10A, C**, $p < 0.05$). At 12 weeks, there is no significant difference between treatment and control,

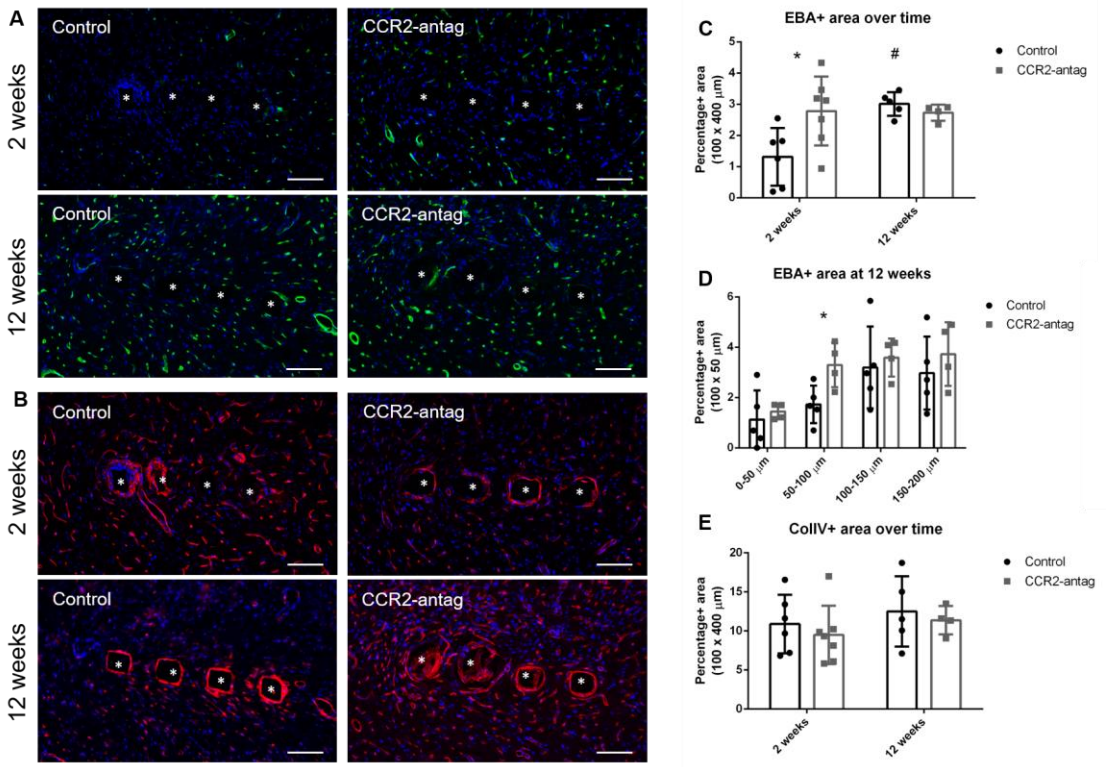

Figure 10 – (A) Representative images of EBA+ vasculature for control and treated animals at 2 and 12 weeks. (B) Representative images of ColIV+ vasculature for control and treated animals at 2 and 12 weeks. (C) Comparison of percentage area of EBA for 2 and 12 weeks (* $p < 0.05$ between treatment, # $p < 0.05$ between time). (D) Binned analysis of EBA for 12 week data. (E) Comparison of percentage area of ColIV for 2 and 12 weeks.

and there was a significant increase in between the control from 2 to 12 weeks (**Figure 10A, C**, $p < 0.05$). In **Figure 10D**, for 12 weeks, the ROI was binned in 100 x 50 µm sections. From 50 – 100 µm, a significant increase was observed in EBA+ area in CCR2-antagonist animals compared to control. However, EBA expression stabilized in the subsequent between the two groups. No difference was seen at 2 or 12 weeks in ColIV expression between treatment and control or over time (**Figure 10B, E**).

1.8.2.3 BBB breach

To evaluate BBB breach, IgG was analyzed. IgG is a common protein found in the blood. This antibody is used as a BBB breach marker as it does not cross an intact BBB, so the presence of this protein denotates leakage. To analyze IgG, a 400 µm x 100 µm rectangle was centered around each electrode and the vertical intensity profile was calculated. The area under the curve was then calculated for each intensity profile for comparison and binned from 0 to 50 µm, 50 to 100 µm, 100 to 150 µm, and 150 to 200 µm. At 2 weeks, there was no significant difference between treatment but at 12 weeks, the CCR2-antagonist had significantly increased (**Figure 11A, B**, $p < 0.05$). **Figure 11D, F** show the binned integrated intensity values for 2 and 12 weeks respectively. For 2 weeks, CCR2-antagonist was significantly lower for each binned distance, while there was no significance at 12 weeks.

To assess live BBB breach, 1 mL of 3% Evans Blue (w/v) in sterile saline was injected 3 hours before euthanasia. Evans Blue binds to albumin, which is a protein found in the blood and is unable to cross the BBB (same as IgG). Evans Blue was present at the

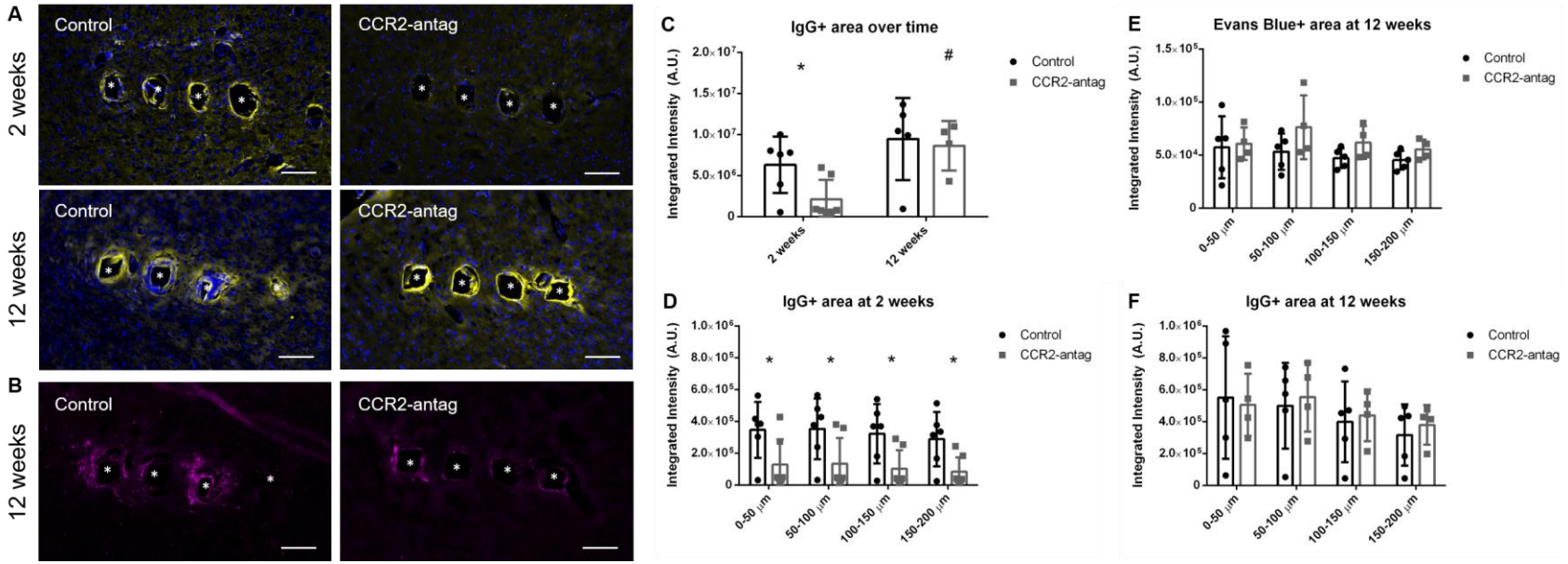

Figure 11 – (A) Representative images of IgG+ expression for control and treated animals at 2 and 12 weeks. (B) Representative images of Evans Blue+ area for control and treated animals at 12 weeks. (C) Comparison of integrated intensity of IgG for 2 and 12 weeks (* $p < 0.05$ between treatment, # $p < 0.05$ between time). (D) Binned analysis of IgG for 12 week data. (E) Binned analysis of Evans Blue for 12 week data. (F) Binned analysis of IgG for 2 week data (* $p < 0.05$).

electrode interface at 12 weeks as seen in **Figure 11B**, and significantly correlated with IgG expression (see supplemental data). However, no differences were observed between the treatment and control (**Figure 11E**).

1.9 Discussion

Elucidating the biological failure mechanisms for intracortical electrodes is crucial for extending the lifetime of the implanted devices. In this work, the CCL2/CCR2 pathway was evaluated in terms of functional electrodes. While no difference was observed with SNR, all CCR2-antagonist treated rats still had active electrodes at 12 weeks, which was a significant improvement compared to controls. At 2 weeks, CCR2 antagonism increased the neural population, reduced BBB leakage, and improved BBB+ vasculature (**See Table 4**). At 12 weeks in CCR2-antagonist treated animals, a significant increase occurred in NeuN+ cells from 0 – 50 µm. There was also a significant increase in EBA+ vasculature from 50 – 100 µm. However, IgG expression in CCR2-antagonist group had significantly increased compared to the 2 week counterparts, and was also positive for Evans Blue.

Table 4 – Overview of changes in antibody expression (++ significant increase, -- significant decrease, N.C. no change, + significant increase at a single binned distance).

Marker	Purpose	2 weeks CCR2-antag /Control	12 weeks CCR2-antag /Control	CCR2-antag 12 weeks /2 weeks	Control 12 weeks /2 weeks
IgG	BBB	−−	N.C.	++	N.C.
EBA	BBB	++	+	N.C.	++
NeuN	Neurons	++	+	N.C.	++
SNR	Signal strength	N.C.	N.C.	−−	−−
Animal %	Signal longevity	N.C.	+	N.C.	−−

CCL2 is most commonly used to recruit CCR2+, pro-inflammatory monocytes. This pathway has been heavily explored in wound healing[155], [156] and foreign body research[157]–[159], and has been extended to neurodegenerative diseases[35], [38]. Use of CCL2 KO models have significantly improved outcomes in rodent neurodegenerative disease models such as multiple sclerosis[160], [161], Alzheimer's disease[162], traumatic brain injury[140], [141], [163], stroke[164], and epilepsy[165], [166]. CCL2 was secreted by microglia cultured from extracted intracortical electrodes[8]. Recent work from the Kyriakides's lab demonstrated the benefits of CCL2 inhibition in an intracortical electrode implant model, and the resulting switch an anti-inflammatory environment[13].

Along with the CCL2 work from the Kyriakides lab[13], others have attempted to modulate the immune response in a single Michigan intracortical electrode model. The Capadona lab has studied the impact of reactive oxygen species and subsequent modulation using curcumin[101] and resveratrol[102], [103]. For both treatments, there were no histological differences chronically (16 weeks) when compared to controls. The electrodes were not functional, so no electrophysiological measurements could be made. Kozai et al implanted functional Michigan electrodes into caspase-1 KO mouse model for 180 days[60]. Caspase-1 has been linked to inflammation and neurodegeneration in neurodegenerative diseases, including stroke. Kozai et al. demonstrated an increase in duration of single units for the caspase-1 KO model.

Chronic local neurodegeneration has been observed at the electrode interface[9], [11], and it is reported that neurons need to be within 100 μm of the electrode site in order to successfully record action potentials[8], [25], [167]. A significant difference was seen in NeuN+ cells within 0 to 50 μm of the electrode interface. While this effect covers a

small area, the health of the neurons remains unknown. Fluorojade C, a common marker for neurodegeneration, would better elucidate the status of the neurons at the electrode interface.

The blood-brain barrier has been identified as an important target in intracortical electrodes[11], [12], [52], [69], [168]. Activation of CCR2 receptors on endothelial cells has been shown to reduce tight junction protein expression[39]–[41], [142], [169], and to also activate angiogenesis[170]–[172], which leads to leaky vasculature[173]–[175]. At 2 weeks, electrode implanted animals treated with the CCR2-antagonist had a significant reduction in IgG expression and a significant increase in EBA expression compared to controls. This data would suggest that CCR2-antagonism decreased BBB leakage and improved tight-junction expression acutely. Also at 2 weeks, NeuN+ cells were significantly increased in CCR2-antagonist animals compared to control.

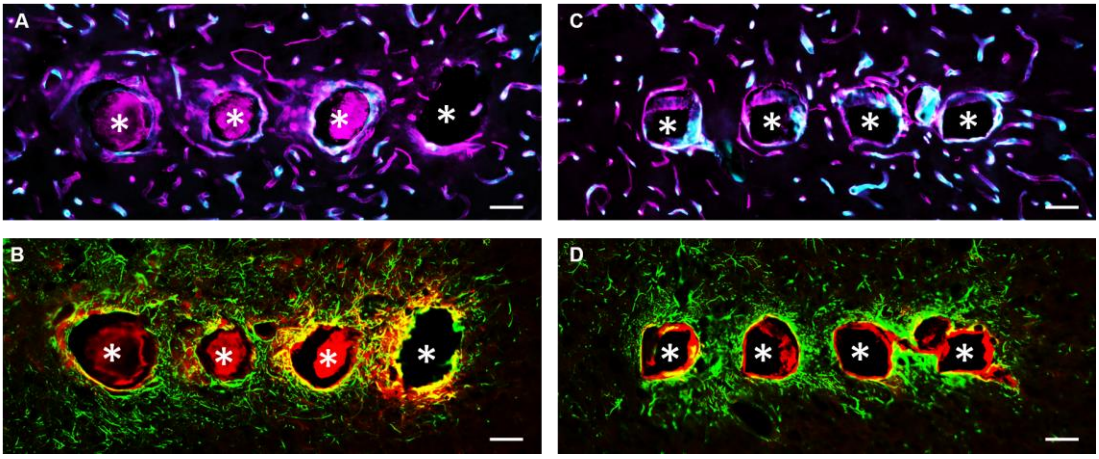

Figure 12 – Control at 12 weeks with (A) ColIV (magenta) and EBA (cyan) merged and with (B) GFAP (green) and IgG (red) merged. CCR2-antagonist at 12 weeks with (A) ColIV (magenta) and EBA (cyan) merged and with (B) GFAP (green) and IgG (red) merged.

Chronically, the differences were subtler. A significant increase was observed in the CCR2-antagonist group for EBA+ vasculature from 50 – 100 µm compared to control (**Figure 12A, C**). This could suggest that the CCR2-antagonist has repaired vasculature closer to the electrode-tissue interface. However, IgG expression in CCR2-antagonist rats had significantly increased at 12 weeks compared to CCR2-antagonist rats at 2 weeks (**Figure 12B, D**). This data was confirmed by Evans Blue, signifying an active breach. Therefore, vasculature has not been completely sealed in the CCR2-antagonist group. DMSO, which was used to dissolve the CCR2-antagonist, RS 102895, is known to facilitate drug permeability through the BBB[176], [177]. However, these effects have been shown to be reversible[178]. Also, IgG leakage was present in control Michigan electrodes at 16 weeks post-implantation[12].

Both biotic and abiotic causes can lead to inflammation and device failure. Micromotion is a mechanism that could have led to the increase in IgG expression at 12 weeks in the CCR2-antagonist treated group (and maintained IgG expression in the control group). A study revealed that micromotion at the electrode interface the day of implantation is caused by respiration (6–11 µm) and heart beat (2–4 µm)[61]. While this effect is reduced by 8 weeks, micromotion is still present[62]. Most notably, this micromotion is observed in an anesthetized, stereotaxed animal and does not include macromotion induced by active movement or by plugging in the connectors for electrophysiological recording. Modeling work has also shown the impact of strain on the surrounding tissue and the electrode itself[57], [63], [64]. Additionally, research has demonstrated a reduced immune response for electrodes that are not anchored to the skull and are truly free floating (not tethered to an off-site connector)[179]–[181].

The use of a CCR2-antagonist did reduce animal variability and led to active electrodes for all treated rats at 12 weeks (compared to only 1 out of 5 for the control rats). The increase of NeuN+ cells from 0 – 50 μm and the increase of EBA+ vasculature from 50 – 100 μm in CCR2-antagonist treated animals may account for this change. Since the histology changes are over a small area, this may explain why no differences were seen in SNR, $V_{p\text{-}p}$, and percentage of active electrodes as these measures may not be sensitive enough to delineate these changes.

1.10 Conclusion

CCR2-antagonism in an electrode implant model has been shown to significantly impact the immune response at an acute time point. Chronically, CCR2-antagonism extended the lifetime of implanted electrodes and had a subtle, but significant effect on neuroinflammation and the BBB. Interestingly, BBB leakage persisted at 12 weeks in the CCR2-antagonist group. Further exploration of abiotic mechanisms such as micromotion is necessary to better understand the chronic cause of BBB leakage.

CORRELATION OF MRNA EXPRESSION TO ASSESS RECORDING VARIABILITY IN A CHRONIC, FUNCTIONAL INTRACORTICAL ELECTRODE MODEL

1.11 Introduction

Clinical trials for brain machine interfaces (BMIs) using intracortical electrodes are showing promising results for restoring functionality to paralysis patients[2], [5], [42], [43]. Intracortical electrodes allow direct interfacing within the brain for single and multi-unit recordings. A major problem in the field is the instability of viable recordings for long durations. Chronic (≥12 weeks) electrode failure, defined as a reduction in signal-to-noise ratio (SNR), continues to be documented across different electrode types in different animal species[12], [22]–[24], [52], [53]. In addition, animal-to-animal recording variability further confounds this problem[52], [54], [182]. Previous work has suggested that the severity and duration of chronic blood-brain barrier (BBB) breach may influence chronic recordings by contributing to local neurodegeneration[11], [12], [52], [183].

Chronic BBB degradation can result from a myriad of biological mechanisms. Initial damage by injury or disease recruits matrix metalloproteinases and reactive oxygen species to the site. This results in The BBB is composed of several cellular layers. Endothelial cells are connected by tight junction proteins, including occludins, claudins, and zona-occludins (ZOs) and adherens junctions, VE-cadherin[29], [81], [184]. Surrounding endothelial cells are pericytes, which aid in blood flow and vessel maintenance[29], [81], [82]. Pericytes are enclosed in basement membrane, which includes

laminin and collagen IV[29], [81]. Astrocyte endfeet, which are rich in aquaporin-4 (AQP-4), directly connect the vasculature to the neurons within the brain[29], [83]. Each of these individual proteins and cells regulate the transport of macromolecules, cytokines, and leukocytes into the brain, and dysfunction at any level can lead to dysregulation of the BBB[29], [184].

With so many points of failure, it might be helpful to investigate the mechanisms by which electrode implantation induces BBB leakage. Previous work from the Capadona lab has focused on an anti-oxidant mechanism (curcumin[101] and resveratrol[102], [103]) for non-functional electrodes, but while both therapies impacted histologically markers at 2 weeks, there was no effect at 16 weeks[101]–[103]. Kozai et al implanted functional electrodes in a general inflammation caspase-1 knockout model with improved single unit recordings[60]. Sawyer et al explored a CCR2 knockout for non-functional electrode implants and saw reduced neuroinflammation histology as well as changes in M1/M2 like expression, suggesting inhibition of pro-inflammatory monocyte recruitment[13]. Other work has focused on correlating histological data with functional recordings[12], [22], [52], [53]. The results have shown a negative correlation between IgG expression (a systemic macromolecule) and SNR at the electrode interface[12], [22], [52]. However, while IgG expression demonstrates BBB leakage, it provides no information on how the BBB has been breached.

For this study, key mechanisms of BBB dysregulation at the mRNA level were explored following electrode implantation. Animal-to-animal recording variability was leveraged to perform correlations with mRNA expression to better elucidate mechanisms associated with electrode failure. To achieve this objective, functional microwire

electrodes were implanted into the rat barrel cortex acutely (for 1 week) and chronically (for 14 weeks). At each endpoint, mRNA was extracted for Fluidigm multi-plex qRT-PCR analysis. The calculated fold changes for each animal were compared to its functional recordings via a Pearson coefficient correlation. Neuroinflammation and markers for BBB integrity were investigated (see **Table 5**).

1.12 Methods

1.12.1 Surgical preparation and electrode implantation

All animal procedures were approved by the Institutional Animal Care and Use Committee (IACUC) at the Georgia Institute of Technology. Adult male Sprague Dawley rats (250 – 300 g) were implanted for 1 week (n = 5) or 14 weeks (n = 6). The implanted electrodes were polyimide coated tungsten microwires (Tucker-Davis Technologies, FL). The array had 16 electrodes arranged in a 2 x 8 pattern spaced 300 µm apart in the x-direction and 500 µm apart in the y-direction (See **Figure 13A**). The electrodes were 50 µm in diameter and 5 mm in length. All microwires were sterilized by ethylene oxide and degassed for 12 hours. Each rat was anesthetized with 2% isoflurane, and their head was shaved and sterilized with chlorohexidine and isopropanol. Each rat's head was stereotaxtically positioned and a subcutaneous injection of lidocaine (Henry Schein, NY) was administered locally prior to incision. Following a midline incision, the periosteum was scraped away and etch gel (Henry Schein, NY) was applied to the skull. Holes for the anchoring screws were then drilled (2 anterior to bregma, 2 posterior to lambda, and 1 opposite the craniotomy), and 5 screws were inserted (See **Figure 13B**). A 3 x 5 mm craniotomy was drilled at 1.5 mm posterior from bregma and 4 mm lateral from the midline

(See **Figure 13B**). The dura was retracted using a bent 25-gauge needle and bleeding was controlled using gel foam (Pfizer, NY) soaked with sterile saline. Grounding wires were wrapped around the anchoring screws prior to insertion. Each array was implanted at a 15-degree angle to a depth of 1200 µm, targeting the IV cortical layer of the barrel cortex. Sterile 1.5% SeaKem agarose (Lonza, NJ) was applied above the craniotomy and UV curing dental cement (Henry Schein, NY) was used to secure the electrodes to the anchor screws and the skull. The incision was wound clipped and animals were injected intramuscularly with buprenorphine. Animals received daily subcutaneous injections of antibiotic, Baytril (Bayer, PA), for 2 weeks.

1.12.2 Electrophysiology and analysis

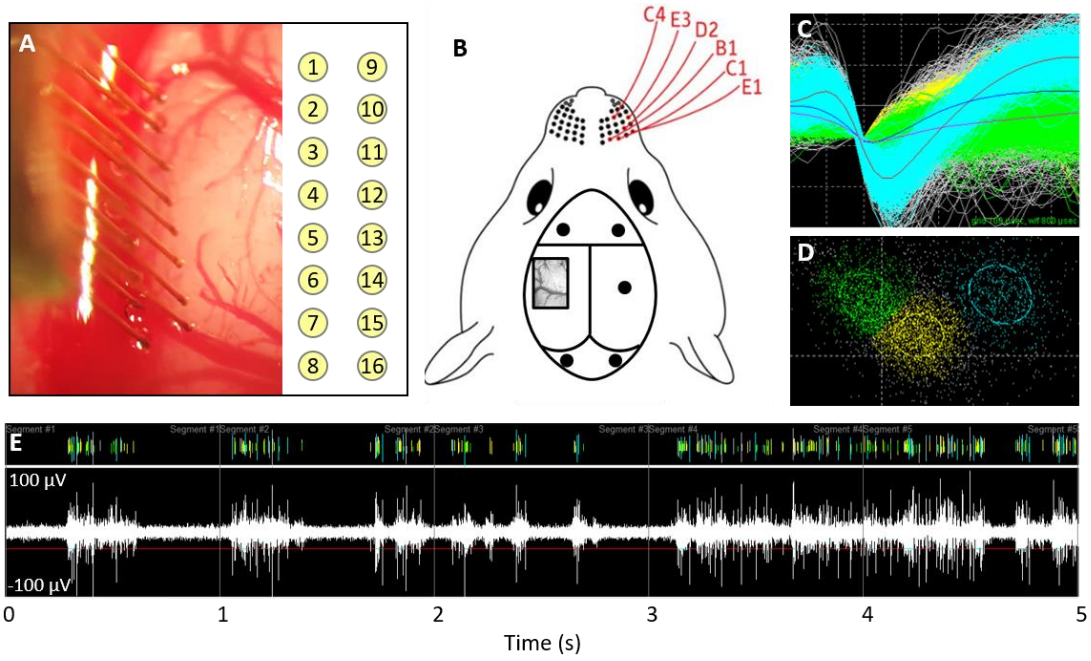

Figure 13 – (A) Implantation of microwire array and electrode site map. (B) Representative image of barrel cortex craniotomy and anchoring/grounding screws. (C) Average waveforms and (D) PCA plot for sorted units. (E) Signal and raster plot of an electrode from a recording session in one animal.

Weekly recordings were collected with a 32-channel data-acquisition system (Plexon, TX). Signals were amplified at 1000 x gain, band-pass filtered at 500-5000 Hz and sampled at 40 kHz. Animals were anesthetized with ketamine/xylazine/acepromazine cocktail as isoflurane suppresses cortical firing in the barrel cortex. For each recording session, two files where recorded: 1) an evoked file in which the rat's whiskers were deflected for ~1 minute, generating action potentials, and 2) a noise file in which no signals were evoked for 10 seconds. In Offline Sorter (Plexon, TX), the channels in the evoked files were thresholded at -4σ (standard orders of deviation) and units were sorted using K means automatic sorting (See **Figure 13C-E**). Units that had fewer than 100 action potentials were excluded. Spontaneous action potentials were removed from the noise file. Sorted files were then exported into Matlab and custom code was used to calculate the SNR by dividing the peak-to-peak voltage ($V_{p\text{-}p}$) by 2 times the standard deviation of noise (**Equation 4**)[151], [152].

Equation 4

$$\boldsymbol{SNR = \frac{V_{p-p}}{2 * Std_{noise}} = \frac{(V_{max} - V_{min})}{2 * \sqrt{\frac{\sum (noise_j - \mu_{noise})^2}{(n-1)}}}}$$

A nested three-way ANOVA model was made to determine significant changes in time. As described in **Equation 5**, μ is the grand mean, τ is the effect of time with *i* as the time index, α is the inter-animal variability with *j* as the index of animals, β is inter-electrode variability with *k* as the electrode index nested within *j* (animals), and ε is error for time, animals and electrodes. If the p-value was less than 0.05, a multiple comparison was run in Matlab.

Equation 5

$$y_{i,j,k} = \mu + \tau_i + \alpha_j + \beta_{k(j)} + \varepsilon_{i,j,k}$$

$$i = 1, \ldots, 14; j = 1, \ldots, 6;\ k = 1, \ldots, 16;$$

1.12.3 qRT-PCR and analysis

At the designated time point, animals were transcardially perfused with sterile PBS (200 mL). The electrodes and headcap were removed and the brain was extracted. A 4-mm biopsy punch was taken at a depth of 2 mm around the electrode implant site. The biopsy punch was immediately frozen in liquid nitrogen and stored at -80 °C. Age matched naïve animals were sacrificed in the same manner as well and the 4-mm biopsy punch was removed from a depth of 2 mm at the same location in the brain. Total RNA was extracted using the RNeasy Plus Universal Kit (Qiagen, CA). RNA integrity was assessed with the Agilent Bioanalyzer using Agilent RNA 6000 Nano Kit (Agilent Technologies, CA) and purity was assessed with the Nanodrop 8000 Spectrophotometer (Thermo Fisher Scientific, MA). For all samples, RNA integrity numbers were above 7, 260/280 were above 1.8, and 260/230 were above 1.0. cDNA was synthesized using the Fluidigm Reverse Transcription kit (#100-6298) (Fluidigm, CA). A 96 qRT-PCR assay using the Fluidigm Biomark HD (Fluidigm, CA) was run in triplicate for each sample using the Duke Center for Genomic and Computational Biology. The Delta Gene Assays (Fluidigm, CA) were designed using the D3 Assay Design (Fluidigm, CA), and the sequences are shown in the supplementary data. CT values were averaged together across triplicates. ΔCT values were calculated by subtracting the geometric mean of four housekeeping genes (GAPDH, HRPT, SDHA, RPL13A) from each CT value. ΔΔCT values were calculated by subtracting the arithmetic average of the naïve samples from the ΔCT values. All statistics were performed in the ΔΔCT space. Fold change was then calculated by taking the base 2 exponent of – ΔΔCT.

A Bonferroni sequential correction[185] was applied to a student's t test to determine significance between 1 and 14 week microwire animals.

1.12.4 Correlation analysis

To correlate the relation between average SNR and mRNA fold change, a Pearson correlation coefficient (r) was calculated in Matlab as well a p-value for each correlation.

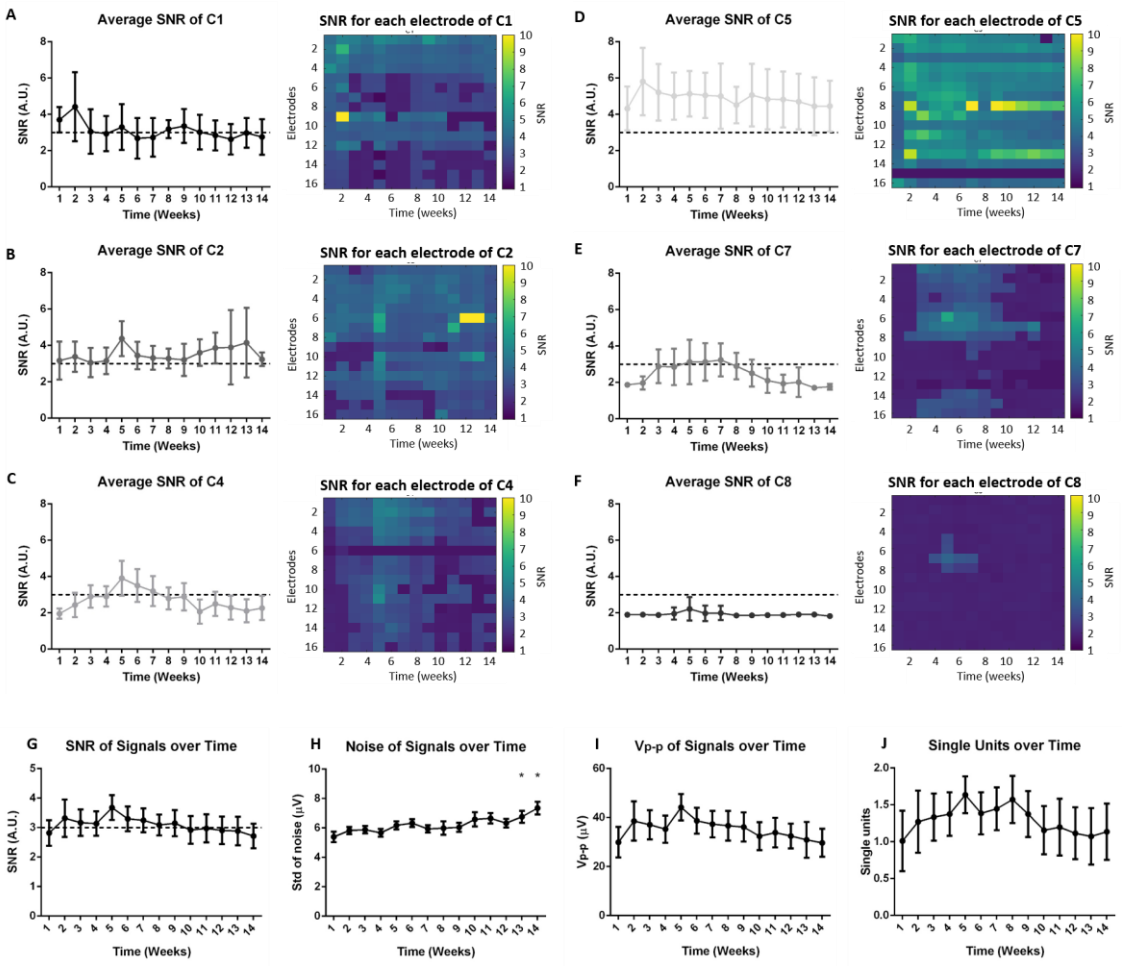

Figure 14 – Average SNRs (x axis is time in weeks and y axis is SNR) and SNR heatmaps (x axis is time in weeks, the y axis is electrode, and the z axis heatmap is SNR) for (A) C1, (B) C2, (C) C4, (D) C5, (E) C7, and (F) C8. The averaged (G) SNR, (H) standard deviation of noise, (I) peak-to-peak voltage, and (J) single units across animals (* $p < 0.05$ compared to week 1).

This was done for both the 1 week and the 14 week cohort. Briefly, electrode SNRs for each animal were averaged at each timepoint. The 14 week SNRs were compared with the mRNA extracted at 14 weeks for each animal.

1.13 Results

1.13.1 Animal-to-animal variability in electrophysiology

Weekly recordings were conducted in the barrel cortex. Rats were anesthetized, and whiskers were deflected to generate evoked potentials. SNRs were calculated for each electrode within each time point within each animal. Eight rats were implanted for the chronic time point, but two were removed from the study due to head cap failure (C3 and C6). **Figure 14A-F** shows the SNR plots for each individual animal. There was no significant change over time in SNR, $V_{p\text{-}p}$, or single units (**Figure 14G,I,J**). However, noise did significantly increase at 11 and 12 weeks (**Figure 14H**). In this study, variability in recording performance amongst animals was significant and was used to investigate possible correlation with underlying molecular differences studied by mRNA expression analysis. Briefly, Pearson correlation coefficients and p-values were calculated for each mRNA primer and the corresponding animal's SNR. Pearson correlation coefficients were considered significant when the p-value ≤ 0.05.

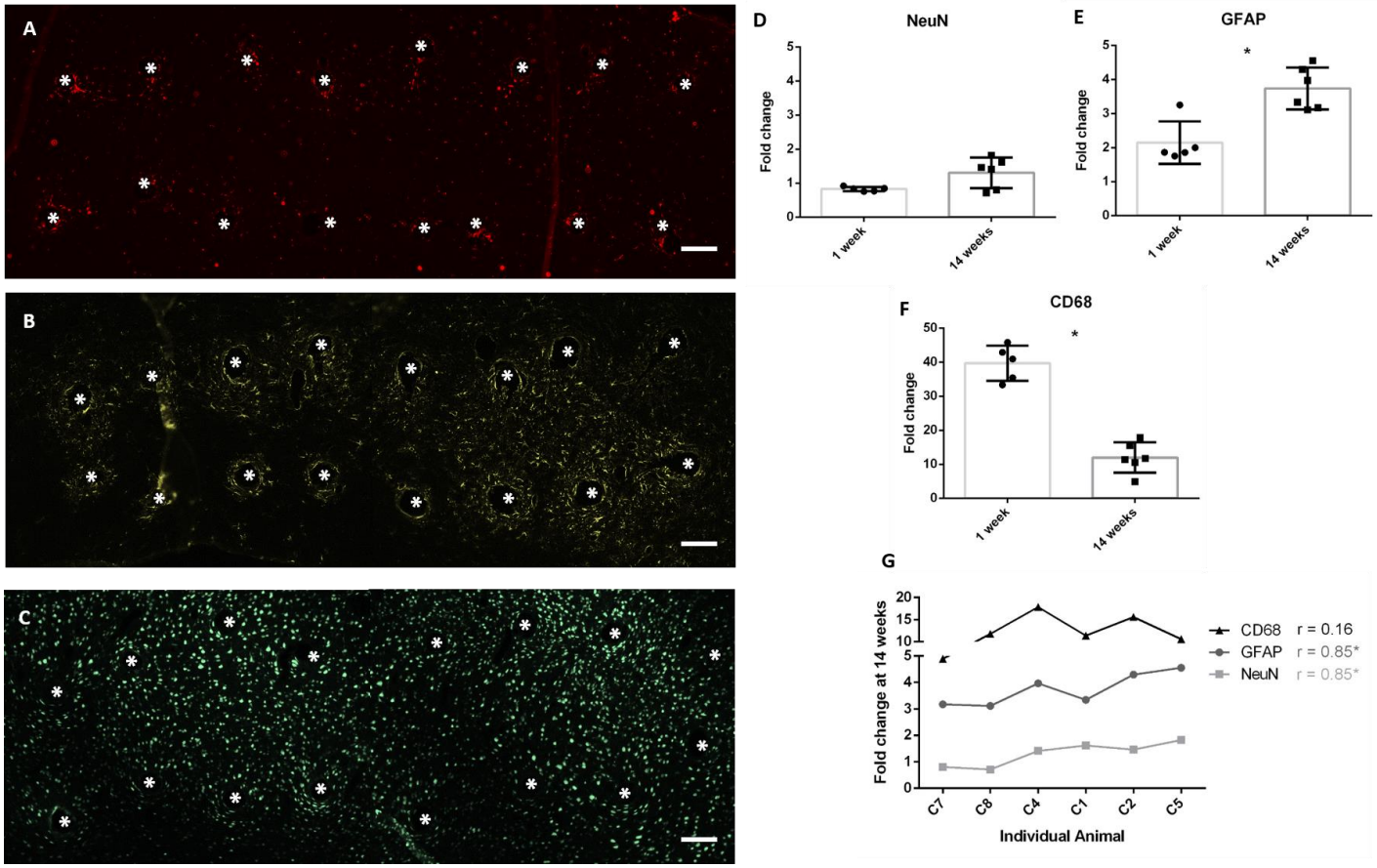

Figure 15 – Representative images of 16 electrode microwire arrays at 1 week with * representing electrode location for (A) CD68, (B) GFAP, and (C) NeuN antibody staining (scale bar = 100 µm). Fold change comparison between 1 and 14 weeks for (D) NeuN, (E) GFAP, and (F) CD68 (* $p < 0.05$, student's t-test, Bonferroni corrected). Each time point was compared to age-matched naïve controls to calculate fold change. (G) Pearson correlation values for CD68, GFAP and CD68 (* $p < 0.05$).

1.13.2 Neuroinflammation

After each time point, mRNA was extracted from biopsied brain tissue and mRNA expression was calculated. Neuroinflammation markers were analyzed in this study. This included CD68 for activated microglia/macrophages, GFAP for astrocytes, and NeuN for neuronal nuclei (**Figure 15A-C**). There was a significant reduction of CD68 expression from 1 to 14 weeks and a significant increase of GFAP 1 to 14 weeks ($p < 0.05$) (**Figure 15E,F**). No change was observed for NeuN expression (**Figure 15D**). At 14 weeks, the Pearson correlation coefficient was positively significant for both NeuN and GFAP ($r = 0.85$, $p < 0.05$, and $r = 0.85$, $p < 0.05$, **Figure 15G**). As NeuN marks neuronal nuclei, the

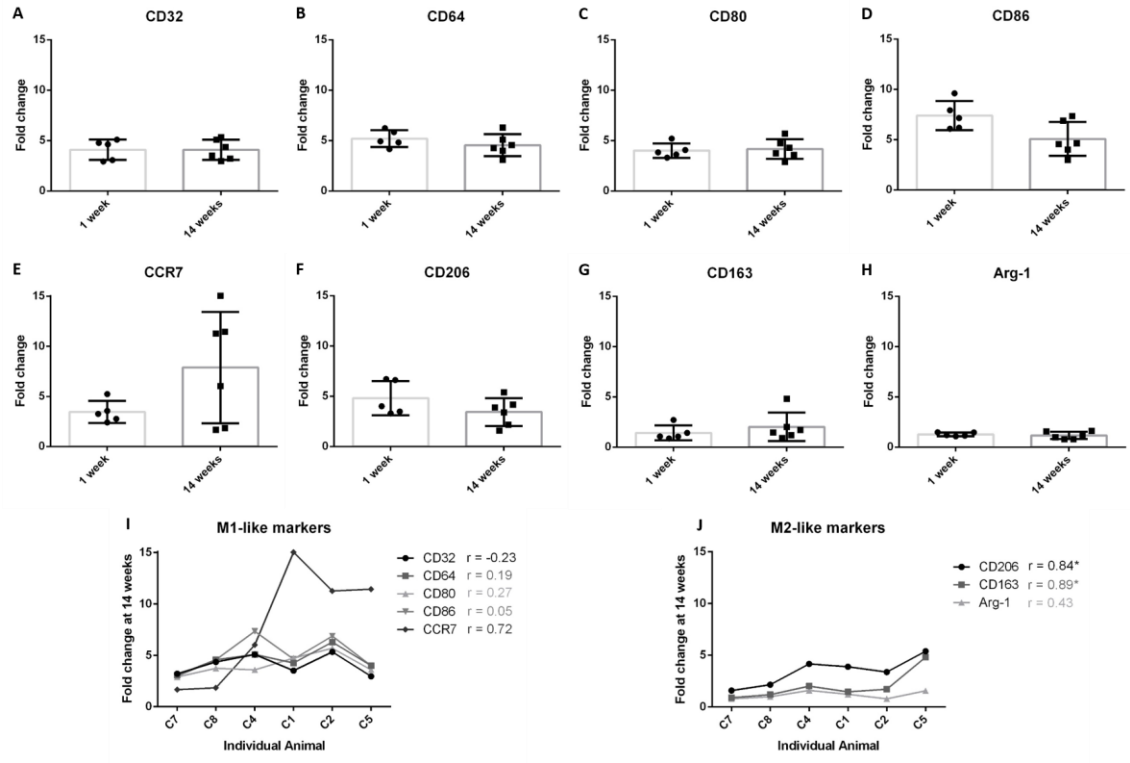

Figure 16 – Fold change comparisons between 1 and 14 weeks for M1-like pro-inflammatory markers (A) CD32, (B) CD64, (C) CD80, (D) CD86, and (E) CCR7, and M2-like anti-inflammatory markers (F) CD206, (G) CD163, and (H) Arg-1. Each time point was compared to age-matched naïve controls to calculate fold change. Pearson correlations for (I) M1-like and (J) M2-like markers (* $p < 0.05$).

positive correlation with SNR is suggestive that SNR represents neuronal health and activity at the electrode interface.

1.13.3 Inflammation milieu

Macrophages are a strong part of the wound healing and regeneration response. Markers for M1-like or pro-inflammatory response were analyzed and were upregulated at both 1 and 14 weeks (**Figure 16A-F**). However, there was no significant change over time. No significance was found for Pearson correlation coefficients for pro-inflammatory markers (**Figure 16I**). For M2-like markers or anti-inflammatory response, CD206 and CD163 had a significant positive Pearson correlation coefficient at 14 weeks (r = 0.84, r = 0.89, $p < 0.05$, **Figure 16J**).

1.13.4 Vascular integrity/BBB breach status

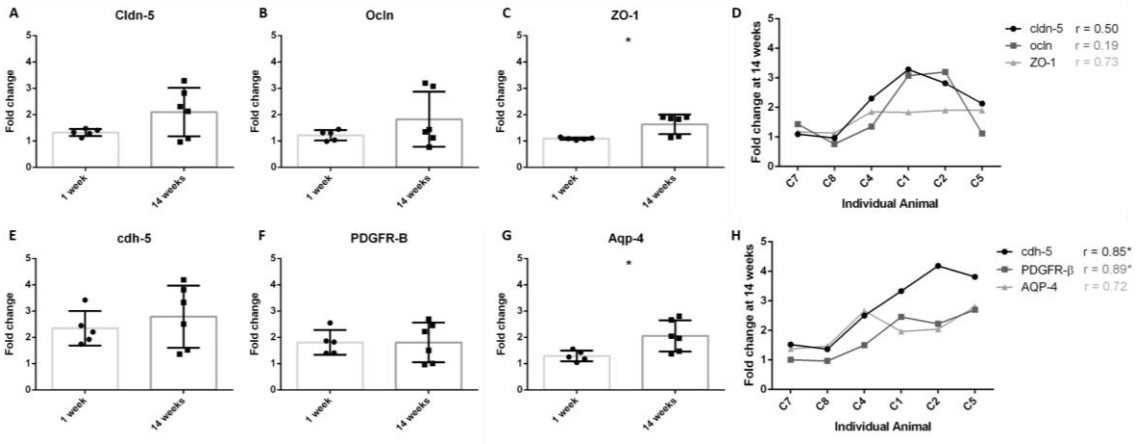

Figure 17 – Fold change comparisons between 1 and 14 weeks for tight junction proteins (A) cldn-5, (B) ocln, (C) and ZO-1, and other BBB markers (E) cdh-5, (F) PDGFR-β, (G) and AQP-4 (* $p < 0.05$, student's t-test, Bonferroni corrected). Each time point was compared to age-matched naïve controls to calculate fold change. Pearson correlations for (D) tight junction protein markers and (H) other BBB markers (* $p < 0.05$).

Previous research has demonstrated the importance of BBB and vasculature to neuronal health. Common markers for BBB tight junctions were first observed. ZO-1 had a significant upregulation at 14 weeks compared to 1 week (**Figure 17C**). No other significant changes from 1 to 14 weeks were observed for claudin-5 (cldn5) or occludin (ocln) (**Figure 17A,B**). No significant Pearson coefficient correlation was found for cldn5, ocln, or ZO-1 at 14 weeks (**Figure 17D**). Additional BBB markers were next evaluated, including cell-to-cell junctions, VE-cadherin (cdh-5), pericytes (PDGFR-β), and astrocyte endfeet (Aqp-4). Aqp-4 was significantly upregulated at 14 weeks compared to 1 week (**Figure 17G**). Expression levels remained the same for cdh-5 and PDGFR- β (**Figure 17E,F**). There was a significant positive Pearson correlation coefficient at 14 weeks for cdh-5 and PDGFR- β ($r = 0.85$, $r = 0.89$, $p < 0.05$, **Figure 17H**). However, no significant correlation was observed for Aqp-4.

1.13.5 Leukocyte recruitment and adhesion

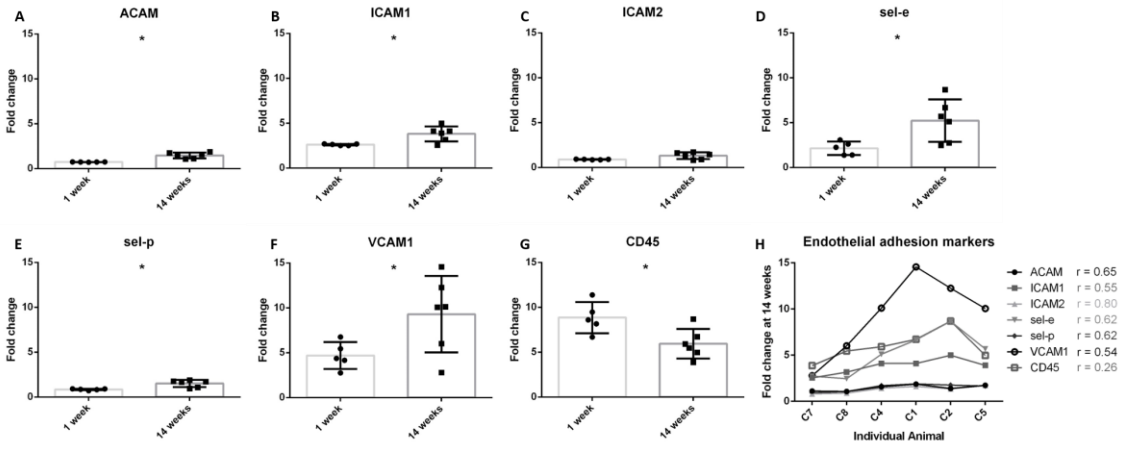

Figure 18 – Fold change comparisons between 1 and 14 weeks for endothelial adhesion markers (A) ACAM, (B) ICAM1, (C) ICAM2, (D) sel-e, (E) sel-p, (F) VCAM1, and pan-leukocyte marker (G) CD45 (* $p < 0.05$, student's t-test, Bonferroni corrected). Each time point was compared to age-matched naïve controls to calculate fold change. (H) Pearson correlation for endothelial adhesion and pan-leukocyte markers (* $p < 0.05$).

A detrimental outcome of BBB leakage is the infiltration of leukocytes. This can be monitored by leukocyte cell markers and endothelial cell adhesion markers. The fold change for the pan-leukocyte marker (CD45) was analyzed and expression significantly decreased at 14 weeks compared to 1 week ($p < 0.05$, **Figure 18G**). However, no significant Pearson correlation was observed with SNR (**Figure 18H**). A variety of adhesion markers were analyzed (ACAM, ICAM1, ICAM2, sel-e, sel-p, VCAM1, **Figure 18A-F**). All were significantly upregulated at 14 weeks (except for ICAM2), suggesting increased leukocyte extravasation, but again, no significant Pearson correlation was found (**Figure 18H**).

1.14 Discussion

If BMIs are to be successful, the signal from the intracortical electrode (i.e. the input) must be able to reliably and robustly record for long durations (on the order of years). Preclinical work has demonstrated the inevitable failure of intracortical electrodes post 12 weeks[12], [22]–[24], [52], [53] as well as animal-to-animal variability[52], [54], [182]. Previously, a relation between BBB integrity and electrode performance has been demonstrated,[12] and here these findings have been extended via an investigation of the underlying molecular mechanisms. Penetration and destruction of vessels during implantation may explain electrode recording variability per animal, and the importance of vascular integrity has been implicated in several studies in regards to neural health and electrodes[12], [52], [77], [168]. However, the direct mechanisms driving BBB dysregulation and electrode failure are not well understood. This data has shown a positive correlation between SNR and different components of the BBB, and this information could better inform therapeutic approaches for reduced electrode failure.

Expression levels for common neuroinflammation markers were evaluated. As seen in **Table 5** and **Figure 15D,E**, significant positive correlation was observed for NeuN and GFAP, but not for CD68. Previous electrode literature has suggested that the development of the astroglial scar at the electrode tissue interface is the primary cause for signal degeneration[25]. This attitude was pervasive through other neurodegenerative fields, however, this view has begun to change. The Sofroniew lab has demonstrated the importance of astrocyte support in a spinal cord injury model, and through knock-out

Table 5 – Overview of significant Pearson correlation at 14 weeks for (A) neuroinflammation markers, (B) Blood-brain barrier markers, (C) leukocyte infiltration markers, and (D) inflammation markers.

Groups	Primers	Pearson correlation ($p < 0.05$)
Neuro-inflammation	CD68	No
	GFAP	Yes
	NeuN	Yes
Blood-brain barrier	cldn5	No
	ocln	No
	ZO-1	No
	cdh5	Yes
	PDGFR-β	Yes
	AQP-4	No
Leukocyte adhesion	CD45	No
	ACAM	No
	ICAM1	No
	ICAM2	No
	sel-e	No
	sel-p	No
	VCAM1	No
Inflammation M1-like	CCR7	No
	CD32	No
	CD64	No
	CD80	No
	CD86	No
Inflammation M2-like	Arg-1	No
	CD163	Yes
	CD206	Yes

models, when the astrocytic scar is ablated, axonal regeneration is in fact impaired[186]. McCreery et al conducted an analysis with Utah electrodes implanted in the cat sensorimotor cortex for almost a year. Histology was correlated with electrophysiology using the Pearson correlation, and a significant positive correlation was found for both NeuN and GFAP within 80 μm of the electrode for signal amplitudes at the experiment endpoint[53]. Our data corroborates McCreery's findings, suggesting that presence of GFAP+ astrocytes is positively correlated with increased SNR. Therefore, developing treatment to improve astrocyte recruitment (as opposed to inhibiting astrocytes) may prove beneficial for chronic intracortical implants.

To investigate the status of the BBB, tight junction protein expression was analyzed (**Table 5, Figure 17A,B**). Tight junctions are crucial to maintaining a healthy, intact BBB, and loss can lead to neurodegeneration[29], [187]–[192]. Interestingly, no significant correlations were observed for these tight junction expressions. Additional components of the BBB were then investigated, including AQP-4, cdh5, and PDGFR-β (**Table 5, Figure 17C,D**). While there was a significant correlation with GFAP expression, there was no correlation with AQP-4, which is a common marker on astrocyte end-feet interacting with the BBB. VE-cadherin (cdh5) had a significant positive correlation with the SNR. VE-cadherin is a cell-to-cell junction for endothelial cells, and the removal of VE-cadherin severely weakens the BBB[81], [193], [194]. Thus far, no work has been done confirming the impact of VE-cadherin loss on neurodegeneration. However, our work suggests the importance of VE-cadherin for functional recordings and may provide a potential therapeutic target.

The data also shows a significant positive correlation between PDGFR-β, a common pericyte receptor, and SNR (See **Table 5, Figure 17C,D**). Pericytes are critical to embryonic blood vessel development, vasculature maintenance, and angiogenesis. PDGFR-β and PDGF-BB crosstalk between pericytes and endothelial cells is key to angiogenesis[195], [196]. Pericytes also regulate blood flow by constricting and dilating the endothelial cells[82]. Evaluation of PDGFR-β knockout mice demonstrated that vascular integrity in the brain was significantly compromised and became more susceptible to macromolecule leakage[111]. The Zlokovic lab built upon this work with the PDGFR-β knockout model showing that pericyte loss reduced cerebral blood flow and degraded BBB tight junction proteins. This resulted in neurodegeneration, and pericyte loss exacerbated amyloid-β clearance in Alzheimer's disease models[87], [197], [198]. The results from this study thus corroborate previously published data describing the importance of pericytes in the neurovascular unit and might suggest the importance of maintaining pericyte health to improve performance for intracortical electrodes.

A common cause/impact of BBB leakage is the increased expression of adhesion markers and leukocytes[33], [34], [84], [199]. Therefore, these markers were investigated in correlation with SNR (**Table 5, Figure 18C,D**). No significant correlation was found for leukocytes (CD45) or adhesion markers (ACAM, ICAM1, ICAM2, sel-e, sel-p, VCAM1). Elahy et al demonstrated that loss of BBB integrity and inflammation does occur in an aging model, but no leukocytes were recruited[200]. Others have shown that while leukocytes are recruited in different BBB leakage models, this cellular presence does not lead to neurodegeneration[201], [202]. Our data may suggest that leukocyte infiltration is not a primary cause for neurodegeneration in an electrode implant model.

The influence of M1-like and M2-like environments on neural health has been an area of study within the central and peripheral nervous systems[13], [146], [203]–[209]. With BBB breach following disease or injury, the influx of innate macrophages can influence the neurological outcomes[204], [207]. Common M1-like (CCR7, CD32, CD64, CD80, CD86) and M2-like (Arg-1, CD163, CD206) markers were evaluated to determine the relation between inflammation and SNR (**Table 5, Figure 16**). At 1 week, M1-like CD80 and M2-like CD206 were both significantly negatively correlated with SNR. At 14 weeks, M2-like CD163 was significantly positively correlated with SNR. CD163 is a general receptor found on all subsets M2-like macrophages, while CD206 is specific for M2a and M2c which is responsible for tissue repair and pro-healing functions[146], [203]. The impact of M1-like and M2-like would need further work to better elucidate the impact and role of these mechanisms.

Overall, this data showed significant positive correlation between SNR and GFAP, VE-cadherin and PDGFR-β. No significant correlations for leukocyte extravasation, inflammatory phenotypes, or tight junction expression were observed. This would suggest the importance of astrocytes (GFAP), adherens junctions (VE-cadherin), and pericytes (PDGFR- β) for maintaining chronic SNR. These data offer insight into potential molecular mechanisms to explore for improving chronic intracortical recordings.

1.15 Conclusion

The objective of this work was to better understand the molecular mechanisms influencing recording fidelity in electrode implant models. Previous work has suggested that BBB breach can influence chronic recordings. By embracing animal variability,

mRNA expression was correlated with SNR. Astrocytes, pericytes, and adherens junctions were identified as potential therapeutic targets to improve chronic intracortical recordings. Additional work with knock-out models and histological analysis is necessary to further validate the effect of these pathways. It is also important to remember that microwires were used for this study, and comparison to commonly used Michigan (research) and Utah (clinical) electrodes would be beneficial. This work provides direction for future studies and identification of BBB integrity markers that may influence and benefit chronic recordings in intracortical electrodes.

PERSPECTIVES AND FUTURE DIRECTIONS

This thesis investigated biological mechanisms that targeted the blood-brain barrier in an intracortical electrode model and evaluated the impact on chronic electrophysiological recordings. In 0, a therapeutic strategy was applied to functional NeuroNexus probes targeting the inflammatory response and BBB breach via the CCL2/CCR2 pathway. CCR2-antagonism significantly reduced inflammation and BBB breach at 2 weeks. At 12 weeks, all CCR2-antagonist treated animals still had active electrodes, while only 1 out of the 5 control animals had active electrodes. A subtle but significant change was observed at the electrode-tissue interface. Animals treated with the CCR2-antagonist had significantly higher NeuN+ cells and EBA+ vasculature within 100 μm of the electrode. In **Error! Reference source not found.**, the objective was to identify dditional molecular pathway activated in the electrode implant model and correlate this data with functional electrophysiology. mRNA expression to implanted microwires was evaluated at 1 and 14 weeks with a focus on neuroinflammation, blood-brain barrier, leukocyte infiltration, and innate inflammation. SNR and mRNA expression were correlated at 14 weeks and significant positive correlation was found for markers of the BBB and M2-like inflammation.

The significance of this work is the increased understanding of the biological mechanisms at play in an intracortical electrode implant model. Additionally, these mechanisms have been correlated with electrophysiology, assessing functionality. Future work includes developing a more detailed understanding of the CCL2/CCR2 pathway, as well as exploring the effects of PDGFR-β, MMP-9, and MMP-2 knock models on

electrophysiology. Alternatively, from a mechanical perspective, the presence of an external connector suggests that the meninges (a part of the BBB) may never close and remain chronically leaky. Exploring wireless technology and the impact of this device design *in vivo* will be crucial for closing the BBB and assessing effects on targeted biological mechanisms and electrophysiology.

1.16 Biological mechanisms and metrics

The focus of this thesis has been on the biological mechanisms that contribute to neurodegeneration at the electrode interface by targeting the blood-brain barrier. When evaluating intracortical electrodes, two biological phenomena occur: 1) acute injury and 2) chronic foreign body response. The chronic foreign body is less understood, and a small histological window has been used to identify microglia, astrocytes, and neurons at the electrode-tissue interface. More characterization studies are needed to better understand the mechanisms activated at these later timepoints. Additionally, expanding the breadth of metrics for classifying neurodegeneration and BBB breach will strengthen this analysis.

1.16.1 Characterization of mechanisms in the intracortical electrode implant model

For analyzing current and future mechanisms, mRNA and protein analysis (Western blots, proteomics) can help characterize the temporal response of the pathway of interest. Additionally, knock-out models can be used to further explore the importance of a gene in terms of healing and recovery. From this thesis, further exploration is needed for the CCL2/CCR2 mechanism. Another mechanism that emerged from **Error! Reference ource not found.** that would be interesting to evaluate is PDGFR-β. Finally, previous

intracortical electrode data suggested the importance of MMP-9 and MMP-2, both acutely and chronically, and future studies can be developed to study this mechanism.

1.16.1.1 CCR2, the BBB, and intracortical electrodes

As a follow-up to the work completed in 0, it would be beneficial to develop a better understanding of a therapeutic window. At the start of this thesis, two schools of thought were discussed for treatment administration: 1) begin treatment immediately and cease at an acute timepoint or 2) begin treatment immediately and continue chronically; however, a third option has become apparent: 3) delay treatment until a determined chronic timepoint. Before testing the many different iterations of these options, it would be beneficial to analyze the mRNA and/or protein of CCL2 and CCR2 at different time points following implantation. From this information, a more informed injection strategy can be implemented.

1.16.1.2 PDGFR-β, the BBB, and intracortical electrodes

PDGFR-β is a common marker on pericytes, which is part of the BBB. Research demonstrated that the absence of PDGFR-β significantly impacted the fidelity of the BBB and directly correlated with pericytes on the vasculature[210]. Pericyte loss has also been heavily implicated in Alzheimer's disease, leading to BBB breach and neurodegeneration[87], [211]. The results from **Error! Reference source not found.** uggest that PDGFR-β is correlated with chronic electrode performance. It would be interesting to explore the role of PDGFR-β in terms of electrode implants and use a PDGFR-β KO model for initial data. As microwires have been shown to robustly record SNRs, implantation of microwires into the PDGFR-β KO model could be used as a rapid

failure model. The PDGFR-β KO model has been validated as having a leaky BBB. Tracking electrode performance with this model could be directly related to BBB breach at the endpoint. Also, electrophysiological and histological outcomes at 16 weeks in the PDGFR-β KO compared to the wild-type can demonstrate if PDGFR-β is an active mechanism in intracortical electrodes.

1.16.1.3 MMPs, the BBB, and intracortical electrodes

Matrix-metalloproteinase-9 (MMP-9) is an enzyme that breaks down extracellular matrix (ECM) and tight junction proteins, which are part of the BBB[85]. MMP-9 has been heavily researched in the stroke community as upregulation has been associated with the intracranial hemorrhage[212], [213]. Acute inhibition of MMP-9 using a KO model[214] or specific inhibition[215] reduces infarct volume and improves behavioral outcome at 24 hours following middle cerebral arterial occlusion (MCAO). Additionally, daily injection of a MMP-2/MMP-9 inhibitor for 6 days following MCAO improved neural survival[215]. Another study used a general MMP inhibitor starting at 7 days post-MCAO and administered daily until 14 days to observe the impact of delayed MMP inhibition. Interestingly, non-specific MMP inhibition increased the infarct size at 14 days[216]. This data would suggest sensitive and acute modulation (< 7 days) of MMP-9 is necessary to produce a reduced infarct and increase behavioral outcomes.

For intracortical implants, an MMP-9 KO model was explored. While minimal differences were observed at 2 and 4 weeks, by 8 weeks, the MMP-9 KO had a significant upregulation of immune cells compared to the wild-type control[217]. MMP-9 mRNA expression was analyzed in Michigan and microwires implanted for 3 days and 16 weeks.

Microwires had significantly less MMP-9 expression at 3 days compared to Michigan and significantly higher expression at 16 weeks[12]. A beneficial experiment would be to analyzed MMP-9 protein concentrations at 0, 3 days and 1 week after Michigan electrode implantation to create a response profile (Michigan electrodes would be used since MMP-9 was significantly upregulated at 3 days[12]). Based on this information, a MMP-2/MMP-9 inhibitor (SB-3CT) can be injected following electrode implantation for 1 day or daily for either 3 or 7 days. Rats would then be euthanized at 2 weeks. If a significant result is observed, the significant injection time can be repeated for a 16 week timepoint. Electrophysiology and protein collection at 16 weeks can also be conducted.

Table 6 – Histological markers and functional tests used to define neurodegeneration in different models.

Disease	Histology
Intracortical Electrodes	NeuN Fluorojade
Multiple Sclerosis	Luxul fast blue Toluidine blue MBP MOG
Stroke	TTC NeuN Cresyl violet Fluorojade
Traumatic Brain Injury	Fluorojade NeuN Cresyl violet Luxul fast blue TUNEL
Spinal Cord Injury	Toluidine blue TUNEL Retrograde tracing

The same electrode study found that MMP-2 was significantly upregulated in microwires at both 3 days and 16 weeks compared to Michigan electrodes[12]. Unlike MMP-9, MMP-2 has been shown to have a pro-healing response in stroke[218], atherosclerosis[219], and spinal cord injury[220]. Analyzing tissue response after daily injections of MMP-2 in a Michigan electrode implant model would be an interesting experiment. Alternatively, Michigan electrodes could be implanted in a MMP-2 KO model and chronic tissue and electrophysiological outcomes could be compared to wild-type controls, with the hypothesis that MMP-2 deletion would result in significantly worse outcomes.

1.16.2 Additional metrics for improved histological analysis

Through this thesis, two questions kept emerging: 1) how to show neurodegeneration, and 2) how to show BBB breach. The histology toolkit of the Bellamkonda is strong. However, to delve more deeply into analyzing neurodegeneration from histology, switching away from immunofluorescence is necessary. For a more detailed understanding of the state of the BBB, increased magnification (to 40 or 100x) is needed to identify tight junction proteins.

1.16.2.1 Methodology for better identifying health of neural tissue

Neurodegeneration is a nebuluous term; its definition varies based on the pathology that is being observed. The exact mechanistic details of neurodegeneration at the electrode-tissue interface are not well-defined. The main analysis tool has been histology, specifically NeuN and FluoroJade C[9], [11], [12], [221], and electrophysiology for functional outcomes[2], [12], [22], [23], [54], [222]. Unfortunately, immunofluorescence can be

limiting for interpreting health of cells. Along with hematoxylin and eosin (H&E), paraffin-embedded immunohistochemistry can provide this information. Common antibodies from other neural diseases could be helpful for studying intracortical electrodes. These antibodies for neurodegeneration are outlined in **Table 6** and are categorized by pathology.

Multiple sclerosis (MS) and spinal cord injury (SCI) have demyelination and damage to axonal tracts. For MS, demyelination is the main neurologic focus. Experimental allergic encephalomyelitis (EAE) is used as the MS pre-clinical model, and histological markers for demyelination include Luxol fast blue, toluidine blue, myelin basic protein (MBP), and myelin oligodendrocyte glycoprotein (MOG) [86], [112], [223]–[229], all of which can be counterstained with cresyl violet, a general stain for neurons[225]. For spinal cord injury, analyzing axonal health is key and toluidine blue, TUNEL, and retrograde tracing is used[230]–[232].

Stroke and traumatic brain injury (TBI) all have a massive injury that occurs in the CNS and results in a lesion with neural death. For stroke, identifying the ischemic region and the resulting neural death is the primary focus. This is done with 2,3,5-triphenyltetrazolium chloride (TTC), a common stain for hypoxia, NeuN, cresyl violet, and fluorojade C[74], [233]–[239]. TBI results in a necrotic core, markers used for neural toxicity include NeuN, fluorojade, cresyl violet, Luxol fast blue, and TUNEL[240]–[243].

From this overview, exploring paraffin-embedding for intracortical electrode histology would be beneficial to expound upon neurodegeneration markers. To start, pathology found in H&E stains can provide information on the morphology of cells at the electrode-tissue interface. From this analysis, the health of the neurons, as well as

classification of astrocytes and microglia, can be analyzed. In addition, antibodies such as cresyl violet, toluidine blue, and Luxol fast blue could better elucidate the state of neural networks.

1.16.2.2 Methodology for better identifying the health of BBB

Several tracers exist to assess the quality of the BBB. Endogenous markers are proteins from the plasma and include albumin, IgG, and fibrinogen[244]. Evans blue binds to albumin and has been used as an injected tracer for BBB breach for decades[244], [245]. A variety of fluorescently-labeled injectable tracers exists including FITC-albumin, Alexafluor-555 cadaverine, and dextran-tetramethylrhodamine[111], [211], [244], [246], as well as fluorescently labeled beads of various micro and nano sizes[247], [248]. The selection of the tracer depends on the objective, but overall, it is good to confirm endogenous histology with a macromolecule tracer. In this thesis, endogenous IgG and Evans Blue were used in histology.

Non-invasive imaging provides great insight into BBB breach. However, the existence of the metallic implant makes imaging difficult. Magnetic resonance imaging (MRI) is a straight-forward tool for assessing brain injury and lesions[249]–[252], as well as BBB breach using gadolinium and albumin labeled with gadolinium as a contrast agent[253]–[256]. A study was conducted using MRI in an intracortical electrode model, but the metallic artifact completely blurred the electrode-tissue interface[12]. Another experiment used infrared imaging to assess BBB leakage using fluorescence molecular tomography (FMT), which was successful. Unfortunately, penetration of the dental cement

headcap is not possible with this modality, so only non-fixed electrodes can be evaluated[12].

To better assess the health of vasculature, images can be taken using a confocal or spinning disk microscope at 40X to 100X. From the convolved z-stacked images, vessel diameter and length can be counted[111]. At this resolution, antibodies for tight junction proteins (ZO-1, occludin, claudin) can be imaged and analyzed for coverage[142], [192]. Along with H&E, transmission electron microscopy is another method to view the morphology of blood vessels at a high resolution[111], [121], [247]. These techniques would yield more in depth data on the state of the BBB at the electrode interface.

1.17 Next generation electrodes – wireless integration

Wireless recording devices are the next frontier for intracortical electrodes[257]. Current clinical intracortical electrodes connect directly from the brain to the exterior of

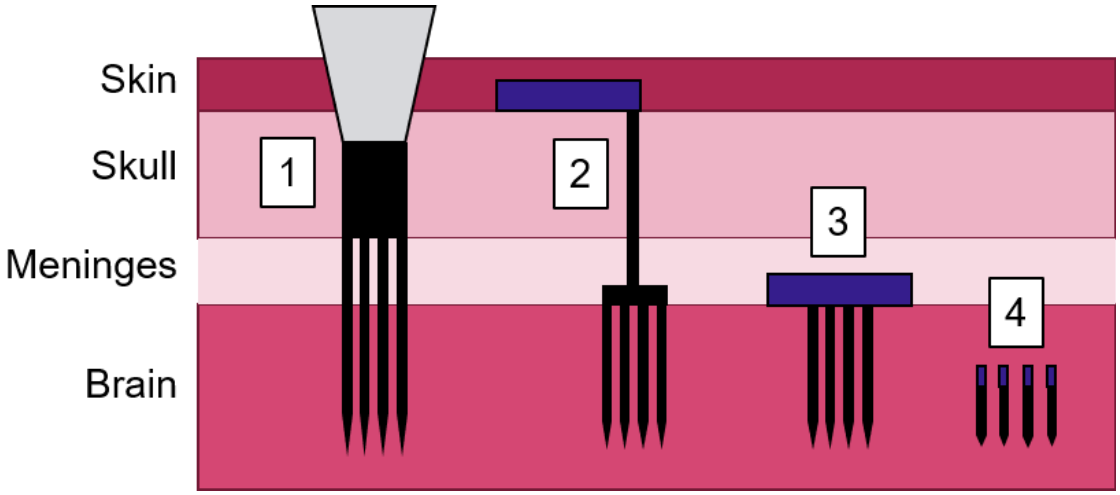

Figure 19 – Examples of anatomical placement for 1) standard fixed electrodes, and 2) trans-cranial, 3) trans-meninges, and 4) sub-meninges wireless electrodes. Blue is the electronics package, while black are the electrodes.

the body[2], [3], [16], [43]. Removing this direct hardware link is crucial to reduce infection and prevent hardware removal, which is a standard requirement for safety as these devices leave research and become available to the public. Additionally, the necessity of tethered cables in current electrode designs further exacerbates the biological response within the brain. Going wireless will reduce the device footprint within the body (and brain).

1.17.1 Biological benefits of a wireless design

For wireless recordings, three types of modalities exist for positioning the electrodes in relation to the skull and meninges, which are shown in **Figure 19**: 2) trans-cranial, 3) trans-meninges, and 4) sub-meninges. While the first iterations of wireless electrodes will be trans-cranial (circuitry resting on skull, covered by skin) and trans-meninges (circuitry resting on the brain, covered by the meninges), a more integrative goal would be to further miniaturize electronics for implants that will rest in the sub-meninges space. With today's fixed and tethered electrode design, the meninges is unable to completely close with electrodes protruding from the brain to the external connector and headcap. While remaining open, cells and proteins from the meninges may coalesce at the tissue-electrode interface. In fact, meningeal inflammation was been correlated with neuronal loss in MS[258]–[260]. Additionally, having the proximal end of the electrode dental cemented to the skull results in micromotion that has an adverse effect on both the electronics and the brain. Research has demonstrated that compared to fixed electrodes, there is a reduced immune response to electrodes that are not connected to the skull[179]–[181]. Moving towards a free floating, functional intracortical electrode can be highly beneficial.

The problem with the trans-cranial design is that while it removes external wires, the electronics package is situated on top of the skull. This design still requires a tethered cable (that is burrowed through the skull) to the electrodes below (See device 2 in **Figure 19**). With the tethered cable, the same issues that are present in the current electrode design will remain at the neural interface (i.e. micromotion and an open meninges)[22]. A good example has been demonstrated with the Utah electrodes in primate work, in which the meninges aggressively encapsulates electrodes, causing complete removal from the neural tissue[54]. The trans-meninges and sub-meninges designs address both problems. Therefore, for future wireless designs, signal penetration through the skull will be a requirement.

When comparing the benefits of the trans-meninges vs the sub-meninges design, the key difference is the location of the electronics package. Ideally, for the trans-meninges device, the meninges will regrow on top of the device with minimal disturbance. However, the location of the electronics could irritate the meninges. Additionally, the electronics package can act as a fixed point and may still result in micromotion at the electrode-tissue interface. A significant reduction in immune response was demonstrated when single electrodes were implanted in the sub-meninges as opposed to the trans-meninges[261]. The immediate restriction with the sub-meninges device is the miniaturization of electronics. But with advancements in semi-conductor technology (and Moore's Law), this will not be a restriction for long.

1.17.1.1 Power and data transmission strategies

Wireless power transmission is a fast expanding field and near field techniques fall into four categories: 1) capacitive coupling, 2) inductive coupling, 3) magneto dynamic coupling, and 4) magnetic resonant coupling[262]. For recording within the brain, several wireless devices have been published using inductive coupling [257], [263]–[265] and magnetic resonant coupling[266], [267]. Radio frequency is the preferred modality for data transmission for these devices. More recently, ultrasound as a data and power transmission media has been demonstrated using millimetre sized recording devices (termed ultrasonic neural dust) in the peripheral nerve[268]. The overall goal for the ultrasonic neural dust is to become a sub-meninges device for implantation within the brain. In summary, the technology exists, it is just a matter of miniaturizing and demonstrating proof-of-concept.

1.17.2 Non-functional studies evaluating micromotion and meninges repair

While functional wireless electrodes are being developed, an important non-functional study would be to compare the immune response of trans-cranial (fixed), trans-meninges, and sub-meninges electrodes. While studies have been conducted[179], [261], the electrodes were only implanted for 4 weeks. It is critical to observe the immune response at a chronic 16 week time point to deduce the impact of micromotion and an unhealed meninges on chronic neural interfaces. This study would also evaluate the impact of the BBB, but from a device design viewpoint, as opposed to a pharmaceutical modulation aim. With this information, the design focus of future wireless electrodes can be adapted to best minimize trauma to the body. Additionally, when exploring biological mechanisms, including a floating electrode as a "negative control" may be valuable.

1.18 EcOGs vs intracortical electrodes

There are currently three categories of recording electrodes for the brain: 1) non-invasive electroencephalography (EEG), 2) extracortical electrocorticography (EcOG), and 3) invasive intracortical electrodes (See **Figure 20A**). Across these modalities, the main difference is the proximity of the electrode interface with the neural tissue. The more invasive the electrode, the better the signal resolution; however, the stability of the electrode decreases and the health risk to the patient increases. Unlike EEG (which is in contact with the scalp) and EcOG (which rests on the surface of the brain), intracortical electrodes directly penetrate the brain. The physical proximity of intracortical electrodes to neurons makes recording of single-unit activity feasible, while the other modalities rely on LFPs, as seen in **Figure 20B**[269].

Several clinical trials have been conducted with EcOG as theses electrodes are used in epilepsy patients to identify seizure loci[270]. EcOGs also have a less invasive surgery and easy post-experiment removal when compared to intracortical electrodes, allowing for short-term recording experiments from epilepsy patients[271]–[273]. Clinical trials have been conducted on paralyzed patients implanted with EcOGs controlling a prosthetic

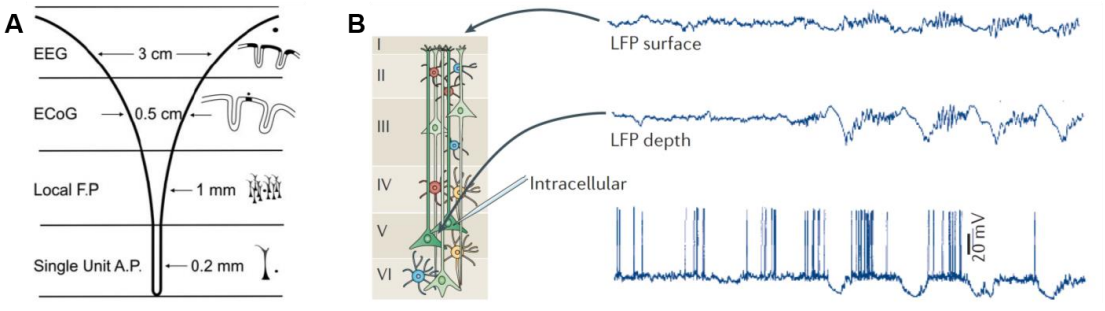

Figure 20 – (A) Types of cortical recording modalities [269]. (B) Types of signals and locations recorded in the brain [286]**.**

arm[273], [274]. In both studies, high gamma frequencies (70 – 200 Hz) offered the most accurate directional control.

As mentioned previously, high gamma is the same physiological range of single and multi-unit spikes. The Brain Gate group is using high gamma and epsilon frequencies (in addition to spikes) as inputs for the neural decoder[3]. Additional work revealed no significant difference in prosthetic control accuracy between neural decoders using spikes versus those using high frequency LFPs[42]. In more recent pre-clinical tests of research EcOG arrays, the electrodes are able to distinguish action potentials from the subdural surface of the brain[275], [270].

As of this moment, it is unclear whether intracortical electrodes or EcOGs are the superior recording device. However, as research continues, EcOGs are able to record more precisely in the frequency ranges used in clinical trials of intracortical electrodes. EcOGs also have the added benefit of immense surface area coverage with minimal tissue damage. No superior device has yet emerged, and it is important for researchers to consider both modalities when attempting to record from within the brain.

1.19 Conclusion – clinical translation

In clinical trials, recorded action potentials from implanted electrodes are the input for machine control. Since signal strength decreases over time, research to improve SNR reliability is necessary. Better understanding the biological cascades induced by implanting a foreign body may be one avenue to increase SNR strength. Through this work, a therapeutic modality (the CCR2/CCL2 pathway) was evaluated and tested in a functional

electrode model. Additionally, mRNA expression of BBB and anti-inflammatory markers were correlated with chronic *in vivo* recordings.

For future work investigating the biological response, further characterization of the CCL2/CCR2 pathway is recommended to develop a stronger timeline for therapy administration. In addition, researching PDGFR-β, MMP-9 and MMP-2 pathways may provide further insight for the role of the BBB in the intracortical electrode model. To better assess the state of neurodegeneration, changing to non-fluorescent immunohistochemistry will allow the visualization of neural morphology and health. For the BBB, a closer view (40 to 100x) is needed to assess the morphology of blood vessels and analyzed the integrity of the tight junction proteins.

As the field moves forward, it is important to look towards the wireless electrode. A design change may eliminate a large part of the immune response currently observed. By removing the external connector, the micromotion from a fixed implant is removed and the meninges can heal over the electrode. It would be interesting to explore this hypothesis in future work. Evaluation of this device design *in vivo* will further elucidate the impact of targeted BBB biological mechanisms and the subsequent electrophysiological performance.

APPENDIX

A.1 Imatinib as a BBB modulation strategy in functional Michigan electrodes

A.1.1 Introduction

Imatinib has shown efficacy in several neurodegenerative and injury models, including spinal cord injury[113], multiple sclerosis[112], [276], ALS[277], traumatic brain injury[278], and stroke[110], [279], [280]. Imatinib targets the vasculature by inhibiting platelet derived growth factor receptors (PDGFRs). The PDGF family (PDGF-A, B, C, and D) has been shown to increase BBB leakiness in an intracerebral hemorrhage stroke model[110], [280]. Su et al showed that imatinib reduced infarct size and reduced the negative impact of tPA by inhibiting the PDGFR-α receptor in a stroke model[110]. As PDGFs are involved in angiogenesis, imatinib may be preventing angiogenesis immediately following trauma. Research has shown that imatinib application reduces vasculature leakiness through abl/arg inhibition which increases VE-cadherin expression[124], [125], [281]. The objective of this study was to use imatinib to seal the blood-brain barrier in an intracortical implant model and observe the impact on electrophysiology.

A.1.2 Methods

Non-functional and functional Michigan electrodes were implanted into Sprague Dawley rats for 2 and 12 weeks. Research grade imatinib (Selleckchem, TX) was administered IP at a dose of 30 mg/kg. Imatinib is insoluble in saline and was dissolved in DMSO at a 10X concentration. The day of injection, the stock was diluted in 0.9 mL of

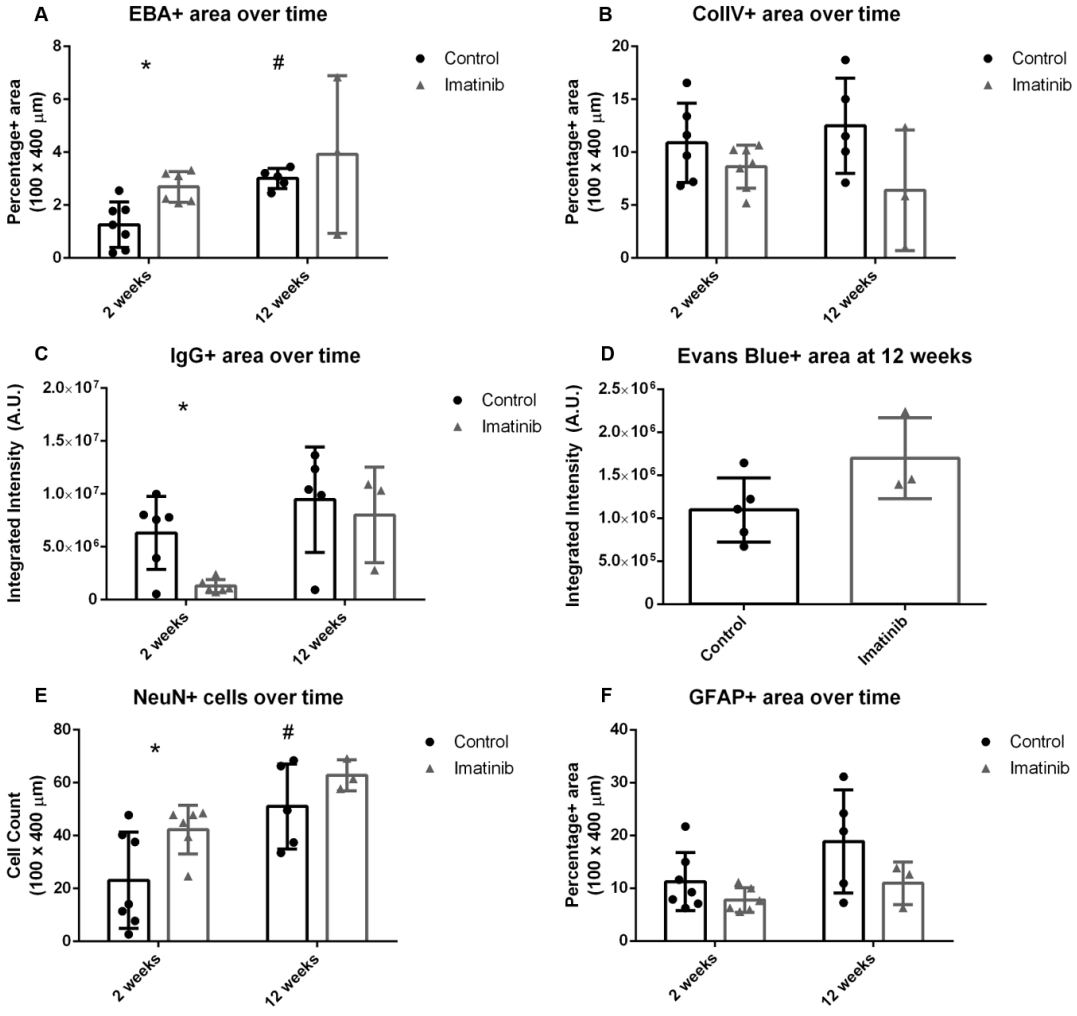

Figure 21 – An overview of the histology analyzed at 2 and 12 weeks. (A) For EBA+ vasculature, there was a significant difference at 2 weeks between treatment and control, and a significant increase in control at 12 weeks compared to control. (B) For ColIV+ vasculature, there was no significant difference. (C) For IgG, there was a significant difference at 2 weeks. (D) For Evans Blue, there was no significance at 12 weeks. (E) For NeuN+ cells, there was a significant difference at 2 weeks between treatment and control, and a significant increase in control at 12 weeks compared to control. (F) For GFAP, there was no significant difference (* $p < 0.05$).

sterile saline for a total of 10% DMSO. For the 12 week study, weekly electrophysiology was conducted. SNR was calculated from the recordings. At the conclusion of the experiment, rats were euthanized via perfusion. Brains were cryosectioned and immunofluorescence staining wasa conducted. Following microscopy, images were analyzed for intensity profiles, cell counts, and percentage of thresholded image.

A.1.3 Results

A.1.3.1 Histology of 2 and 12 week study (Imatinib 30 mg/kg)

The antibodies listed in **Table 3** were used for the histology for this experiment. At 2 weeks, imatinib increased EBA+ vasculature, reduced IgG expression, and increased NeuN+ cells (**Figure 21A,C,E**, 4-way nested ANOVA). However, by 12 weeks, there was no significant difference between treatment and control. There was no difference for ColIV+ vasculature, Evans blue leakage at 12 weeks, and GFAP expression (**Figure 21B,D,F**).

A.1.3.2 Electrophysiology

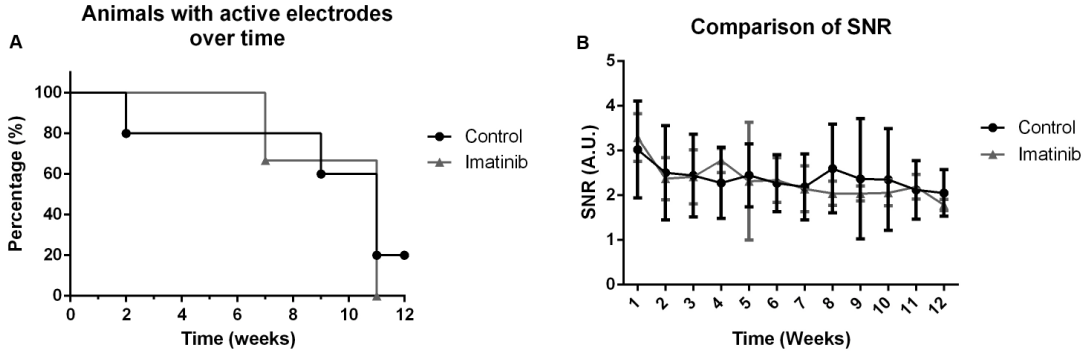

Figure 22 – (A) Percent of animals with active electrodes over time. (B) SNR over time.

Weekly electrophysiological recordings were conducted until 12 weeks. As seen in **Figure 22B**, there was no significant difference in SNR between treatment and control. Additionally, there was no change in the percentage of animals with active electrodes compared to control (**Figure 22A**). In the imatinib group, the first rat stopped recording at week 7, while the other 2 failed at week 11.

A.1.3.3 Imatinib effect on weight change

An initial study using imatinib at a dosage of 60 mg/kg revealed that rats injected daily with imatinib were not gaining weight, and there was a significant difference compared to the control counterparts (**Figure 23A**). Following FDA guidelines[282], the dosage was reduced by half to 30 mg/kg. For the 2 week study, rats injected daily had normal weight gain (data not shown). Over 12 weeks, imatinib injected rats did start to gain less weight compared to controls, starting at 9 weeks (**Figure 23B**, 2-way ANOVA).

A.1.4 Discussion

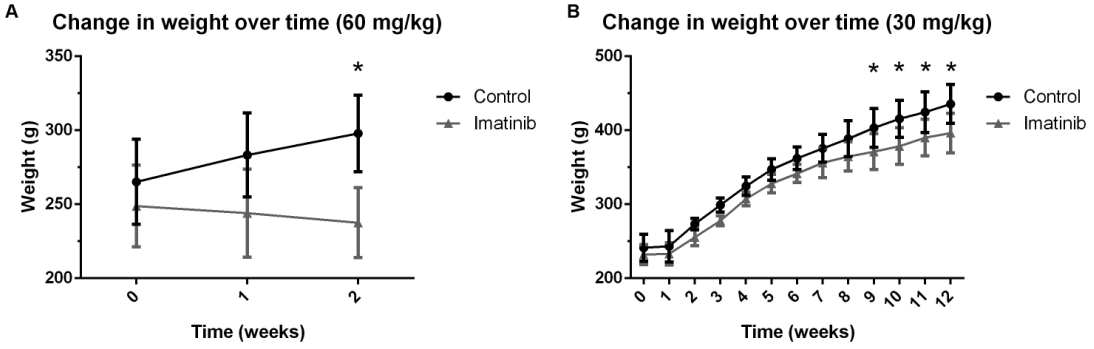

Figure 23 – (A) Weight change over time of imatinib injected rats (60 mg/kg) compared to control (* $p < 0.05$). (B) Weight change over time of imatinib injected rats (30 mg/kg) compared to control (* $p < 0.05$).

Imatinib significantly changed the immune response at 2 weeks in a Michigan intracortical electrode implant model. However, at 12 weeks, there was no difference in electrophysiological or histological outcomes. Imatinib is PDGFR inhibitor and one concern using this pharmaceutical is the chronic effect. Inhibiting angiogenesis may be beneficial acutely, but the impact of preventing communication between pericytes and endothelial cells chronically is unknown. From the histological data, daily administration of imatinib may not worsen the immune response at the electrode interface when compared to controls.

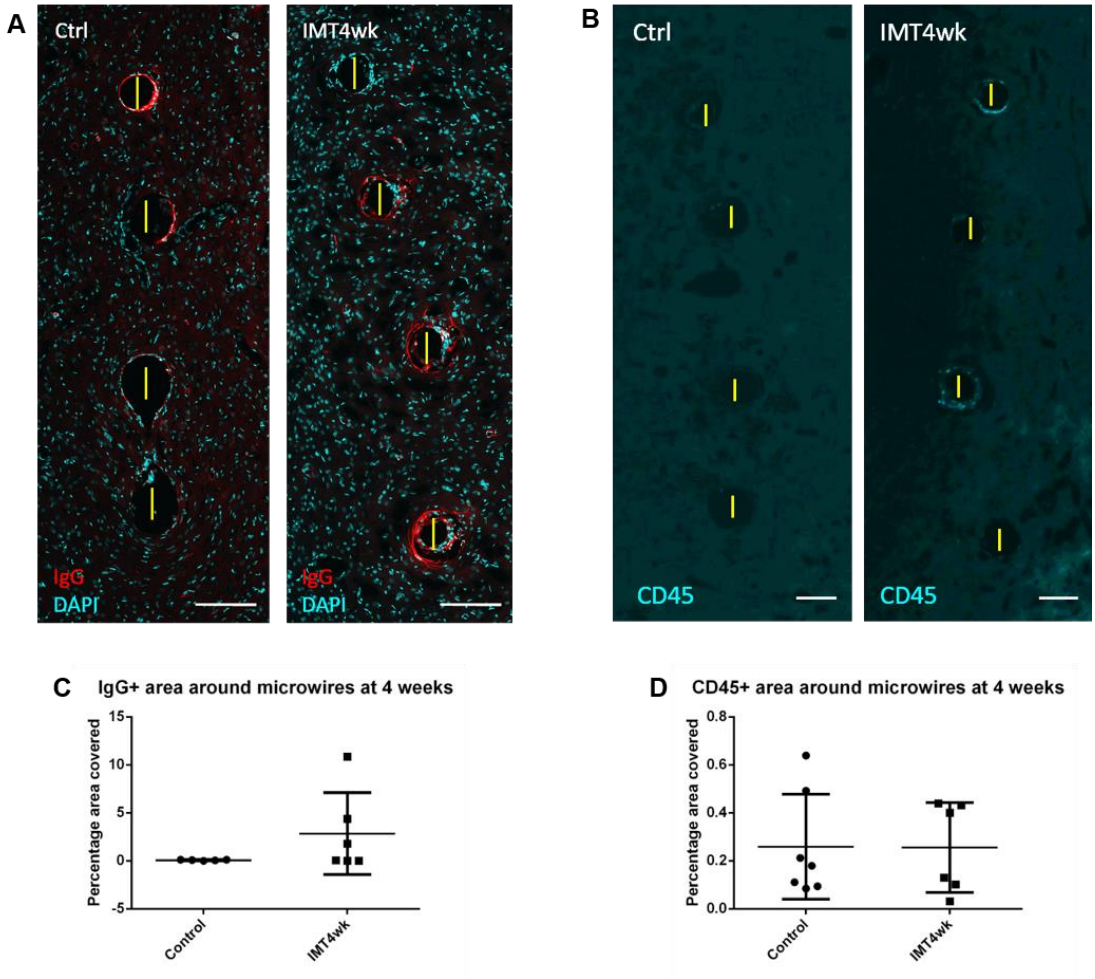

Figure 24 – Representative images of IgG (A) and CD45 (B) intensity for, as well as (C) IgG and (D) CD45 percentage area covered.

A1.4.1 Injected imatinib is more toxic than reported in literature

It is important to acknowledge that the concentration of imatinib was reduced for the microwire experiment (from 60 mg/kg to 30 mg/kg). It was observed after the 2 week study that the imatinib-treated animals (60 mg/kg) did not gain weight (which is abnormal for young male rats). During perfusion, peritoneal adhesions on the liver were observed. A literature search revealed two papers which had reported similar findings. Han et al 2009

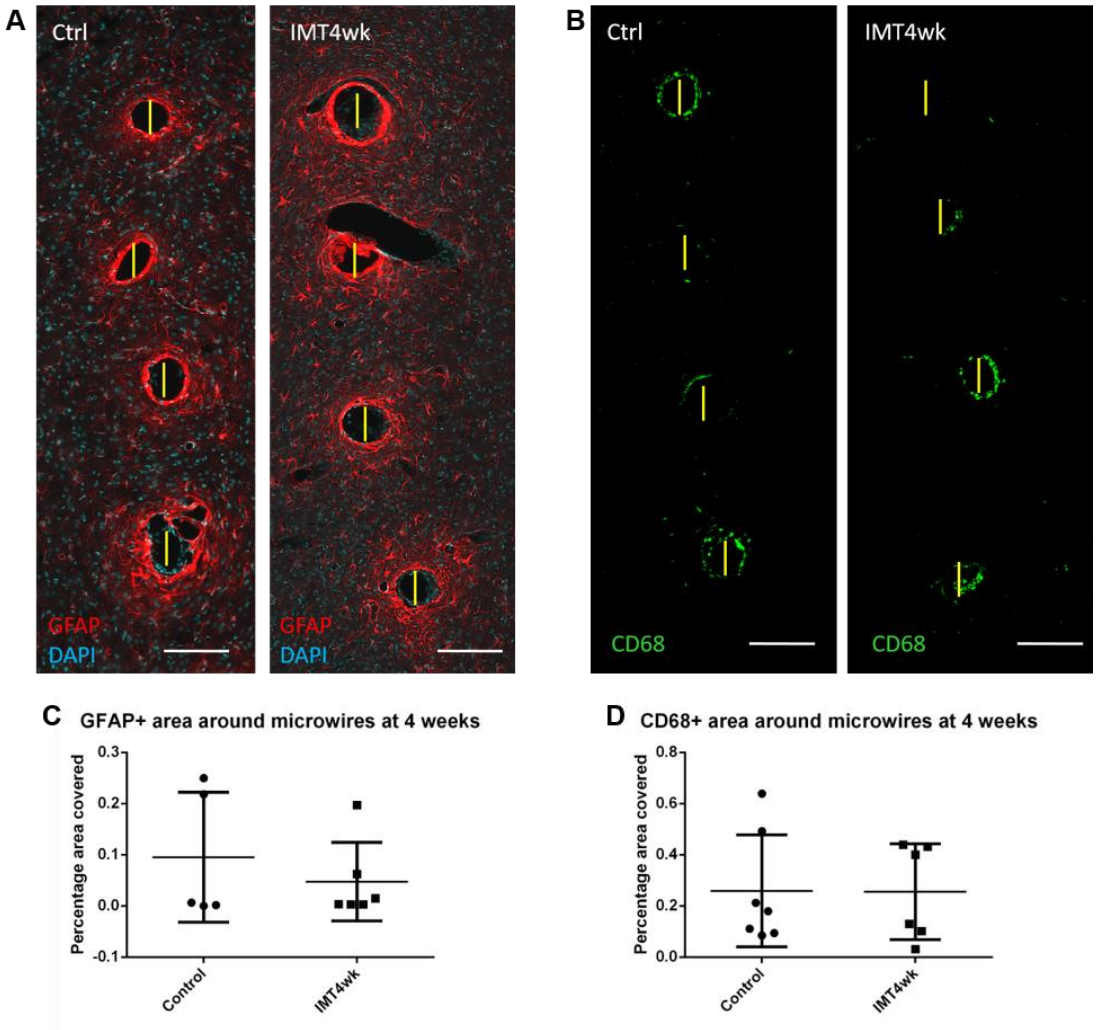

Figure 25 – Representative images of (A) GFAP and (B) CD68 intensity for control and 4 week imatinib treatment. (C) IgG and (D) CD45 percentage area covered.

reported that db/db mice given IP injections of 50 – 75 mg/kg of imatinib had peritoneal adhesions and general weakness[283]. Wolf et al 2010 reported severe toxicity (and death) in C57BL/6 mice that received 200 mg/kg daily IP doses of imatinib. Mice that received 50 mg/kg IP imatinib were sacrificed at 22 days due to local toxicity (lesions in the abdominal organs). However, in the same study, mice that received 400 mg/kg of imatinib orally displayed no symptoms[284]. When the toxicity of the 60 mg/kg IP dose was revealed, the dose for the rats was reduced to 30 mg/kg based on FDA recommendations[282]. The 60 mg/kg dosing was suggested for mice, but as rats have a lower metabolism (by 50%), the dosing was reduced by half. Initially, imatinib had no impact on weight gain. However, by 9 weeks, rats in the imatinib treatment had started to gain significantly less weight.

A.1.5 Conclusion

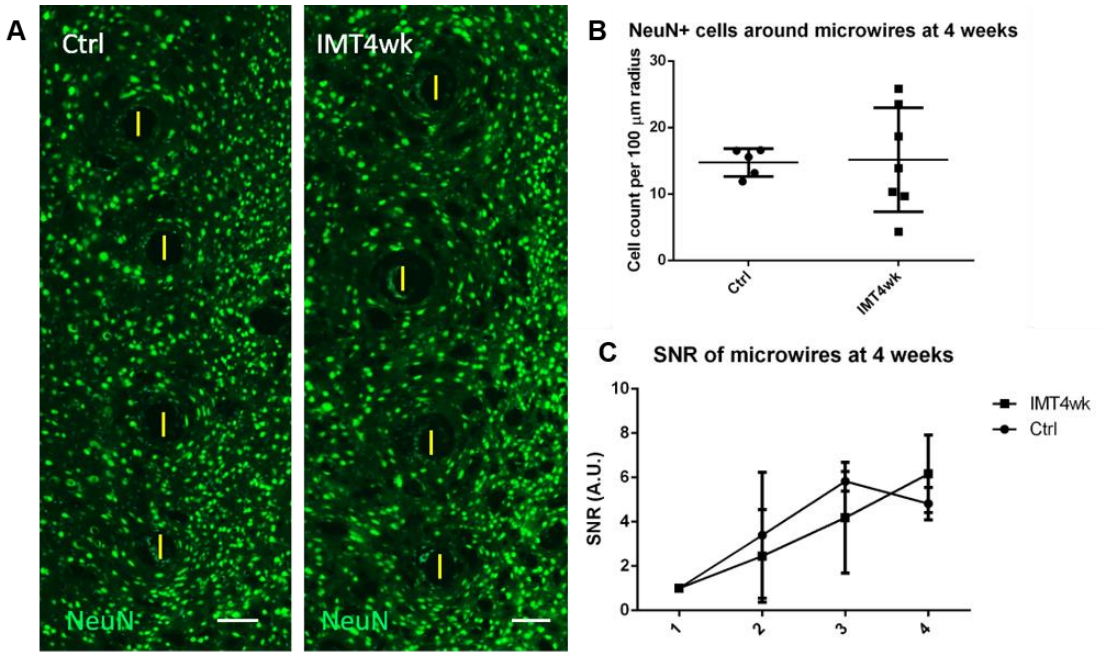

Figure 26 – Representative images of (A) NeuN intensity for control and 4 week imatinib treatment. (B) NeuN cell count and (C) SNR.

At 2 weeks, imatinib appears to have reduced the immune response by several viable histological markers. However, the 12 week data shows no differences across electrophysiology or histology. Imatinib did not have any significant impact chronically in the intracortical electrode model.

A.2 Imatinib as a BBB modulation strategy in functional microwires electrodes

A.2.1 Results

Contrary to the results observed in the 2 week Michigan electrode study, no significant difference was observed in IgG accumulation between the imatinib-treated and control animals (**Figure 24a,b,e**). CD45+ cells were also evaluated. Again no significant difference was seen (**Figure 24c,d,f**).

A well-defined astrocyte scar was observed encapsulating the control microwires (**Figure 25a**). However, no difference was seen between the imatinib-treated and control animals in GFAP coverage (**Figure 25a,b,e**). Interestingly, at 4 weeks around microwires, CD68+ cells were observed at the electrode interface. When compared to the 2 week Michigan electrode data, CD68+ cells are no longer present at 2 weeks and onwards (which has been shown in the literature [11]). However, no difference was seen in CD68 expression between the control and imatinib-treated animals (**Figure 25c-f**).

Neuronal density was histological evaluated by counting NeuN+ cells in a 100 μm radius circle around the electrode. This analysis revealed no differences between the control and imatinib-treated group (**Figure 26a-c**). Signal-to-noise ratios were also calculated over the 4 week time course of the experiment. No significant differences were

observed either (**Figure 26d**). However, there was significant difference between time points, with the maximum SNRs occurring at 3 and 4 weeks.

A.3 mRNA analysis at 2 weeks for Michigan probes comparing CCR2-antagonist

After 2 weeks of implantation of Michigan electrodes, in which the treatment group received daily CCR2-antagonist injection, tissue was extracted. Total mRNA was extracted, and cDNA was amplified. mRNA primers for M1-like and M2-like phenotypes were selected from previous work (CD68, CCR7, CD80, CD163, CD206, Arg-1)[13]. A 96-channel Fluidigm qRT-PCR was run, and fold change was calculated from the resulting CT values. No significant differences were found between treatment and control across the 6 selected primers (**Figure 27**).

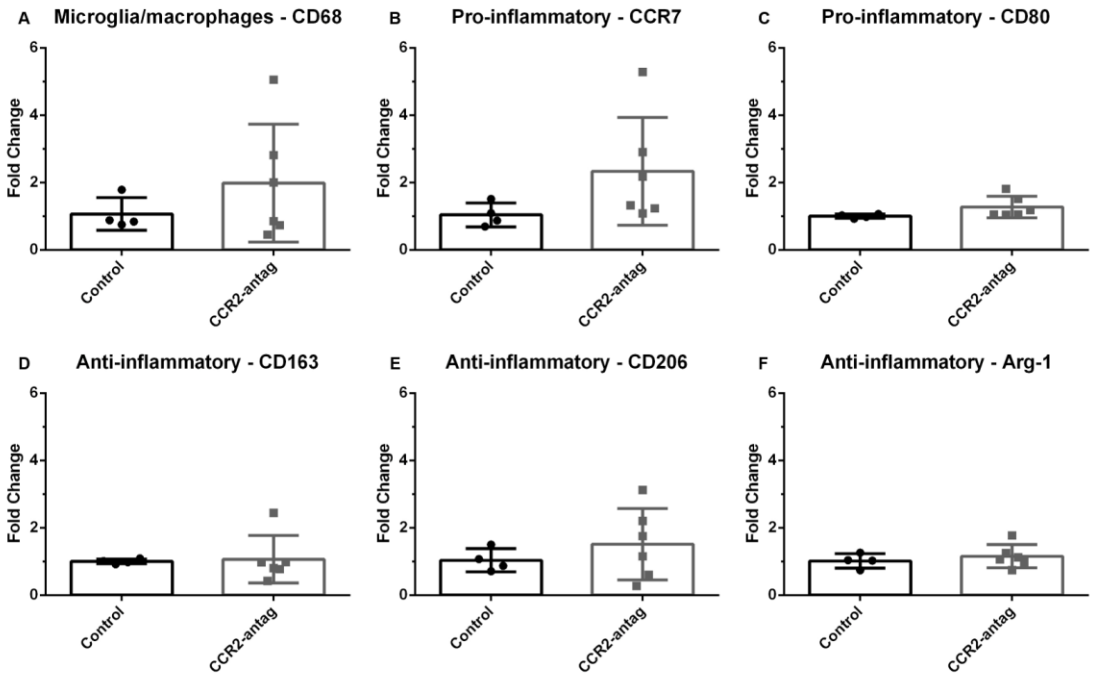

Figure 27 – Fold change from qRT-PCR for (A) activated microglia/macrophages (CD68), (B,C) M1-like pro-inflammatory markers (CCR7, CD80), and (D-F) M2-like anti-inflammatory markers (CD163, CD206, Arg-1).

A.4 TDT Microwires vs NeuroNexus Probes

This thesis dealt with two common research intracortical probes, TDT microwires and NeuroNexus electrodes. Previous work from this lab reported to improved SNR strength and longevity of microwires compared to NeuroNexus probes. The same study noted that microwires had significantly less IgG accumulation at 16 weeks when compared to NeuroNexus electrodes, suggesting a correlation between BBB breach and electrophysiological performance[12]. Electrophysiology between Chapter 3 and Chapter 4 was compared, and the same results were found where microwires outperformed NeuroNexus probes over 12 weeks (**Figure 28A, B**).

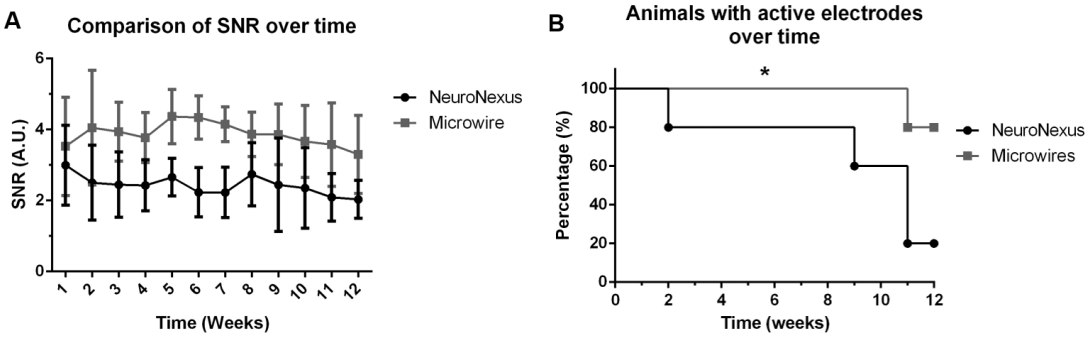

Figure 28 – Comparison between microwire array and NeuroNexus for (A) SNR and (B) animals with active electrodes (n = 5 for NeuroNexus and n = 7 for microwires.

REFERENCES

[1] S. N. Flesher *et al.*, "Intracortical microstimulation of human somatosensory cortex," *Sci. Transl. Med.*, vol. 8, no. 361, p. 361ra141-361ra141, 2016.

[2] C. E. Bouton *et al.*, "Restoring cortical control of functional movement in a human with quadriplegia.," *Nature*, vol. 0, no. 7602, pp. 1–13, 2016.

[3] A. B. Ajiboye *et al.*, "Restoration of reaching and grasping in a person with tetraplegia through brain-controlled muscle stimulation: a proof-of-concept demonstratio," *Lancet*, vol. 6736, no. 17, p. (In press), 2017.

[4] V. Gilja *et al.*, "Clinical translation of a high-performance neural prosthesis," *Nat. Med.*, vol. 21, no. 10, pp. 1142–1145, Sep. 2015.

[5] J. L. Collinger *et al.*, "High-performance neuroprosthetic control by an individual with tetraplegia," *Lancet*, vol. 381, no. 9866, pp. 557–564, Feb. 2013.

[6] J. E. Downey *et al.*, "Blending of brain-machine interface and vision-guided autonomous robotics improves neuroprosthetic arm performance during grasping," *J. Neuroeng. Rehabil.*, vol. 13, no. 1, p. 28, 2016.

[7] V. S. Polikov, M. L. Block, J.-M. Fellous, J.-S. Hong, and W. M. Reichert, "In vitro model of glial scarring around neuroelectrodes chronically implanted in the CNS.," *Biomaterials*, vol. 27, no. 31, pp. 5368–76, Nov. 2006.

[8] R. Biran, D. C. Martin, and P. a Tresco, "Neuronal cell loss accompanies the brain tissue response to chronically implanted silicon microelectrode arrays.," *Exp. Neurol.*, vol. 195, no. 1, pp. 115–26, Sep. 2005.

[9] G. C. McConnell, H. D. Rees, A. I. Levey, C.-A. Gutekunst, R. E. Gross, and R. V Bellamkonda, "Implanted neural electrodes cause chronic, local inflammation that is correlated with local neurodegeneration.," *J. Neural Eng.*, vol. 6, no. 5, pp. 1–12, Oct. 2009.

[10] B. D. Winslow, M. B. Christensen, W.-K. Yang, F. Solzbacher, and P. a Tresco, "A comparison of the tissue response to chronically implanted Parylene-C-coated and uncoated planar silicon microelectrode arrays in rat cortex.," *Biomaterials*, vol. 31, no. 35, pp. 9163–72, Dec. 2010.

[11] K. A. Potter, A. C. Buck, W. K. Self, and J. R. Capadona, "Stab injury and device implantation within the brain results in inversely multiphasic neuroinflammatory and neurodegenerative responses," *J. Neural Eng.*, vol. 9, no. 4, pp. 1–14, Aug. 2012.

[12] T. Saxena *et al.*, "The impact of chronic blood-brain barrier breach on intracortical

electrode function.,” *Biomaterials*, vol. 34, no. 20, pp. 4703–4713, Jul. 2013.

[13] A. J. Sawyer *et al.*, “The effect of inflammatory cell-derived MCP-1 loss on neuronal survival during chronic neuroinflammation,” *Biomaterials*, vol. 35, pp. 6698–6706, 2014.

[14] B. S. Armour, E. A. Courtney-Long, M. H. Fox, H. Fredine, and A. Cahill, “Prevalence and Causes of Paralysis—United States, 2013,” *Am. J. Public Health*, vol. 106, no. 10, pp. 1855–1857, 2016.

[15] L. R. Hochberg *et al.*, “Neuronal ensemble control of prosthetic devices by a human with tetraplegia.,” *Nature*, vol. 442, no. 7099, pp. 164–71, Jul. 2006.

[16] L. R. Hochberg *et al.*, “Reach and grasp by people with tetraplegia using a neurally controlled robotic arm.,” *Nature*, vol. 485, no. 7398, pp. 372–375, May 2012.

[17] M. Capogrosso *et al.*, “A brain-spinal interface alleviating gait deficits after spinal cord injury in primates,” *Nature*, vol. In Press, no. 7628, pp. 284–288, 2016.

[18] F. J. Santos, R. M. Costa, and F. Tecuapetla, “Stimulation on demand: Closing the loop on deep brain stimulation,” *Neuron*, vol. 72, no. 2, pp. 197–198, 2011.

[19] N. C. Swann *et al.*, “Chronic multisite brain recordings from a totally implantable bidirectional neural interface: experience in 5 patients with Parkinson’s disease,” *J. Neurosurg.*, pp. 1–12, Apr. 2017.

[20] B. Rosin *et al.*, “Closed-loop deep brain stimulation is superior in ameliorating parkinsonism.,” *Neuron*, vol. 72, no. 2, pp. 370–84, Oct. 2011.

[21] K. Nowak *et al.*, “Optimizing a rodent model of Parkinson’s disease for exploring the effects and mechanisms of deep brain stimulation.,” *Parkinsons. Dis.*, vol. 2011, p. 414682, Jan. 2011.

[22] L. Karumbaiah *et al.*, “Relationship between intracortical electrode design and chronic recording function.,” *Biomaterials*, vol. 34, no. 33, pp. 8061–8074, Nov. 2013.

[23] T. D. Y. Kozai *et al.*, “Comprehensive chronic laminar single-unit, multi-unit, and local field potential recording performance with planar single shank electrode arrays,” *J. Neurosci. Methods*, vol. 242, pp. 15–40, 2015.

[24] G. Sharma *et al.*, “Time Stability and Coherence Analysis of Multiunit , Single-Unit and Local Field Potential Neuronal Signals in Chronically Implanted Brain Electrodes,” *Bioelectron. Med.*, vol. 2, pp. 63–71, 2015.

[25] V. S. Polikov, P. A. Tresco, and W. M. Reichert, “Response of brain tissue to chronically implanted neural electrodes.,” *J. Neurosci. Methods*, vol. 148, no. 1, pp. 1–18, Oct. 2005.

[26] W. He and R. Bellamkonda, “A Molecular Perspective on Understanding and Modulating the Performance of Chronic Central Nervous System (CNS) Recording Electrodes,” in *Indwelling Neural Implants: Strategies for Contending with the In Vivo Environment (Frontiers in Neuroscience)*, W. Reichert, Ed. CRC Press, 2008.

[27] B. D. Winslow and P. a. Tresco, “Quantitative analysis of the tissue response to chronically implanted microwire electrodes in rat cortex.,” *Biomaterials*, vol. 31, no. 7, pp. 1558–67, Mar. 2010.

[28] B. V Zlokovic, “Neurovascular pathways to neurodegeneration in Alzheimer’s disease and other disorders.,” *Nat. Rev. Neurosci.*, vol. 12, no. 12, pp. 723–38, Dec. 2011.

[29] N. J. Abbott, L. Rönnbäck, and E. Hansson, “Astrocyte-endothelial interactions at the blood-brain barrier.,” *Nat. Rev. Neurosci.*, vol. 7, no. 1, pp. 41–53, Jan. 2006.

[30] K. E. Sandoval and K. a Witt, “Blood-brain barrier tight junction permeability and ischemic stroke.,” *Neurobiol. Dis.*, vol. 32, no. 2, pp. 200–19, Nov. 2008.

[31] D. Davalos *et al.*, “Fibrinogen-induced perivascular microglial clustering is required for the development of axonal damage in neuroinflammation.,” *Nat. Commun.*, vol. 3, p. 1227, Jan. 2012.

[32] S. Bardehle, V. a. Rafalski, and K. Akassoglou, “Breaking boundaries—coagulation and fibrinolysis at the neurovascular interface,” *Front. Cell. Neurosci.*, vol. 9, no. September, pp. 1–9, 2015.

[33] J. Greenwood, S. J. Heasman, J. I. Alvarez, A. Prat, R. Lyck, and B. Engelhardt, “Review: Leucocyte-endothelial cell crosstalk at the blood-brain barrier: A prerequisite for successful immune cell entry to the brain,” *Neuropathol. Appl. Neurobiol.*, vol. 37, no. 1, pp. 24–39, 2011.

[34] R. Shechter, A. London, and M. Schwartz, “Orchestrated leukocyte recruitment to immune-privileged sites: absolute barriers versus educational gates.,” *Nat. Rev. Immunol.*, vol. 13, no. 3, pp. 206–18, Mar. 2013.

[35] S. Bose and J. Cho, “Role of chemokine CCL2 and its receptor CCR2 in neurodegenerative diseases,” *Arch. Pharm. Res.*, vol. 36, no. 9, pp. 1039–1050, 2013.

[36] H. X. Chu, T. V Arumugam, M. Gelderblom, T. Magnus, G. R. Drummond, and C. G. Sobey, “Role of CCR2 in inflammatory conditions of the central nervous system.,” *J. Cereb. Blood Flow Metab.*, vol. 34, no. 9, pp. 1425–9, Sep. 2014.

[37] B. D. Semple, T. Kossmann, and M. C. Morganti-Kossmann, “Role of chemokines in CNS health and pathology: a focus on the CCL2/CCR2 and CXCL8/CXCR2 networks.,” *J. Cereb. Blood Flow Metab.*, vol. 30, no. 3, pp. 459–473, 2010.

[38] G. Conductier, N. Blondeau, A. Guyon, J. L. Nahon, and C. Rov??re, “The role of monocyte chemoattractant protein MCP1/CCL2 in neuroinflammatory diseases,” *J. Neuroimmunol.*, vol. 224, no. 1–2, pp. 93–100, 2010.

[39] S. M. Stamatovic, R. F. Keep, S. L. Kunkel, and A. V Andjelkovic, “Potential role of MCP-1 in endothelial cell tight junction ‘opening’: signaling via Rho and Rho kinase.,” *J. Cell Sci.*, vol. 116, no. Pt 22, pp. 4615–4628, 2003.

[40] O. B. Dimitrijevic, S. M. Stamatovic, R. F. Keep, and A. V Andjelkovic, “Effects of the chemokine CCL2 on blood-brain barrier permeability during ischemia-reperfusion injury,” *J Cereb Blood Flow Metab*, vol. 26, no. 6, pp. 797–810, 2006.

[41] S. M. Stamatovic *et al.*, “Monocyte chemoattractant protein-1 regulation of blood-brain barrier permeability.,” *J. Cereb. Blood Flow Metab.*, vol. 25, no. 5, pp. 593–606, 2005.

[42] J. A. Perge *et al.*, “Reliability of directional information in unsorted spikes and local field potentials recorded in human motor cortex.,” *J. Neural Eng.*, vol. 11, no. 4, pp. 1–14, Jun. 2014.

[43] J. D. Simeral, S.-P. Kim, M. J. Black, J. P. Donoghue, and L. R. Hochberg, “Neural control of cursor trajectory and click by a human with tetraplegia 1000 days after implant of an intracortical microelectrode array.,” *J. Neural Eng.*, vol. 8, no. 2, pp. 1–24, Apr. 2011.

[44] E. Başar, C. Başar-Eroglu, S. Karakaş, and M. Schürmann, “Gamma, alpha, delta, and theta oscillations govern cognitive processes,” *Int. J. Psychophysiol.*, vol. 39, no. 2–3, pp. 241–248, Jan. 2001.

[45] S. P. Kim, J. D. Simeral, L. R. Hochberg, J. P. Donoghue, and M. J. Black, “Neural control of computer cursor velocity by decoding motor cortical spiking activity in humans with tetraplegia,” *J. Neural Eng.*, vol. 5, no. 4, p. 455, 2008.

[46] D. A. Friedenberg *et al.*, “Neuroprosthetic-enabled control of graded arm muscle contraction in a paralyzed human,” *Sci. Rep.*, vol. 7, no. 1, p. 8386, 2017.

[47] E. K. Chadwick *et al.*, “Continuous neuronal ensemble control of simulated arm reaching by a human with tetraplegia,” *J. Neural Eng.*, vol. 8, no. 3, p. 34003, Jun. 2011.

[48] D. A. Nowak, J. Hermsdörfer, S. Glasauer, J. Philipp, L. Meyer, and N. Mai, “The effects of digital anaesthesia on predictive grip force adjustments during vertical movements of a grasped object,” *Eur. J. Neurosci.*, vol. 14, no. 4, pp. 756–762, Aug. 2002.

[49] R. S. Johansson and G. Westling, “Signals in tactile afferents from the fingers eliciting adaptive motor responses during precision grip,” *Exp. Brain Res.*, vol. 66, no. 1, pp. 141–154, Mar. 1987.

[50] R. S. Johansson and J. R. Flanagan, “Coding and use of tactile signals from the fingertips in object manipulation tasks,” *Nat. Rev. Neurosci.*, vol. 10, no. 5, pp. 345–359, May 2009.

[51] K. V. Shenoy and J. M. Carmena, “Combining decoder design and neural adaptation in brain-machine interfaces,” *Neuron*, vol. 84, no. 4, pp. 665–680, 2014.

[52] N. F. Nolta, M. B. Christensen, P. D. Crane, J. L. Skousen, and P. A. Tresco, “BBB leakage, astrogliosis, and tissue loss correlate with silicon microelectrode array recording performance,” *Biomaterials*, vol. 53, pp. 753–762, 2015.

[53] D. Mccreery, S. Cogan, S. Kane, and V. Pikov, “Correlations between histology and neuronal activity recorded by microelectrodes implanted chronically in the cerebral cortex,” *J. Neural Eng.*, vol. 13, no. 3, pp. 1–17, 2016.

[54] J. C. Barrese *et al.*, “Failure mode analysis of silicon-based intracortical microelectrode arrays in non-human primates.,” *J. Neural Eng.*, vol. 10, no. 6, pp. 1–23, Nov. 2013.

[55] A. Prasad *et al.*, “Comprehensive characterization and failure modes of tungsten microwire arrays in chronic neural implants,” *J. Neural Eng.*, vol. 9, no. 5, p. 56015, Oct. 2012.

[56] A. Prasad *et al.*, “Abiotic-biotic characterization of Pt/Ir microelectrode arrays in chronic implants.,” *Front. Neuroeng.*, vol. 7, no. February, p. 2, Jan. 2014.

[57] T. D. Y. Kozai *et al.*, “Mechanical failure modes of chronically implanted planar silicon-based neural probes for laminar recording,” *Biomaterials*, pp. 1–15, Oct. 2014.

[58] J. C. Barrese, J. Aceros, and J. P. Donoghue, “Scanning electron microscopy of chronically implanted intracortical microelectrode arrays in non-human primates,” *J. Neural Eng.*, vol. 13, no. 2, p. 26003, Apr. 2016.

[59] P. Takmakov, K. Ruda, K. Scott Phillips, I. S. Isayeva, V. Krauthamer, and C. G. Welle, “Rapid evaluation of the durability of cortical neural implants using accelerated aging with reactive oxygen species,” *J. Neural Eng.*, vol. 12, no. 2, p. 26003, Apr. 2015.

[60] T. D. Y. Kozai *et al.*, “Effects of caspase-1 knockout on chronic neural recording quality and longevity: Insight into cellular and molecular mechanisms of the reactive tissue response.,” *Biomaterials*, pp. 1–15, Aug. 2014.

[61] A. Gilletti and J. Muthuswamy, “Brain micromotion around implants in the rodent somatosensory cortex,” *J. Neural Eng.*, vol. 3, no. 3, pp. 189–195, Sep. 2006.

[62] A. Sridharan, S. D. Rajan, and J. Muthuswamy, “Long-term changes in the material properties of brain tissue at the implant-tissue interface.,” *J. Neural Eng.*, vol. 10,

no. 6, p. 66001, Oct. 2013.

[63] H. Lee, R. V Bellamkonda, W. Sun, and M. E. Levenston, “Biomechanical analysis of silicon microelectrode-induced strain in the brain.,” *J. Neural Eng.*, vol. 2, no. 4, pp. 81–9, Dec. 2005.

[64] J. Subbaroyan, D. C. Martin, and D. R. Kipke, “A finite-element model of the mechanical effects of implantable microelectrodes in the cerebral cortex,” *J. Neural Eng.*, vol. 2, no. 4, pp. 103–113, 2005.

[65] J. K. Nguyen *et al.*, “Mechanically-compliant intracortical implants reduce the neuroinflammatory response.,” *J. Neural Eng.*, vol. 11, no. 5, pp. 1–15, Oct. 2014.

[66] J. P. Harris *et al.*, “Mechanically adaptive intracortical implants improve the proximity of neuronal cell bodies.,” *J. Neural Eng.*, vol. 8, no. 6, p. 66011, Nov. 2011.

[67] T. Suzuki, K. Mabuchi, and S. Takeuchi, “A 3D flexible parylene probe array for multichannel neural recording,” in *First International IEEE EMBS Conference on Neural Engineering, 2003. Conference Proceedings.*, pp. 154–156.

[68] T. Ware *et al.*, “Thiol-ene/acrylate substrates for softening intracortical electrodes.,” *J. Biomed. Mater. Res. B. Appl. Biomater.*, vol. 102, no. 1, pp. 1–11, Jan. 2014.

[69] T. D. Y. Kozai *et al.*, “Ultrasmall implantable composite microelectrodes with bioactive surfaces for chronic neural interfaces,” *Nat. Mater.*, vol. 11, no. 11, pp. 1–9, Nov. 2012.

[70] P. R. Patel *et al.*, “Insertion of linear 8.4 μ m diameter 16 channel carbon fiber electrode arrays for single unit recordings,” *J. Neural Eng.*, vol. 12, no. 4, p. 46009, 2015.

[71] H. S. Sohal *et al.*, “The sinusoidal probe: a new approach to improve electrode longevity,” *Front. Neuroeng.*, vol. 7, no. April, pp. 1–14, 2014.

[72] C. L. Kolarcik *et al.*, “Elastomeric and soft conducting microwires for implantable neural interfaces,” *Soft Matter*, vol. 11, no. 24, pp. 4847–4861, Jun. 2015.

[73] W. Shen *et al.*, “Extracellular matrix-based intracortical microelectrodes: Toward a microfabricated neural interface based on natural materials,” *Microsystems Nanoeng.*, vol. 1, 2015.

[74] T. Kozai and D. Kipke, “Insertion shuttle with carboxyl terminated self-assembled monolayer coatings for implanting flexible polymer neural probes in the brain,” *J. Neurosci. Methods*, vol. 184, no. 2, pp. 199–205, 2009.

[75] D. Lewitus, K. L. Smith, W. Shain, and J. Kohn, “Ultrafast resorbing polymers for use as carriers for cortical neural probes,” *Acta Biomater.*, vol. 7, no. 6, pp. 2483–

2491, 2011.

[76] G. C. McConnell, R. J. Butera, and R. V Bellamkonda, “Bioimpedance modeling to monitor astrocytic response to chronically implanted electrodes.,” *J. Neural Eng.*, vol. 6, no. 5, p. 55005, Oct. 2009.

[77] A. Y. Shih *et al.*, “The smallest stroke: occlusion of one penetrating vessel leads to infarction and a cognitive deficit,” *Nat. Neurosci.*, vol. 16, no. 1, pp. 55–63, Dec. 2012.

[78] Chipolla, “Chapter 2 Anatomy and ultrastructure,” *Boek*, no. Figure 3, pp. 3–8, 2009.

[79] Cipolla MJ., “Chapter 6 Barriers of the CNS,” in *The Cerebral Circulation.*, Morgan & Claypool Life Sciences, 2009, pp. 185–187.

[80] N. J. Abbott, A. a K. Patabendige, D. E. M. Dolman, S. R. Yusof, and D. J. Begley, “Structure and function of the blood-brain barrier.,” *Neurobiol. Dis.*, vol. 37, no. 1, pp. 13–25, Jan. 2010.

[81] S. Tietz and B. Engelhardt, “Brain barriers: Crosstalk between complex tight junctions and adherens junctions.,” *J. Cell Biol.*, vol. 209, no. 4, pp. 493–506, 2015.

[82] G. Bergers and S. Song, “The role of pericytes in blood-vessel formation and maintenance.,” *Neuro. Oncol.*, vol. 7, no. 4, pp. 452–64, Oct. 2005.

[83] G. E. Barreto, J. Gonzalez, Y. Torres, and L. Morales, “Astrocytic-neuronal crosstalk: Implications for neuroprotection from brain injury.,” *Neurosci. Res.*, vol. 71, no. 2, pp. 107–13, Oct. 2011.

[84] B. Obermeier, R. Daneman, and R. M. Ransohoff, “Development, maintenance and disruption of the blood-brain barrier.,” *Nat. Med.*, vol. 19, no. 12, pp. 1584–96, Dec. 2013.

[85] S. E. Lakhan, A. Kirchgessner, D. Tepper, and A. Leonard, “Matrix metalloproteinases and blood-brain barrier disruption in acute ischemic stroke.,” *Front. Neurol.*, vol. 4, no. 32, pp. 1–15, Jan. 2013.

[86] J. K. Ryu *et al.*, “Blood coagulation protein fibrinogen promotes autoimmunity and demyelination via chemokine release and antigen presentation,” *Nat. Commun.*, vol. 6, p. 8164, Sep. 2015.

[87] A. P. Sagare *et al.*, “Pericyte loss influences Alzheimer-like neurodegeneration in mice,” *Nat. Commun.*, vol. 4, pp. 1–14, Dec. 2013.

[88] J. I. Alvarez *et al.*, “Focal disturbances in the blood-brain barrier are associated with formation of neuroinflammatory lesions,” *Neurobiol. Dis.*, vol. 74, no. November, pp. 14–24, 2015.

[89] E. Seiffert *et al.*, “Lasting blood-brain barrier disruption induces epileptic focus in the rat somatosensory cortex.,” *J. Neurosci.*, vol. 24, no. 36, pp. 7829–7836, Sep. 2004.

[90] E. A. van Vliet *et al.*, “Blood-brain barrier leakage may lead to progression of temporal lobe epilepsy.,” *Brain*, vol. 130, no. Pt 2, pp. 521–534, Mar. 2007.

[91] S. Ivens *et al.*, “TGF-beta receptor-mediated albumin uptake into astrocytes is involved in neocortical epileptogenesis.,” *Brain*, vol. 130, no. Pt 2, pp. 535–47, Feb. 2007.

[92] G. A. Rosenberg and Y. Yang, “Vasogenic edema due to tight junction disruption by matrix metalloproteinases in cerebral ischemia.,” *Neurosurg. Focus*, vol. 22, no. 5, p. E4, May 2007.

[93] D. Wang, S.-P. Li, J.-S. Fu, S. Zhang, L. Bai, and L. Guo, “Resveratrol defends blood-brain barrier integrity in experimental autoimmune encephalomyelitis mice,” *J. Neurophysiol.*, vol. 116, no. 5, pp. 2173–2179, Nov. 2016.

[94] C. Moussa *et al.*, “Resveratrol regulates neuro-inflammation and induces adaptive immunity in Alzheimer’s disease,” *J. Neuroinflammation*, vol. 14, no. 1, p. 1, 2017.

[95] A. Y. Sun, Q. Wang, A. Simonyi, and G. Y. Sun, “Resveratrol as a therapeutic agent for neurodegenerative diseases.,” *Mol. Neurobiol.*, vol. 41, no. 2–3, pp. 375–83, Jun. 2010.

[96] P. B. L. Pun, J. Lu, and S. Moochhala, “Involvement of ROS in BBB dysfunction.,” *Free Radic. Res.*, vol. 43, no. 4, pp. 348–64, Apr. 2009.

[97] M. S. Lin, Y. H. Lee, W. T. Chiu, and K. S. Hung, “Curcumin provides neuroprotection after spinal cord injury,” *J. Surg. Res.*, vol. 166, no. 2, pp. 280–289, 2011.

[98] J. Jiang, W. Wang, Y. J. Sun, M. Hu, F. Li, and D. Y. Zhu, “Neuroprotective effect of curcumin on focal cerebral ischemic rats by preventing blood-brain barrier damage.,” *Eur. J. Pharmacol.*, vol. 561, no. 1–3, pp. 54–62, Apr. 2007.

[99] M. Thiyagarajan and S. S. Sharma, “Neuroprotective effect of curcumin in middle cerebral artery occlusion induced focal cerebral ischemia in rats,” *Life Sci.*, vol. 74, no. 8, pp. 969–985, 2004.

[100] T. Ishrat *et al.*, “Amelioration of cognitive deficits and neurodegeneration by curcumin in rat model of sporadic dementia of Alzheimer’s type (SDAT),” *Eur. Neuropsychopharmacol.*, vol. 19, no. 9, pp. 636–647, 2009.

[101] K. a Potter, M. Jorfi, K. T. Householder, E. J. Foster, C. Weder, and J. R. Capadona, “Curcumin-releasing mechanically adaptive intracortical implants improve the proximal neuronal density and blood-brain barrier stability.,” *Acta Biomater.*, vol.

10, no. 5, pp. 2209–22, May 2014.

[102] K. A. Potter, A. C. Buck, W. K. Self, M. E. Callanan, S. Sunil, and J. R. Capadona, "The effect of resveratrol on neurodegeneration and blood brain barrier stability surrounding intracortical microelectrodes.," *Biomaterials*, vol. 34, no. 29, pp. 7001–7015, Sep. 2013.

[103] K. A. Potter-Baker *et al.*, "Implications of chronic daily anti-oxidant administration on the inflammatory response to intracortical microelectrodes," *J. Neural Eng.*, vol. 12, no. 4, pp. 1–15, 2015.

[104] R. M. Friedlander *et al.*, "Inhibition of caspase-1 slows disease progression in a mouse model of Huntington's disease.," *Nature*, vol. 399, no. 6733, pp. 263–267, May 1999.

[105] R. M. Friedlander, "Role of Caspase 1 in Neurologic Disease," *Arch. Neurol.*, vol. 57, no. 9, pp. 1273–1276, Sep. 2000.

[106] R. M. Friedlander and J. Yuan, "ICE, neuronal apoptosis and neurodegeneration.," *Cell Death Differ.*, vol. 5, no. 10, pp. 823–31, 1998.

[107] H. Hara *et al.*, "Inhibition of interleukin 1beta converting enzyme family proteases reduces ischemic and excitotoxic neuronal damage.," *Proc. Natl. Acad. Sci. U. S. A.*, vol. 94, no. 5, pp. 2007–12, 1997.

[108] H. Hara *et al.*, "Attenuation of transient focal cerebral ischemic injury in transgenic mice expressing a mutant ICE inhibitory protein.," *J. Cereb. Blood Flow Metab.*, vol. 17, no. 4, pp. 370–5, Apr. 1997.

[109] R. Rennaker and J. Miller, "Minocycline increases quality and longevity of chronic neural recordings," *J. neural …*, vol. 4, no. 2, pp. 1–10, 2007.

[110] E. J. Su *et al.*, "Activation of PDGF-CC by tissue plasminogen activator impairs blood-brain barrier integrity during ischemic stroke.," *Nat. Med.*, vol. 14, no. 7, pp. 731–737, Jul. 2008.

[111] A. Armulik *et al.*, "Pericytes regulate the blood-brain barrier.," *Nature*, vol. 468, no. 7323, pp. 557–561, Dec. 2010.

[112] M. Z. Adzemovic, M. Zeitelhofer, U. Eriksson, T. Olsson, and I. Nilsson, "Imatinib ameliorates neuroinflammation in a rat model of multiple sclerosis by enhancing blood-brain barrier integrity and by modulating the peripheral immune response.," *PLoS One*, vol. 8, no. 2, pp. 1–15, Jan. 2013.

[113] M. B. Abrams *et al.*, "Imatinib enhances functional outcome after spinal cord injury.," *PLoS One*, vol. 7, no. 6, pp. 1–12, Jan. 2012.

[114] E. Tejima *et al.*, "Astrocytic induction of matrix metalloproteinase-9 and edema in

brain hemorrhage.," *J. Cereb. Blood Flow Metab.*, vol. 27, no. 3, pp. 460–8, Mar. 2007.

[115] C.-M. Yang, H.-L. Hsieh, P.-H. Yu, C.-C. Lin, and S.-W. Liu, "IL-1β Induces MMP-9-Dependent Brain Astrocytic Migration via Transactivation of PDGF Receptor/NADPH Oxidase 2-Derived Reactive Oxygen Species Signals.," *Mol. Neurobiol.*, Aug. 2014.

[116] C.-Y. Wu, H.-L. Hsieh, C.-C. Sun, C.-P. Tseng, and C.-M. Yang, "IL-1 beta induces proMMP-9 expression via c-Src-dependent PDGFR/PI3K/Akt/p300 cascade in rat brain astrocytes.," *J. Neurochem.*, vol. 105, no. 4, pp. 1499–512, May 2008.

[117] Q. Ma *et al.*, "PDGFR-α inhibition preserves blood-brain barrier after intracerebral hemorrhage.," *Ann. Neurol.*, vol. 70, no. 6, pp. 920–931, Dec. 2011.

[118] G. Bergers, S. Song, N. Meyer-Morse, E. Bergsland, and D. Hanahan, "Benefits of targeting both pericytes and endothelial cells in the tumor vasculature with kinase inhibitors.," *J. Clin. Invest.*, vol. 111, no. 9, pp. 1287–95, May 2003.

[119] J. Ruan *et al.*, "Imatinib disrupts lymphoma angiogenesis by targeting vascular pericytes," *Blood*, vol. 121, no. 26, pp. 5192–5202, Jun. 2013.

[120] K. Hosaka *et al.*, "Tumour PDGF-BB expression levels determine dual effects of anti-PDGF drugs on vascular remodelling and metastasis.," *Nat. Commun.*, vol. 4, p. 2129, Jan. 2013.

[121] J. L. Wilkinson-Berka *et al.*, "Inhibition of platelet-derived growth factor promotes pericyte loss and angiogenesis in ischemic retinopathy.," *Am. J. Pathol.*, vol. 164, no. 4, pp. 1263–73, Apr. 2004.

[122] M. Franco, P. Roswall, E. Cortez, D. Hanahan, and K. Pietras, "Pericytes promote endothelial cell survival through induction of autocrine VEGF-A signaling and Bcl-w expression.," *Blood*, vol. 118, no. 10, pp. 2906–17, Sep. 2011.

[123] G. Vlahovic *et al.*, "Treatment with imatinib improves drug delivery and efficacy in NSCLC xenografts.," *Br. J. Cancer*, vol. 97, no. 6, pp. 735–40, Sep. 2007.

[124] E. M. Chislock and A. M. Pendergast, "Abl family kinases regulate endothelial barrier function in vitro and in mice.," *PLoS One*, vol. 8, no. 12, pp. 1–17, Jan. 2013.

[125] J. Aman *et al.*, "Effective treatment of edema and endothelial barrier dysfunction with imatinib.," *Circulation*, vol. 126, no. 23, pp. 2728–38, Dec. 2012.

[126] J. Xu, M. Millard, X. Ren, O. T. Cox, and A. Erdreich-Epstein, "c-Abl mediates endothelial apoptosis induced by inhibition of integrins alphavbeta3 and alphavbeta5 and by disruption of actin.," *Blood*, vol. 115, no. 13, pp. 2709–18, Apr. 2010.

[127] R. S. Stephens, L. E. Servinsky, O. Rentsendorj, T. M. Kolb, A. Pfeifer, and D. B. Pearse, "Protein kinase G increases antioxidant function in lung microvascular endothelial cells by inhibiting the c-Abl tyrosine kinase.," *Am. J. Physiol. Cell Physiol.*, vol. 306, no. 6, pp. C559-69, Mar. 2014.

[128] Y. Nio *et al.*, "Monocyte chemoattractant protein-1 (MCP-1) deficiency enhances alternatively activated M2 macrophages and ameliorates insulin resistance and fatty liver in lipoatrophic diabetic A-ZIP transgenic mice," *Diabetologia*, vol. 55, no. 12, pp. 3350–3358, 2012.

[129] B. Lu *et al.*, "Abnormalities in monocyte recruitment and cytokine expression in monocyte chemoattractant protein 1-deficient mice.," *J. Exp. Med.*, vol. 187, no. 4, pp. 601–8, 1998.

[130] C. Shi and E. G. Pamer, "Monocyte recruitment during infection and inflammation.," *Nat. Rev. Immunol.*, vol. 11, no. 11, pp. 762–74, 2011.

[131] C. McManus, J. W. Berman, F. M. Brett, H. Staunton, M. Farrell, and C. F. Brosnan, "MCP-1, MCP-2 and MCP-3 expression in multiple sclerosis lesions: an immunohistochemical and in situ hybridization study," *J. Neuroimmunol.*, vol. 86, no. 1, pp. 20–29, 1998.

[132] J. Simpson, P. Rezaie, J. Newcombe, M. L. L. Cuzner, D. Male, and M. N. N. Woodroofe, "Expression of the β-chemokine receptors CCR2, CCR3 and CCR5 in multiple sclerosis central nervous system tissue," *J. Neuroimmunol.*, vol. 108, no. 1–2, pp. 192–200, 2000.

[133] B. T. Fife, G. B. Huffnagle, W. A. Kuziel, and W. J. Karpus, "Cc Chemokine Receptor 2 Is Critical for Induction of Experimental Autoimmune Encephalomyelitis," *J. Exp. Med.*, vol. 192, no. 6, pp. 899–906, Sep. 2000.

[134] D. Huang, J. Wang, P. Kivisakk, B. J. Rollins, and R. M. Ransohoff, "Absence of Monocyte Chemoattractant Protein 1 in Mice Leads to Decreased Local Macrophage Recruitment and Antigen-Specific T Helper Cell Type 1 Immune Response in Experimental Autoimmune Encephalomyelitis," *J. Exp. Med.*, vol. 193, no. 6, pp. 713–726, Mar. 2001.

[135] A. R. Glabinski, M. Tani, V. K. Tuohy, R. J. Tuthill, and R. M. Ransohoff, "Central Nervous System Chemokine mRNA Accumulation Follows Initial Leukocyte Entry at the Onset of Acute Murine Experimental Autoimmune Encephalomyelitis," *Brain. Behav. Immun.*, vol. 9, no. 4, pp. 315–330, 1995.

[136] A. Arakelyan, J. Petrkova, Z. Hermanova, A. Boyajyan, J. Lukl, and M. Petrek, "Serum Levels of the MCP-1 Chemokine in Patients With Ischemic Stroke and Myocardial Infarction," *Mediators Inflamm.*, vol. 2005, no. 3, pp. 175–179, 2005.

[137] J. Zaremba and J. Losy, "Early TNF-alpha levels correlate with ischaemic stroke severity," *Acta Neurol. Scand.*, vol. 104, no. 5, pp. 288–295, Nov. 2001.

[138] O. B. Dimitrijevic, S. M. Stamatovic, R. F. Keep, and A. V. Andjelkovic, “Absence of the chemokine receptor CCR2 protects against cerebral ischemia/reperfusion injury in mice,” *Stroke*, vol. 38, no. 4, pp. 1345–1353, 2007.

[139] Y. Chen *et al.*, “Overexpression of monocyte chemoattractant protein 1 in the brain exacerbates ischemic brain injury and is associated with recruitment of inflammatory cells.,” *J. Cereb. Blood Flow Metab.*, vol. 23, no. 6, pp. 748–55, Jun. 2003.

[140] B. D. Semple, N. Bye, M. Rancan, J. M. Ziebell, and M. C. Morganti-Kossmann, “Role of CCL2 (MCP-1) in traumatic brain injury (TBI): evidence from severe TBI patients and CCL2-/- mice.,” *J. Cereb. Blood Flow Metab.*, vol. 30, no. 4, pp. 769–82, 2010.

[141] S. Gyoneva, D. Kim, A. Katsumoto, O. N. Kokiko-Cochran, B. T. Lamb, and R. M. Ransohoff, “Ccr2 deletion dissociates cavity size and tau pathology after mild traumatic brain injury,” *J. Neuroinflammation*, vol. 12, no. 1, p. 228, 2015.

[142] L. Song and J. S. Pachter, “Monocyte chemoattractant protein-1 alters expression of tight junction-associated proteins in brain microvascular endothelial cells,” *Microvasc. Res.*, vol. 67, no. 1, pp. 78–89, 2004.

[143] P. Italiani and D. Boraschi, “From monocytes to M1/M2 macrophages: Phenotypical vs. functional differentiation,” *Front. Immunol.*, vol. 5, no. OCT, pp. 1–22, 2014.

[144] N. Mokarram and R. V. Bellamkonda, “Overcoming endogenous constraints on neuronal regeneration,” *IEEE Trans. Biomed. Eng.*, vol. 58, no. 7, pp. 1900–1906, 2011.

[145] D. Strauss-Ayali, S. M. Conrad, and D. M. Mosser, “Monocyte subpopulations and their differentiation patterns during infection.,” *J. Leukoc. Biol.*, vol. 82, no. 2, pp. 244–52, Aug. 2007.

[146] S. David and A. Kroner, “Repertoire of microglial and macrophage responses after spinal cord injury,” *Nat. Rev. Neurosci.*, vol. 12, no. 7, pp. 388–399, 2011.

[147] M. Ravikumar *et al.*, “The roles of blood-derived macrophages and resident microglia in the neuroinflammatory response to implanted Intracortical microelectrodes.,” *Biomaterials*, vol. 35, no. 28, pp. 8049–64, Sep. 2014.

[148] X.-J. Feng, B. Greenwald, H. Rabitz, E. Shea-Brown, and R. Kosut, “Toward closed-loop optimization of deep brain stimulation for Parkinson’s disease: concepts and lessons from a computational model.,” *J. Neural Eng.*, vol. 4, no. 2, pp. L14–L21, Jun. 2007.

[149] J. N. Turner *et al.*, “Cerebral astrocyte response to micromachined silicon implants.,” *Exp. Neurol.*, vol. 156, no. 1, pp. 33–49, 1999.

[150] R. D. Bell and B. V Zlokovic, “Neurovascular mechanisms and blood-brain barrier disorder in Alzheimer’s disease.,” *Acta Neuropathol.*, vol. 118, no. 1, pp. 103–13, Jul. 2009.

[151] A. Srinivasan *et al.*, “A regenerative microchannel device for recording multiple single-unit action potentials in awake, ambulatory animals,” *Eur. J. Neurosci.*, vol. 43, no. 3, pp. 474–485, 2016.

[152] C. T. Nordhausen, E. M. Maynard, and R. a Normann, “Single unit recording capabilities of a 100 microelectrode array.,” *Brain Res.*, vol. 726, no. 1–2, pp. 129–40, Jul. 1996.

[153] S. Suner, M. R. Fellows, C. Vargas-Irwin, G. K. Nakata, and J. P. Donoghue, “Reliability of signals from a chronically implanted, silicon-based electrode array in non-human primate primary motor cortex.,” *IEEE Trans. neural Syst. Rehabil. Eng.*, vol. 13, no. 4, pp. 524–41, Dec. 2005.

[154] J. Schindelin *et al.*, “Fiji: an open-source platform for biological-image analysis,” *Nat. Methods*, vol. 9, no. 7, pp. 676–682, Jun. 2012.

[155] R. Gillitzer and M. Goebeler, “Chemokines in cutaneous wound healing.,” *J. Leukoc. Biol.*, vol. 69, no. 4, pp. 513–21, Apr. 2001.

[156] O. Dewald, “CCL2/Monocyte Chemoattractant Protein-1 Regulates Inflammatory Responses Critical to Healing Myocardial Infarcts,” *Circ. Res.*, vol. 96, no. 8, pp. 881–889, Mar. 2005.

[157] T. R. Kyriakides *et al.*, “The CC Chemokine Ligand, CCL2/MCP1, Participates in Macrophage Fusion and Foreign Body Giant Cell Formation,” *Am. J. Pathol.*, vol. 165, no. 6, pp. 2157–2166, 2004.

[158] J. M. Anderson, A. Rodriguez, and D. T. Chang, “Foreign body reaction to biomaterials,” *Semin. Immunol.*, vol. 20, no. 2, pp. 86–100, Apr. 2008.

[159] P. R. Castro *et al.*, “Deletion of the chemokine receptor CCR2 attenuates foreign body reaction to implants in mice,” *Microvasc. Res.*, vol. 95, no. 1, pp. 37–45, 2014.

[160] D. J. Mahad and R. M. Ransohoff, “The role of MCP-1 (CCL2) and CCR2 in multiple sclerosis and experimental autoimmune encephalomyelitis (EAE),” *Seminars in Immunology*, vol. 15, no. 1. Academic Press, pp. 23–32, 01-Feb-2003.

[161] M. Moreno *et al.*, “Conditional Ablation of Astroglial CCL2 Suppresses CNS Accumulation of M1 Macrophages and Preserves Axons in Mice with MOG Peptide EAE,” *J. Neurosci.*, vol. 34, no. 24, pp. 8175–8185, Jun. 2014.

[162] T. Kiyota *et al.*, “CCL2 Accelerates Microglia-Mediated Aβ Oligomer Formation and Progression of Neurocognitive Dysfunction,” *PLoS One*, vol. 4, no. 7, p. e6197, Jul. 2009.

[163] S. Liu, L. Zhang, Q. Wu, Q. Wu, and T. Wang, "Chemokine CCL2 Induces Apoptosis in Cortex Following Traumatic Brain Injury," *J. Mol. Neurosci.*, vol. 51, no. 3, pp. 1021–1029, Nov. 2013.

[164] N. Tei *et al.*, "Expression of MCP-1 and fractalkine on endothelial cells and astrocytes may contribute to the invasion and migration of brain macrophages in ischemic rat brain lesions," *J. Neurosci. Res.*, vol. 91, no. 5, pp. 681–693, 2013.

[165] N. H. Varvel *et al.*, "Infiltrating monocytes promote brain inflammation and exacerbate neuronal damage after status epilepticus," *Proc. Natl. Acad. Sci.*, vol. 113, no. 38, pp. E5665–E5674, Sep. 2016.

[166] D.-S. Tian *et al.*, "Chemokine CCL2–CCR2 Signaling Induces Neuronal Cell Death via STAT3 Activation and IL-1β Production after Status Epilepticus," *J. Neurosci.*, vol. 37, no. 33, pp. 7878–7892, Aug. 2017.

[167] G. Buzsáki, "Large-scale recording of neuronal ensembles," *Nat. Neurosci.*, vol. 7, no. 5, pp. 446–451, 2004.

[168] T. D. Y. Kozai *et al.*, "Reduction of neurovascular damage resulting from microelectrode insertion into the cerebral cortex using in vivo two-photon mapping.," *J. Neural Eng.*, vol. 7, no. 4, pp. 1–12, Aug. 2010.

[169] S. M. Stamatovic, O. B. Dimitrijevic, R. F. Keep, and A. V. Andjelkovic, "Protein kinase C??-RhoA cross-talk in CCL2-induced alterations in brain endothelial permeability," *J. Biol. Chem.*, vol. 281, no. 13, pp. 8379–8388, 2006.

[170] K. S. Weber, P. J. Nelson, H. J. Gröne, and C. Weber, "Expression of CCR2 by endothelial cells : implications for MCP-1 mediated wound injury repair and In vivo inflammatory activation of endothelium.," *Arterioscler. Thromb. Vasc. Biol.*, vol. 19, no. 9, pp. 2085–93, Sep. 1999.

[171] K. A. Dzenko, L. Song, S. Ge, W. A. Kuziel, and J. S. Pachter, "CCR2 expression by brain microvascular endothelial cells is critical for macrophage transendothelial migration in response to CCL2," *Microvasc. Res.*, vol. 70, no. 1–2, pp. 53–64, Jul. 2005.

[172] K. H. Hong *et al.*, "Monocyte chemoattractant protein-1-induced angiogenesis is mediated by vascular endothelial growth factor-A.," *Blood*, vol. 105, no. 4, pp. 1405–7, Feb. 2005.

[173] V. Rigau *et al.*, "Angiogenesis is associated with blood-brain barrier permeability in temporal lobe epilepsy.," *Brain*, vol. 130, no. Pt 7, pp. 1942–56, Jul. 2007.

[174] Z. G. Zhang *et al.*, "VEGF enhances angiogenesis and promotes blood-brain barrier leakage in the ischemic brain.," *J. Clin. Invest.*, vol. 106, no. 7, pp. 829–38, Oct. 2000.

[175] Y. Yang *et al.*, “Early inhibition of MMP activity in ischemic rat brain promotes expression of tight junction proteins and angiogenesis during recovery.,” *J. Cereb. Blood Flow Metab.*, vol. 33, no. 7, pp. 1104–14, Jul. 2013.

[176] P. C. Iwen and N. G. Miller, “Enhancement of ketoconazole penetration across the blood-brain barrier of mice by dimethyl sulfoxide.,” *Antimicrob. Agents Chemother.*, vol. 30, no. 4, pp. 617–8, Oct. 1986.

[177] W. M. Pardridge, “Blood-brain barrier delivery,” *Drug Discovery Today*, vol. 12, no. 1–2. Elsevier Current Trends, pp. 54–61, 01-Jan-2007.

[178] R. D. Broadwell, M. Salcman, and R. S. Kaplan, “Morphologic effect of dimethyl sulfoxide on the blood-brain barrier.,” *Science*, vol. 217, no. 4555, pp. 164–6, Jul. 1982.

[179] Y.-T. Kim, R. W. Hitchcock, M. J. Bridge, and P. a Tresco, “Chronic response of adult rat brain tissue to implants anchored to the skull,” *Biomaterials*, vol. 25, no. 12, pp. 2229–2237, May 2004.

[180] R. Biran, D. C. Martin, and P. A. Tresco, “The brain tissue response to implanted silicon microelectrode arrays is increased when the device is tethered to the skull,” *J. Biomed. Mater. Res. Part A*, vol. 82A, no. 1, pp. 169–178, Jul. 2007.

[181] J. Thelin *et al.*, “Implant size and fixation mode strongly influence tissue reactions in the CNS,” *PLoS One*, vol. 6, no. 1, 2011.

[182] R. J. Vetter, J. C. Williams, J. F. Hetke, E. a Nunamaker, and D. R. Kipke, “Chronic neural recording using silicon-substrate microelectrode arrays implanted in cerebral cortex.,” *IEEE Trans. Biomed. Eng.*, vol. 51, no. 6, pp. 896–904, Jun. 2004.

[183] T. D. Y. Kozai, J. R. Eles, A. L. Vazquez, and X. T. Cui, “Two-photon imaging of chronically implanted neural electrodes: Sealing methods and new insights,” *J. Neurosci. Methods*, vol. 258, pp. 46–55, 2016.

[184] B. V Zlokovic, “The blood-brain barrier in health and chronic neurodegenerative disorders.,” *Neuron*, vol. 57, no. 2, pp. 178–201, Jan. 2008.

[185] Y. Benjamini and Y. Hochberg, “Controlling the false discovery rate: a practical and powerful approach to multiple testing,” *Journal of the Royal Statistical Society B*, vol. 57, no. 1. pp. 289–300, 1995.

[186] M. A. Anderson *et al.*, “Astrocyte scar formation aids central nervous system axon regeneration.,” *Nature*, vol. 532, no. 7598, pp. 195–200, Apr. 2016.

[187] Z. Zhong *et al.*, “ALS-causing SOD1 mutants generate vascular changes prior to motor neuron degeneration.,” *Nat. Neurosci.*, vol. 11, no. 4, pp. 420–422, 2008.

[188] J. Liu, X. Jin, K. J. K. J. Liu, and W. Liu, “Matrix metalloproteinase-2-mediated

occludin degradation and caveolin-1-mediated claudin-5 redistribution contribute to blood-brain barrier damage in early ischemic stroke stage.," *J. Neurosci.*, vol. 32, no. 9, pp. 3044–57, Feb. 2012.

[189] A. T. Argaw, B. T. Gurfein, Y. Zhang, A. Zameer, and G. R. John, "VEGF-mediated disruption of endothelial CLN-5 promotes blood-brain barrier breakdown.," *Proc. Natl. Acad. Sci. U. S. A.*, vol. 106, no. 6, pp. 1977–1982, 2009.

[190] T. Kanda, Y. Numata, and H. Mizusawa, "Chronic inflammatory demyelinating polyneuropathy: decreased claudin-5 and relocated ZO-1.," *J. Neurol. Neurosurg. Psychiatry*, vol. 75, no. 5, pp. 765–769, May 2004.

[191] J. S. Henkel, D. R. Beers, S. Wen, R. Bowser, and S. H. Appel, "Decreased mRNA expression of tight junction proteins in lumbar spinal cords of patients with ALS," *Neurology*, vol. 72, no. 18, pp. 1614–1616, May 2009.

[192] D. Paul, A. E. Cowan, S. Ge, and J. S. Pachter, "Novel 3D analysis of Claudin-5 reveals significant endothelial heterogeneity among CNS microvessels.," *Microvasc. Res.*, vol. 86, pp. 1–10, Mar. 2013.

[193] Y. Wallez and P. Huber, "Endothelial adherens and tight junctions in vascular homeostasis, inflammation and angiogenesis," *Biochim. Biophys. Acta - Biomembr.*, vol. 1778, no. 3, pp. 794–809, 2008.

[194] M. Giannotta, M. Trani, and E. Dejana, "VE-cadherin and endothelial adherens junctions: Active guardians of vascular integrity," *Dev. Cell*, vol. 26, no. 5, pp. 441–454, 2013.

[195] M. Hellström *et al.*, "Role of PDGF-B and PDGFR-beta in recruitment of vascular smooth muscle cells and pericytes during embryonic blood vessel formation in the mouse.," *Development*, vol. 126, no. 14, pp. 3047–55, Jun. 1999.

[196] E. A. Winkler, R. D. Bell, and B. V Zlokovic, "Pericyte-specific expression of PDGF beta receptor in mouse models with normal and deficient PDGF beta receptor signaling.," *Mol. Neurodegener.*, vol. 5, p. 32, 2010.

[197] R. D. Bell *et al.*, "Pericytes control key neurovascular functions and neuronal phenotype in the adult brain and during brain aging.," *Neuron*, vol. 68, no. 3, pp. 409–27, Nov. 2010.

[198] M. R. Halliday *et al.*, "Accelerated pericyte degeneration and blood–brain barrier breakdown in apolipoprotein E4 carriers with Alzheimer's disease," *J. Cereb. Blood Flow Metab.*, no. November 2014, pp. 1–9, 2015.

[199] H. E. de Vries, G. Kooij, D. Frenkel, S. Georgopoulos, A. Monsonego, and D. Janigro, "Inflammatory events at blood-brain barrier in neuroinflammatory and neurodegenerative disorders: Implications for clinical disease," *Epilepsia*, vol. 53, pp. 45–52, Nov. 2012.

[200] M. Elahy *et al.*, "Blood-brain barrier dysfunction developed during normal aging is associated with inflammation and loss of tight junctions but not with leukocyte recruitment.," *Immun. Ageing*, vol. 12, p. 2, Jan. 2015.

[201] K. Boztug, M. J. Carson, N. Pham-Mitchell, V. C. Asensio, J. DeMartino, and I. L. Campbell, "Leukocyte Infiltration, But Not Neurodegeneration, in the CNS of Transgenic Mice with Astrocyte Production of the CXC Chemokine Ligand 10," *J. Immunol.*, vol. 169, no. 3, 2002.

[202] S. S. Shaftel, T. J. Carlson, J. A. Olschowka, S. Kyrkanides, S. B. Matousek, and M. K. O'Banion, "Chronic Interleukin-1β Expression in Mouse Brain Leads to Leukocyte Infiltration and Neutrophil-Independent Blood–Brain Barrier Permeability without Overt Neurodegeneration," *J. Neurosci.*, vol. 27, no. 35, 2007.

[203] N. Mokarram, A. Merchant, V. Mukhatyar, G. Patel, and R. V Bellamkonda, "Effect of modulating macrophage phenotype on peripheral nerve repair.," *Biomaterials*, vol. 33, no. 34, pp. 8793–801, Dec. 2012.

[204] K. a Kigerl, J. C. Gensel, D. P. Ankeny, J. K. Alexander, D. J. Donnelly, and P. G. Popovich, "Identification of two distinct macrophage subsets with divergent effects causing either neurotoxicity or regeneration in the injured mouse spinal cord.," *J. Neurosci.*, vol. 29, no. 43, pp. 13435–13444, Oct. 2009.

[205] Y. K. Kim, K. S. Na, A. M. Myint, and B. E. Leonard, "The role of pro-inflammatory cytokines in neuroinflammation, neurogenesis and the neuroendocrine system in major depression," *Prog. Neuro-Psychopharmacology Biol. Psychiatry*, vol. 64, pp. 277–284, 2016.

[206] D. Y. Vogel *et al.*, "Macrophages in inflammatory multiple sclerosis lesions have an intermediate activation status," *J. Neuroinflammation*, vol. 10, no. 1, p. 35, 2013.

[207] J. Mikita *et al.*, "Altered M1/M2 activation patterns of monocytes in severe relapsing experimental rat model of multiple sclerosis. Amelioration of clinical status by M2 activated monocyte administration.," *Mult. Scler.*, vol. 17, no. 1, pp. 2–15, 2011.

[208] J. D. Cherry, J. A. Olschowka, and M. O'Banion, "Neuroinflammation and M2 microglia: the good, the bad, and the inflamed," *J. Neuroinflammation*, vol. 11, no. 1, p. 98, 2014.

[209] Y. Tang and W. Le, "Differential Roles of M1 and M2 Microglia in Neurodegenerative Diseases," *Mol. Neurobiol.*, vol. 53, no. 2, pp. 1181–1194, 2016.

[210] M. Mäe, A. Armulik, and C. Betsholtz, "Getting to know the cast - cellular interactions and signaling at the neurovascular unit.," *Curr. Pharm. Des.*, vol. 17, no. 26, pp. 2750–4, Jan. 2011.

[211] R. D. Bell *et al.*, "Apolipoprotein E controls cerebrovascular integrity via cyclophilin A.," *Nature*, vol. 485, no. 7399, pp. 512–6, May 2012.

[212] J. Montaner *et al.*, "Matrix metalloproteinase-9 pretreatment level predicts intracranial hemorrhagic complications after thrombolysis in human stroke.," *Circulation*, vol. 107, no. 4, pp. 598–603, Feb. 2003.

[213] A. W. Clark, C. A. Krekoski, S. S. Bou, K. R. Chapman, and D. R. Edwards, "Increased gelatinase A (MMP-2) and gelatinase B (MMP-9) activities in human brain after focal ischemia," *Neurosci. Lett.*, vol. 238, no. 1–2, pp. 53–56, Nov. 1997.

[214] M. Asahi *et al.*, "Effects of matrix metalloproteinase-9 gene knock-out on the proteolysis of blood-brain barrier and white matter components after cerebral ischemia.," *J. Neurosci.*, vol. 21, no. 19, pp. 7724–32, Oct. 2001.

[215] J. Cui *et al.*, "Inhibition of MMP-9 by a selective gelatinase inhibitor protects neurovasculature from embolic focal cerebral ischemia.," *Mol. Neurodegener.*, vol. 7, no. 21, pp. 1–15, Jan. 2012.

[216] B.-Q. Zhao *et al.*, "Role of matrix metalloproteinases in delayed cortical responses after stroke.," *Nat. Med.*, vol. 12, no. 4, pp. 441–445, Apr. 2006.

[217] W. Tian and T. R. Kyriakides, "Matrix metalloproteinase-9 deficiency leads to prolonged foreign body response in the brain associated with increased IL-1beta levels and leakage of the blood-brain barrier.," *Matrix Biol.*, vol. 28, no. 3, pp. 148–59, Apr. 2009.

[218] V. Lucivero *et al.*, "Different roles of matrix metalloproteinases-2 and -9 after human ischaemic stroke," *Neurol. Sci.*, vol. 28, no. 4, pp. 165–170, Aug. 2007.

[219] I. M. Loftus *et al.*, "Increased matrix metalloproteinase-9 activity in unstable carotid plaques. A potential role in acute plaque disruption.," *Stroke*, vol. 31, no. 1, pp. 40–7, Jan. 2000.

[220] J.-Y. C. Hsu *et al.*, "Matrix metalloproteinase-2 facilitates wound healing events that promote functional recovery after spinal cord injury.," *J. Neurosci.*, vol. 26, no. 39, pp. 9841–9850, Sep. 2006.

[221] K. a Potter-Baker *et al.*, "A comparison of neuroinflammation to implanted microelectrodes in rat and mouse models.," *Biomaterials*, vol. 35, no. 22, pp. 5637–46, Jul. 2014.

[222] M. A. L. Nicolelis *et al.*, "Chronic, multisite, multielectrode recordings in macaque monkeys.," *Proc. Natl. Acad. Sci. U. S. A.*, vol. 100, no. 19, pp. 11041–6, Sep. 2003.

[223] I. M. Pomeroy, P. M. Matthews, J. a. Frank, E. K. Jordan, and M. M. Esiri, "Demyelinated neocortical lesions in marmoset autoimmune encephalomyelitis mimic those in multiple sclerosis," *Brain*, vol. 128, no. 11, pp. 2713–2721, 2005.

[224] T. Chitnis *et al.*, "Elevated neuronal expression of CD200 protects Wlds mice from inflammation-mediated neurodegeneration.," *Am. J. Pathol.*, vol. 170, no. 5, pp.

1695–1712, May 2007.

[225] S. Love, “Demyelinating diseases,” *J. Clin. Pathol.*, vol. 59, no. 11, pp. 1151–1159, Nov. 2006.

[226] M. Spadaro *et al.*, “Histopathology and clinical course of MOG-antibody-associated encephalomyelitis.,” *Ann. Clin. Transl. Neurol.*, vol. 2, no. 3, pp. 295–301, Mar. 2015.

[227] W. Lin *et al.*, “The integrated stress response prevents demyelination by protecting oligodendrocytes against immune-mediated damage,” *J. Clin. Invest.*, vol. 117, no. 2, pp. 448–456, Feb. 2007.

[228] P. Kozlowski, D. Raj, J. Liu, C. Lam, A. C. Yung, and W. Tetzlaff, “Characterizing White Matter Damage in Rat Spinal Cord with Quantitative MRI and Histology,” *J. Neurotrauma*, vol. 25, no. 6, pp. 653–676, Jun. 2008.

[229] Z. Xiang *et al.*, “Detection of myelination using a novel histological probe.,” *J. Histochem. Cytochem.*, vol. 53, no. 12, pp. 1511–6, Dec. 2005.

[230] J. E. A. Wells, “Neuroprotection by minocycline facilitates significant recovery from spinal cord injury in mice,” *Brain*, vol. 126, no. 7, pp. 1628–1637, Apr. 2003.

[231] T. Schallert, S. M. Fleming, J. L. Leasure, J. L. Tillerson, and S. T. Bland, “CNS plasticity and assessment of forelimb sensorimotor outcome in unilateral rat models of stroke, cortical ablation, parkinsonism and spinal cord injury,” *Neuropharmacology*, vol. 39, no. 5, pp. 777–787, Apr. 2000.

[232] H. Yaginuma *et al.*, “A novel type of programmed neuronal death in the cervical spinal cord of the chick embryo.,” *J. Neurosci.*, vol. 16, no. 11, pp. 3685–703, Jun. 1996.

[233] R. Abu Fanne *et al.*, “Blood-brain barrier permeability and tPA-mediated neurotoxicity.,” *Neuropharmacology*, vol. 58, no. 7, pp. 972–80, Jun. 2010.

[234] G. Yang *et al.*, “Neuronal MCP-1 mediates microglia recruitment and neurodegeneration induced by the mild impairment of oxidative metabolism.,” *Brain Pathol.*, vol. 21, no. 3, pp. 279–97, 2011.

[235] H. Chu, Y. Tang, and Q. Dong, “Protection of Vascular Endothelial Growth Factor to Brain Edema Following Intracerebral Hemorrhage and Its Involved Mechanisms: Effect of Aquaporin-4.,” *PLoS One*, vol. 8, no. 6, p. e66051, Jan. 2013.

[236] P. Wolinski and A. Glabinski, “Chemokines and neurodegeneration in the early stage of experimental ischemic stroke,” *Mediators Inflamm.*, vol. 2013, 2013.

[237] M. K. Schuhmann *et al.*, “CD28 superagonist-mediated boost of regulatory T cells increases thrombo-inflammation and ischemic neurodegeneration during the acute

phase of experimental stroke.," *J. Cereb. Blood Flow Metab.*, vol. 35, no. 1, pp. 6–10, Oct. 2014.

[238] M. Kramer *et al.*, "TTC staining of damaged brain areas after MCA occlusion in the rat does not constrict quantitative gene and protein analyses," *J. Neurosci. Methods*, vol. 187, no. 1, pp. 84–89, Mar. 2010.

[239] F. Liu, D. P. Schafer, and L. D. McCullough, "TTC, fluoro-Jade B and NeuN staining confirm evolving phases of infarction induced by middle cerebral artery occlusion.," *J. Neurosci. Methods*, vol. 179, no. 1, pp. 1–8, Apr. 2009.

[240] C.-C. Chen *et al.*, "Berberine Protects against Neuronal Damage via Suppression of Glia-Mediated Inflammation in Traumatic Brain Injury.," *PLoS One*, vol. 9, no. 12, p. e115694, Jan. 2014.

[241] E. D. Hall, Y. D. Bryant, W. Cho, and P. G. Sullivan, "Evolution of Post-Traumatic Neurodegeneration after Controlled Cortical Impact Traumatic Brain Injury in Mice and Rats as Assessed by the De Olmos Silver and Fluorojade Staining Methods," *J. Neurotrauma*, vol. 25, no. 3, pp. 235–247, Mar. 2008.

[242] D. J. Loane, A. Kumar, B. A. Stoica, R. Cabatbat, and A. I. Faden, "Progressive neurodegeneration after experimental brain trauma: association with chronic microglial activation.," *J. Neuropathol. Exp. Neurol.*, vol. 73, no. 1, pp. 14–29, Jan. 2014.

[243] D. A. Shear *et al.*, "Neural progenitor cell transplants promote long-term functional recovery after traumatic brain injury," *Brain Res.*, vol. 1026, no. 1, pp. 11–22, Nov. 2004.

[244] N. R. Saunders, K. M. Dziegielewska, K. Møllgård, and M. D. Habgood, "Markers for blood-brain barrier integrity: How appropriate is Evans blue in the twenty-first century and what are the alternatives?," *Front. Neurosci.*, vol. 9, no. OCT, pp. 1–16, 2015.

[245] A. Saria and J. M. Lundberg, "Evans blue fluorescence: quantitative and morphological evaluation of vascular permeability in animal tissues," *J. Neurosci. Methods*, vol. 8, no. 1, pp. 41–49, May 1983.

[246] J. Pelz *et al.*, "Endothelial barrier antigen-immunoreactivity is conversely associated with blood-brain barrier dysfunction after embolic stroke in rats.," *Eur. J. Histochem.*, vol. 57, no. 4, p. e38, Jan. 2013.

[247] A. J. Sawyer and T. R. Kyriakides, "Nanoparticle-based evaluation of blood-brain barrier leakage during the foreign body response.," *J. Neural Eng.*, vol. 10, no. 1, p. 16013, Jan. 2013.

[248] T. Saxena *et al.*, "Nanocarrier-mediated inhibition of macrophage migration inhibitory factor attenuates secondary injury after spinal cord injury," *ACS Nano*,

vol. 9, no. 2, pp. 1492–1505, 2015.

[249] Y. Yang, V. M. Salayandia, J. F. Thompson, L. Y. Yang, E. Y. Estrada, and Y. Yang, "Attenuation of acute stroke injury in rat brain by minocycline promotes blood–brain barrier remodeling and alternative microglia/macrophage activation during recovery," *J. Neuroinflammation*, vol. 12, no. 1, pp. 1–15, 2015.

[250] Z. Wang *et al.*, "Chronic valproate treatment enhances postischemic angiogenesis and promotes functional recovery in a rat model of ischemic stroke.," *Stroke.*, vol. 43, no. 9, pp. 2430–6, Sep. 2012.

[251] T. W. McAllister, L. A. Flashman, B. C. McDonald, and A. J. Saykin, "Mechanisms of Working Memory Dysfunction after Mild and Moderate TBI: Evidence from Functional MRI and Neurogenetics," *J. Neurotrauma*, vol. 23, no. 10, pp. 1450–1467, Oct. 2006.

[252] M. Filippi *et al.*, "Quantitative brain MRI lesion load predicts the course of clinically isolated syndromes suggestive of multiple sclerosis.," *Neurology*, vol. 44, no. 4, pp. 635–41, Apr. 1994.

[253] M. Kinoshita, N. McDannold, F. A. Jolesz, and K. Hynynen, "Targeted delivery of antibodies through the blood-brain barrier by MRI-guided focused ultrasound," *Biochem. Biophys. Res. Commun.*, vol. 340, no. 4, pp. 1085–1090, Feb. 2006.

[254] D. H. Carr *et al.*, "Gadolinium-DTPA as a contrast agent in MRI: Initial clinical experience in 20 patients," *Am. J. Roentgenol.*, vol. 143, no. 2, pp. 215–224, Aug. 1984.

[255] A. G. Kermode *et al.*, "Breakdown of the blood-brain barrier precedes symptoms and other mri signs of new lesions in multiple sclerosis: Pathogenetic and clinical implications," *Brain*, vol. 113, no. 5, pp. 1477–1489, Oct. 1990.

[256] P. S. Tofts and A. G. Kermode, "Measurement of the blood-brain barrier permeability and leakage space using dynamic MR imaging. 1. Fundamental concepts," *Magn. Reson. Med.*, vol. 17, no. 2, pp. 357–367, Feb. 1991.

[257] K. Wise, D. Anderson, J. Hetke, D. Kipke, and K. Najafi, "Wireless Implantable Microsystems : High-Density Electronic Interfaces to the Nervous System," *Proc. IEEE*, vol. 92, no. 1, pp. 76–97, 2004.

[258] S. R. Choi *et al.*, "Meningeal inflammation plays a role in the pathology of primary progressive multiple sclerosis," *Brain*, vol. 135, no. 10, pp. 2925–2937, Oct. 2012.

[259] R. Magliozzi *et al.*, "A Gradient of neuronal loss and meningeal inflammation in multiple sclerosis," *Ann. Neurol.*, vol. 68, no. 4, pp. 477–493, Oct. 2010.

[260] O. W. Howell *et al.*, "Meningeal inflammation is widespread and linked to cortical pathology in multiple sclerosis," *Brain*, vol. 134, no. 9, pp. 2755–2771, Sep. 2011.

[261] N. T. Markwardt, J. Stokol, and R. L. Rennaker, “Sub-meninges implantation reduces immune response to neural implants.,” *J. Neurosci. Methods*, vol. 214, no. 2, pp. 119–25, Apr. 2013.

[262] A. M. Jawad, R. Nordin, S. K. Gharghan, H. M. Jawad, and M. Ismail, “Opportunities and Challenges for Near-Field Wireless Power Transfer: A Review,” *Energies*, vol. 10, no. 7, p. 1022, 2017.

[263] A. M. Sodagar, K. D. Wise, and K. Najafi, “A wireless implantable microsystem for multichannel neural recording,” *IEEE Trans. Microw. Theory Tech.*, vol. 57, no. 10, pp. 2565–2573, 2009.

[264] C. S. Mestais, G. Charvet, F. Sauter-Starace, M. Foerster, D. Ratel, and A. L. Benabid, “WIMAGINE: Wireless 64-Channel ECoG Recording Implant for Long Term Clinical Applications,” *IEEE Trans. Neural Syst. Rehabil. Eng.*, vol. 23, no. 1, pp. 10–21, Jan. 2015.

[265] R. R. Harrison *et al.*, “A Low-Power Integrated Circuit for a Wireless 100-Electrode Neural Recording System,” *IEEE J. Solid-State Circuits*, vol. 42, no. 1, pp. 123–133, Jan. 2007.

[266] M. Kiani, Uei-Ming Jow, and M. Ghovanloo, “Design and Optimization of a 3-Coil Inductive Link for Efficient Wireless Power Transmission,” *IEEE Trans. Biomed. Circuits Syst.*, vol. 5, no. 6, pp. 579–591, Dec. 2011.

[267] D. Ahn and M. Ghovanloo, “Optimal Design of Wireless Power Transmission Links for Millimeter-Sized Biomedical Implants,” *IEEE Trans. Biomed. Circuits Syst.*, vol. 10, no. 1, pp. 125–137, 2016.

[268] D. Seo *et al.*, “Wireless Recording in the Peripheral Nervous System with Ultrasonic Neural Dust,” *Neuron*, vol. 91, no. 3, pp. 529–539, 2016.

[269] A. B. Schwartz, X. T. Cui, D. J. Weber, and D. W. Moran, “Brain-controlled interfaces: movement restoration with neural prosthetics.,” *Neuron*, vol. 52, no. 1, pp. 205–20, Oct. 2006.

[270] J. Viventi *et al.*, “Flexible, foldable, actively multiplexed, high-density electrode array for mapping brain activity in vivo,” *Nat. Neurosci.*, vol. 14, no. 12, pp. 1599–1605, Nov. 2011.

[271] D. Khodagholy *et al.*, “NeuroGrid: recording action potentials from the surface of the brain,” *Nat. Neurosci.*, vol. 18, no. 2, pp. 310–316, Dec. 2014.

[272] E. C. Leuthardt, G. Schalk, J. R. Wolpaw, J. G. Ojemann, and D. W. Moran, “A brain-computer interface using electrocorticographic signals in humans.,” *J. Neural Eng.*, vol. 1, no. 2, pp. 63–71, Jun. 2004.

[273] G. Schalk *et al.*, “Two-dimensional movement control using electrocorticographic

signals in humans," *J. Neural Eng.*, vol. 5, no. 1, pp. 75–84, 2008.

[274] W. Wang *et al.*, "An Electrocorticographic Brain Interface in an Individual with Tetraplegia," *PLoS One*, vol. 8, no. 2, pp. 1–8, Feb. 2013.

[275] S. Dangi, K. So, A. L. Orsborn, M. C. Gastpar, and J. M. Carmena, "Brain-machine interface control using broadband spectral power from local field potentials.," *Conf. Proc. IEEE Eng. Med. Biol. Soc.*, vol. 2013, pp. 285–8, 2013.

[276] G. Azizi *et al.*, "Effects of Imatinib Mesylate in Mouse Models of Multiple Sclerosis and In vitro Determinants.," *Iran. J. Allergy. Asthma. Immunol.*, vol. 13, no. 3, pp. 198–206, Jun. 2014.

[277] S. A. Lewandowski *et al.*, "Presymptomatic activation of the PDGF-CC pathway accelerates onset of ALS neurodegeneration," *Acta Neuropathol.*, 2015.

[278] E. J. Su *et al.*, "Imatinib treatment reduces brain injury in a murine model of traumatic brain injury," *Front. Cell. Neurosci.*, vol. 9, no. October, pp. 1–12, 2015.

[279] Y. Zhan *et al.*, "Imatinib preserves blood-brain barrier integrity following experimental subarachnoid hemorrhage in rats.," *J. Neurosci. Res.*, vol. 0, Sep. 2014.

[280] P. Yang *et al.*, "Role of PDGF-D and PDGFR-β in neuroinflammation in experimental ICH mice model," *Exp. Neurol.*, vol. 283, pp. 157–164, 2016.

[281] a. N. Rizzo, J. Aman, G. P. van Nieuw Amerongen, and S. M. Dudek, "Targeting Abl Kinases to Regulate Vascular Leak During Sepsis and Acute Respiratory Distress Syndrome," *Arterioscler. Thromb. Vasc. Biol.*, pp. 1–10, 2015.

[282] C. US DHHS, FDA, "Guidance for Industry – Estimating the maximum safe starting dose in initial clinical trials for therapeutics in adult healthy volunteers," 2005.

[283] M. Han, K. Chung, and H. Cheon, "Imatinib mesylate reduces endoplasmic reticulum stress and induces remission of diabetes in db/db mice," *Diabetes*, vol. 58, no. February, pp. 329–336, 2009.

[284] A. Wolf *et al.*, "Imatinib does not induce cardiotoxicity at clinically relevant concentrations in preclinical studies.," *Leuk. Res.*, vol. 34, no. 9, pp. 1180–8, Sep. 2010.

[285] S. Nassiri, I. Zakeri, M. S. Weingarten, and K. L. Spiller, "Relative Expression of Proinflammatory and Antiinflammatory Genes Reveals Differences between Healing and Nonhealing Human Chronic Diabetic Foot Ulcers," *J. Invest. Dermatol.*, vol. 135, 2015.

[286] G. Buzsáki, C. a Anastassiou, and C. Koch, "The origin of extracellular fields and currents--EEG, ECoG, LFP and spikes.," *Nat. Rev. Neurosci.*, vol. 13, no. 6, pp. 407–20, 2012.